ASSESSMENT AND DEVELOPMENT OF A TROPOSPHERIC DELAY MODEL FOR AIRCRAFT USERS OF THE GLOBAL POSITIONING SYSTEM

JOHN PAUL COLLINS

September 1999

ASSESSMENT AND DEVELOPMENT OF A TROPOSPHERIC DELAY MODEL FOR AIRCRAFT USERS OF THE GLOBAL POSITIONING SYSTEM

John Paul Collins

Department of Geodesy and Geomatics Engineering
University of New Brunswick
P.O. Box 4400
Fredericton, N.B.
Canada
E3B 5A3

September 1999

PREFACE

This technical report is a reproduction of a thesis submitted in partial fulfillment of the requirements for the degree of Master of Science in Engineering in the Department of Geodesy and Geomatics Engineering, September 1999. The research was supervised by Dr. Richard Langley, and it was supported by Nav Canada.

This technical report supersedes our previously published Technical Report No. 187.

As with any copyrighted material, permission to reprint or quote extensively from this report must be received from the author. The citation to this work should appear as follows:

Collins, J. P. (1999). *Assessment and Development of a Tropospheric Delay Model for Aircraft Users of the Global Positioning System.* M.Sc.E. thesis, Department of Geodesy and Geomatics Engineering Technical Report No. 203, University of New Brunswick, Fredericton, New Brunswick, Canada, 174 pp.

ABSTRACT

There currently exist several tropospheric delay models that are specifically intended for use in GPS navigation applications. The basic algorithms were designed approximately 25 to 30 years ago however, and are somewhat inaccurate. As an alternative to these models, some use has been made of the models currently used in precise geodetic positioning. No coherent modelling approach has emerged however, and an opportunity exists to provide an accurate model suitable for a wide range of GPS navigation purposes.

To this end, all the existing tropospheric zenith delay models and mapping functions used in geodesy were examined and a combined model of the best ones were chosen to be compared with the navigation-type models. Enhancements of this "composite" UNB model are based on improving the meteorological parameter values that must be input to drive the model. The final recommended version, denoted UNB3, uses a look up table of meteorological parameters derived from the 1966 U.S. Standard Atmosphere Supplements whose values vary over latitude and season.

The models have been tested using two different data sets: simultaneous GPS and meteorological observations recorded in-flight on a test aircraft; and ray-traced values of the tropospheric delay derived from radiosonde data. The accuracy improvement of the UNB models over that of the initially proposed WAAS model, for example, is between two and four times. For example, the mean height position error at or near the surface is reduced from -0.26 m using the initially proposed WAAS model to -0.06 m using the

UNB3 model. At the same time, the peak-to-peak height position differences were reduced from 1.98 m to 1.01 m.

An attempt was made to define the error bounds of these models. The position error induced by mis-modelling the troposphere during extreme weather conditions may range between 2.5 and 5 metres in height. Two important points must be made regarding the impact of severe weather conditions. First, unless real-time input values are provided, any tropospheric delay model may fail to correctly model the delay under conditions of extremely high or low pressure and/or humidity. Second, these conditions are exceedingly rare and usually of a transient nature, however they do represent theoretical limits.

Despite this qualifier, it is possible to accurately determine the tropospheric delay for an aircraft in flight without access to real-time meteorological information. Under a wide range of general atmospheric conditions, the composite UNB models consistently perform better than the simpler navigation-type models. These improvements have been achieved through the use of models that more accurately represent the physics of the atmosphere and through the use of long-term climatological data (such as that represented in the Standard Atmospheres) to better model the variation of the atmosphere and hence the tropospheric delay.

ACKNOWLEDGEMENTS

TABLE OF CONTENTS

LIST OF TABLES

LIST OF FIGURES

LIST OF SYMBOLS

c	(m/s)	vacuum speed of light (299,792,458 m/s)
d_{trop}	(m)	total propagation delay due to the neutral atmosphere
d_{hyd}^z	(m)	hydrostatic portion of the zenith delay
d_{wet}^z	(m)	wet portion of the zenith delay
$e\ (e_0)$	(mbar)	partial pressure of water vapour (sea-level value)
E	(rad)	true (unrefracted) elevation angle of raypath
g	(m/s^2)	gravitational acceleration
H	(m)	user's height above mean-sea-level
k_1	(K/mbar)	refractive effect of induced molecular polarization of dry gases
k_2	(K/mbar)	refractive effect of induced molecular polarization of water vapour
k_3	(K^2/mbar)	refractive effect of the permanent dipole moment of water vapour
m_{hyd}	(unitless)	hydrostatic mapping function
m_{wet}	(unitless)	wet mapping function
M_d	(kg/kmol)	mean molecular weight of dry air
M_w	(kg/kmol)	molecular weight of water vapour
n	(unitless)	total refractive index
N	(N-units)	total refractivity
N_{dry}	(N-units)	refractivity due to dry gases
N_{wet}	(N-units)	refractivity due to water vapour
P_d	(mbar)	partial pressure of dry gases
$P\ (P_0)$	(mbar)	total atmospheric pressure (sea-level value)
r	(m)	radial distance from the geocentre
R_d	(J/kg/K)	mean specific gas constant for dry air
S	(m)	electromagnetic path in the neutral atmosphere
$T\ (T_0)$	(Kelvin)	absolute temperature (sea-level value)
T_m	(Kelvin)	mean tropospheric temperature
v	(m/s)	media speed of electromagnetic signal
$w\ (w_0)$	(unitless)	mixing ratio of water vapour to dry air (sea-level value)
$z\ (z_0)$	(rad)	true (unrefracted) zenith angle of raypath (sea-level value)
Z_d^{-1}	(unitless)	compressibility factor for dry air

Z_w^{-1}	(unitless)	compressibility factor for water vapour
β	(K/m)	temperature lapse rate
ε	(farad/m)	electric permittivity
κ_{hyd}	(unitless)	hydrostatic delay scaling factor
κ_{wet}	(unitless)	wet delay scaling factor
λ	(unitless)	water vapour "lapse-rate" parameter
λ'	(unitless)	$\lambda + 1$
μ	(henry/m)	magnetic permeability
ρ	(m)	rectilinear (unrefracted) path length in the neutral atmosphere
ρ	(kg/m^3)	total atmospheric density
τ_{hyd}^z	(m/mbar)	hydrostatic delay sensitivity
τ_{wet}^z	(K·m/mbar)	wet delay sensitivity
ζ	(rad)	apparent (refracted) raypath zenith angle

CHAPTER ONE
INTRODUCTION

This thesis describes an investigation into the potential error effects of the neutral atmosphere on the position determination of an aircraft using the Global Positioning System (GPS). An accurate algorithm to model these effects is recommended for use in an aircraft navigation environment. The motivation and background for the work is presented in this chapter. A summary of tropospheric error modelling, as well as GPS and Wide Area Differential GPS (WADGPS) is provided, along with references. The field of aircraft satellite navigation is emphasised throughout, having provided most of the focus for this research.

1.1 Motivation

At its inception, the satellite-based Global Positioning System (GPS) was primarily designed to be a military navigation system, however it was quickly realised that civil use would far outstrip military use. Prior to the availability of the full satellite constellation, civil use has concentrated upon the precise static positioning capabilities available through post-processing of recorded data. While the possibilities for civil aviation have long been recognised (see e.g., *McDonald* [1991]), it was only with the declaration of Full Operational Capability on July 17, 1995, that the potential for GPS use in this field came to the fore.

The full GPS satellite constellation nominally consists of twenty-four space vehicles (SVs) located in six, near-circular, orbital planes. Each satellite transmits electromagnetic signals at 1575.42 MHz (L1) and 1227.60 MHz (L2) containing ranging codes, satellite ephemerides and other information. Non-authorised (primarily civil) users are provided with the Standard Positioning Service (SPS) which restricts access to the Coarse / Acquisition (C/A) code and carrier signals on the L1 frequency only. These signals are constrained to provide standalone (single isolated receiver) position accuracies of 100 m (2 drms) horizontally and 156 m (95%) vertically. This limitation is mainly achieved through the deliberate dithering of the satellite atomic clocks through a process known as Selective Availability (SA) [*Georgiadou and Doucet*, 1990; *Langley*, 1997].

It is primarily because of SA that the Standard Positioning Service falls short of most of the accuracy requirements for civil aviation. To be able to use GPS in this field, corrections and augmentations to the signals must be considered. One possible solution is Differential GPS (DGPS), whereby a receiver located at an accurately coordinated reference station records GPS pseudorange signals from all visible satellites, computes a scalar correction and correction rate for each satellite, and then broadcasts them to potential users in the vicinity.

Due to the de-correlation of satellite and atmospheric error sources, DGPS systems can only provide metre level accuracies over distances of the order of 50 km around the reference station [*Parkinson and Enge*, 1995]. Hence, for continent- or country-wide navigation using GPS, an extension of the DGPS technique must be used. This has led to the Wide Area DGPS (WADGPS) concept [*Kee et al*., 1991], wherein a network of

reference stations record dual-frequency observations from all the visible satellites and transmit the data to a master station. The master station computes a vector of corrections consisting of the satellite positions, the satellite clocks and, usually, a grid of ionospheric corrections. These are then transmitted to the users to be incorporated into the position determination. The separation of the error components allows them to be updated at different time intervals depending on their rates of change and, in the case of the ionospheric corrections, for different user locations.

The use of GPS as a satellite-based navigation system for civil aircraft in North America is being overseen in the United States by the Federal Aviation Administration (FAA), and in Canada by Nav Canada (previously Transport Canada Aviation). The WADGPS system that will provide the accuracy, availability and safety requirements for the en-route to category-one (CAT I) precision approach phases of flight is called the Wide Area Augmentation System (WAAS) [*Loh*, 1995].

This particular WADGPS will consist of the usual network of reference stations (WRSs) located throughout North America connected to one or more master stations (WMSs) which will compute the necessary corrections. The corrections will then be uplinked to one or more geostationary satellites via a ground-earth station (GES) to be relayed to the users. The system will give service to such a large portion of the earth that international co-operation could result in global coverage with three or four similar systems [*Loh*, 1996].

The use of geostationary communications satellites is an important aspect of WAAS, making it more than just a WADGPS correction service. Not only will differential corrections be transmitted, but also a GPS Integrity Broadcast (GIB) and GPS-like ranging signals on the L1 frequency. Combined together, these features form a system that will provide greater positioning accuracy, plus improved availability, integrity and reliability for civil aviation users. More information on the background, implementation and early tests of WAAS can be found in *Loh* [1993] and *Loh et al.* [1995].

The impact of the neutral atmosphere will be felt in two ways in a WADGPS. First, the effect must be modelled in the analysis of the GPS signals received at the reference stations so that the broadcast corrections will not be contaminated by tropospheric delay errors. Second, the receiver on board the user's aircraft must also model the effect at the current location. While in theory, some input could be provided from the aircraft's barometer and temperature sensors, the current consensus is that economical considerations preclude widespread use of this option.

1.2 Troposphere Modelling Overview

The retardation and bending of electromagnetic waves by the electrically neutral atmosphere was first studied to a large extent in the 1950s and 1960s, when much of the focus was on representing the structure, or general profile, of the neutral atmosphere in terms of the refractivity of the constituent gases. Much of the work in the field of "radio meteorology", as it was called, was undertaken in the United States at what was then the

Central Radio Propagation Laboratory (CRPL), in Boulder, Colorado (see *Bean and Dutton* [1966]). Some of this work went towards improving the performance of one of the first major air navigation aids – radar.

The research undertaken by CRPL has proved to be useful in the fields of space geodesy and radio astronomy. One of the fundamental results of the CRPL investigations was that the delay and bending of electromagnetic waves could be computed to a high accuracy by ray-tracing suitable refractivity profiles specified with only surface refractivity values. In fact, it was found that only a few examples of different profiles need be used, provided that accurate measurements of the surface refractivity were available. Simple polynomial approximations of the results were used for speed and convenience. It is models such as these, based directly on the work of CRPL (e.g. *Altshuler* [1971]), that are currently recommended for navigational uses of GPS. All such models are generally termed tropospheric delay models, because the bulk of the effect is experienced in the tropospheric portion of the neutral atmosphere.

Similar empirical techniques have also been applied to space geodesy positioning, although generally with some refinements such as separating the zenith effects from the elevation angle dependent effects. Most current models also separate the refractivity effect into two parts – one due to the dry gases and one due to the wet gases in the atmosphere. Models formulated in this way were developed for use with Very Long Baseline Interferometry (VLBI), Satellite Laser Ranging (SLR), Transit and GPS high accuracy positioning techniques.

As these positioning techniques were continually refined, it became obvious that the imperfect modelling of the tropospheric delay was one of the major limiting factors in the achievable position accuracies. What was perhaps the most problematic part was the modelling of the elevation angle dependence of the delay, and a great deal of work has gone into improving this aspect of the delay modelling (see e.g., *Davis et al.* [1985]; *Ifadis* [1986]; *Herring* [1992]; *Niell* [1996]).

The latest models of the elevation angle dependence (the so-called "mapping functions" or "obliquity factors") have proved to be so accurate (see e.g., *Mendes and Langley* [1994]; *Estefan and Sovers* [1994]), that nearly the only limit to precisely determining the tropospheric delay is provided by the temporal and spatial variability of the atmospheric structure and its constituent gases. The primary problem remains the inhomogeneous nature of atmospheric water vapour. While certain radiometric instruments have been developed to directly measure the contribution of the atmospheric water vapour (e.g. the Water Vapour Radiometer), their operation is not trivial and alternative techniques, such as the estimation of the unmodelled delay from the measurement data were originally proven, if anything, to be better (e.g. *Dixon and Kornreich Wolf* [1990] and *Tralli et al.* [1992]). The later introduction of "pointed" WVR instruments to directly measure "line-of-sight" water vapour content were an improvement over the original, zenith only, instruments (see e.g., *Ware et al.* [1993]), however the major limitations, such as poor operation in rain, remain.

The estimation techniques used to improve the modelling of the tropospheric effect are primarily least-squares parametric or stochastic techniques, and are often implemented at

static reference stations. For an aircraft receiver however, a real-time estimation procedure — although theoretically feasible with carrier phase measurements [*Collins and Langley*, 1997] — requires further investigation and will likely not be implemented in the near future. As such, aircraft users will have to rely solely on an empirical model, and one without access to measurements of the ambient meteorological conditions.

1.3 Research Objectives

Despite the recent advances in tropospheric delay modelling for geodetic applications of GPS, the models currently used, or proposed for use, in navigation applications of GPS are often those initially developed between 25 and 30 years ago. The advances made in both computing power and knowledge of the atmosphere since then renders these models as somewhat out-of-date, in addition to being comparatively inaccurate. At the same time, the application of more recent geodetic-type models to this field of GPS has not been comprehensively explained, precluding greater insight into the nature of the atmospheric effect. Therefore, an opportunity exists to clarify the potential improvements available for modelling the tropospheric delay in GPS navigation.

Hence, the primary task of this research was to test the navigation-type tropospheric delay models alongside the best of the current geodetic-type models, as modified to work at an aircraft in flight. In this way, the accurate methods of tropospheric delay determination from space geodesy have been applied to the navigation field of GPS.

1.4 Thesis Overview

A brief description of the impact of the neutral atmosphere on electromagnetic waves is described in Chapter Two, along with the algorithms for modelling the effect. Chapter Three describes the composite models developed at UNB to deal with this problem and their testing with GPS flight data. Chapter Four describes further testing with radiosonde data. The rationale and methodology for both types of test is fully described in each chapter. A numerical study of the potential limits of any unmodelled errors is described in Chapter Five. Chapter Six contains a summary, the conclusions, and the recommendations for possible future work. The appendices consist of a short mathematical derivation left out of the main part of the report, the algorithms of some of the older models, relevant figures from the two tests, and a section on the practical implementation of the recommended tropospheric delay model.

1.5 Terminology

This thesis has been written with a background in geodesy in mind and therefore geodetic terminology predominates. Some phrases will re-occur that are slightly at variance from those used in aviation circles. The most prominent of these is the use of "height" instead of "altitude" and "height error" instead of "vertical bias". The former refers to the vertical position above a reference surface, usually the ellipsoid that best approximates mean-sea level, and the latter for the error in the computed aircraft position from its true location.

CHAPTER TWO
THE TROPOSPHERIC EFFECT

This section describes the effect of the neutral atmosphere on the GPS signals. A brief development from a physical perspective is given followed by a description of the empirical models of the propagation delay generally used for navigation purposes. This approach leads towards the solution of the tropospheric delay as generally approached in space geodesy and to the extension of those methods to aircraft navigation.

2.1 Refraction in the Neutral Atmosphere

An electromagnetic signal propagating through the neutral atmosphere is impeded because the refractive index of the constituent gases is slightly greater than unity. The resulting decrease in velocity increases the time taken for the signal to reach a receiver's antenna, thereby increasing the equivalent path length (both often referred to as the "delay"). Refraction also bends the raypath and thereby lengthens it, further increasing the delay.

Like all electromagnetic waves, the ranging signals broadcast by the GPS satellites can be described by Maxwell's equations. The propagation media in those equations is characterised by μ and ε, the magnetic permeability and the electric permittivity. The velocity of an electromagnetic wave is characterised by the refractive index, n. This represents the ratio of the vacuum speed (c) of an electromagnetic wave to its media speed (v) and is related by Maxwell's formula [*Brunner*, 1992]:

$$n = \frac{c}{v} = \sqrt{\varepsilon\mu}\,. \qquad (2.1)$$

Solutions of Maxwell's equations can be difficult to obtain if μ and ε are functions of position. Hence it is usual to use the approximate solution provided by geometrical optics [*Bohn*, 1968]. In this approximation the wave is described by a geometric curve or ray. The use of geometric optics is valid provided that the wave extent is very large compared to the wavelength [*Kerker*, 1969]. Maxwell's equations can then be reduced to the fundamental differential equation for geometric optics:

$$(\nabla S)^2 = n^2\,. \qquad (2.2)$$

This is the eikonal equation [*Kline and Kay*, 1965] where ∇ (del), the gradient operator, is applied to the electromagnetic path S. All the laws of geometrical optics, including Snell's Law, can be derived from this equation. As such, it is subject to Fermat's principle of minimum time travel of a ray.

The electromagnetic path length can be determined from equation (2.2) as:

$$S = \int_S |\nabla S|\, ds = \int_{P_1}^{P_2} n\, ds\,. \qquad (2.3)$$

where P_1, and P_2 are the end points of S. In geodetic GPS work it is common to characterise the electromagnetic path length in the neutral atmosphere as:

$$S = \rho + d_{trop}, \qquad (2.4)$$

where ρ represents the rectilinear, *in-vacuo,* distance between P_1, and P_2 and d_{trop} represents the excess path length due to the refractive index differing from unity over the ray path. The refractive index is a function referenced in three dimensional space,

however in the neutral atmosphere several simplifying assumptions can be made to simplify equation (2.3). First, the atmosphere is assumed to be spherically symmetric; that is, the earth is a sphere and the properties of the atmosphere vary only with geocentric radius. In this way the atmosphere can be considered layered with a refractive index characterising each layer. Second, the atmosphere is usually assumed to be azimuthally symmetric; that is with no variation in azimuth of the refractive index in each layer. In this way the electromagnetic ray is confined to a plane defined by the start and end points of the ray and the geocentre. These assumptions allow us to represent the refractive index profile as a function of geocentric radial distance only, $n(r)$. Equations (2.3) and (2.4) can then be written as:

$$\rho + d_{trop} = \int_{r_0}^{r_1} n(r)\sec\zeta(r)\,dr \qquad\qquad (\,2.5\,)$$

where the refractive index is integrated along the path between points r_0 – the geocentric distance of the user's antenna and r_1 – the geocentric distance of the "top" of the neutral atmosphere. Angle ζ is the actual (refracted) zenith angle of the raypath at distance r (see Figure 2.1). The path delay is caused by the variation of n from unity, hence:

$$\rho + d_{trop} = \int_{r_0}^{r_1}\left[n(r)-1\right]\sec\zeta(r)\,dr + \int_{r_0}^{r_1}\sec\zeta(r)\,dr \qquad\qquad (\,2.6\,)$$

gives in the first term the excess delay equivalent path length and in the second term the geometric length along the curved path. To obtain the total tropospheric delay we can subtract the *in-vacuo* distance to get the following integral equation [*Langley*, 1996]:

$$d_{trop} = \int_{r_0}^{r_1}[n(r)-1]\sec\zeta(r)\,dr + \left[\int_{r_0}^{r_1}\sec\zeta(r)\,dr - \int_{r_0}^{r_1}\sec z_0\,dr\right] \qquad (\,2.7\,)$$

Angle z_0 is the true (unrefracted) satellite zenith angle and hence constant along the unrefracted path. To summarise: the first integral accounts for the difference between the electromagnetic distance and the geometric distance along the ray path and the bracketed integrals account for the curvature of the ray path; i.e., the difference between the refracted and rectilinear geometric distances.
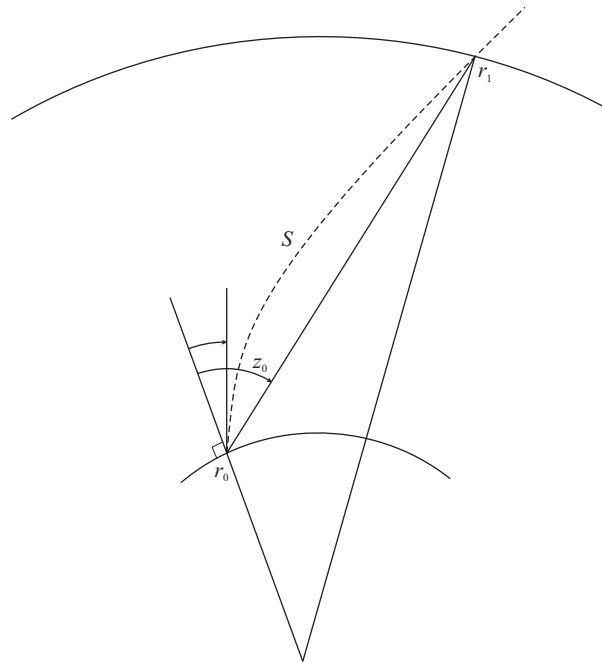
Figure 2.1. Tropospheric delay geometry.

The tropospheric delay is usually considered in two parts: the delay experienced in the zenith direction and the magnification of that delay to the delay experienced at the zenith angle of the raypath of the observed signal. The ratio of these two values is usually termed the "mapping function" (which has tended to replace the phrase "obliquity

factor"). In addition, because the refraction is primarily a function of the (mainly dry) atmospheric gases in hydrostatic equilibrium and of water vapour alone, their contributions are often considered separately. This leads to the common formulation of zenith delays and mapping functions seen in the geodetic GPS literature. Following *Davis et al.* [1985], the typical formulation of the tropospheric delay is given as:

$$d_{trop} = d^z_{hyd} \cdot m_{hyd} + d^z_{wet} \cdot m_{wet}, \quad\quad\quad (2.8)$$

where the total delay d_{trop} is a function of the hydrostatic zenith delay d^z_{hyd} and its mapping function m_{hyd}, and the wet zenith delay d^z_{wet} and its mapping function m_{wet}. If the bending of the raypath is taken into account, it is usually incorporated into the hydrostatic mapping function. It is common in the literature describing some older geodetic models to find the total delay partitioned into the slightly different "dry" and "wet" components. In addition, the wet portion has also been described as the "non-hydrostatic" portion [*Mendes*, 1999].

2.2 Explicit Definition of the Tropospheric Delay

Part of the appeal of using the current geodetic-GPS positioning models as an alternative to the current navigation-GPS models is that many are based on an extended analysis of the physics of the atmosphere. In addition, previous work at UNB has indicated that they can be very precise and accurate [*Janes et al.*, 1991; *Mendes*, 1999], especially compared to the navigation models [*Mendes et al.*, 1995]. For this reason and because they form the backbone of this work, their derivation will be described in full.

2.2.1 Zenith Delays

Considering only the delay in the zenith direction, equation (2.7) reduces to:

$$d_{trop}^{z} = \int_{r_0}^{r_1} [n(r) - 1] \, dr = 10^{-6} \int_{r_0}^{r_1} N(r) \, dr, \qquad (2.9)$$

where N is the refractivity. The refractivity is primarily dependent upon the ambient atmospheric gases and can be written in two parts, that due to the dry gases (primarily nitrogen and oxygen) and that due to water vapour [*Thayer*, 1974]:

$$\begin{aligned} N &= N_{dry} + N_{wet} \\ &= k_1 \left(\frac{P_d}{T} \right) Z_d^{-1} + \left(k_2 \frac{e}{T} + k_3 \frac{e}{T^2} \right) Z_w^{-1}, \end{aligned} \qquad (2.10)$$

where N_{dry} and N_{wet} are the refractivity contributions from the dry and wet gases respectively, P_d is the partial pressure of dry air (mbar), T is the absolute temperature (K), e is the partial pressure of water vapour (mbar) and Z_d and Z_w are compressibility factors to account for non-ideal gas behaviour [*Owens*, 1967]. The constants k_1, k_2 and k_3 represent the molecular polarization of the dry gases and water vapour and the permanent dipole moment of water vapour respectively and are empirically derived. Small refraction effects due to hydrometeors (such as rain, suspended water droplets, clouds, snow and ice) and aerosols (such as smog) are usually considered to be negligible and are ignored. Using the equation of state, equation (2.10) can be recast as a function of the total atmospheric density, ρ, specifically:

$$N = k_1 R_d \rho + \left(k_2' \frac{e}{T} + k_3 \frac{e}{T^2} \right) Z_w^{-1}, \qquad (2.11)$$

where, $k_2' = (k_2 - k_1 [M_w / M_d])$, M_w and M_d are the molar masses of water vapour and

dry air respectively and R_d is the molar gas constant. The first term in equation (2.11) represents the contribution of that fraction of moist air that is in hydrostatic equilibrium and is referred to as the hydrostatic component of refractivity. Combining equations (2.9) and (2.11) and ignoring the compressibility factors (which differ from unity by a few parts per thousand at most), we get:

$$
\begin{aligned}
d^z_{trop} &= d^z_{hyd} + d^z_{wet} \\
&= \frac{10^{-6} k_1 R_d}{g_m} \cdot P + 10^{-6} \int_{r_0}^{r_1} \left(k'_2 \frac{e}{T} + k_3 \frac{e}{T^2} \right) dr,
\end{aligned}
\qquad (\,2.12\,)
$$

where the assumption of hydrostatic equilibrium in the atmosphere has allowed the integration of the hydrostatic component. Gravity acceleration at the atmospheric column centroid is given by g_m, a function of latitude and height of the antenna. The hydrostatic zenith delay normally accounts for about 95% of the total zenith delay and can be modelled with sub-millimetre accuracy provided accurate measurements of pressure (P) at the user's antenna are available [*Davis et al.*, 1985]. We will choose to write the hydrostatic zenith delay as:

$$
\begin{aligned}
d^z_{hyd} &= \frac{10^{-6} k_1 R_d}{g_m} \cdot P \\
&= \tau^z_{hyd} \cdot P
\end{aligned}
\qquad (\,2.13\,)
$$

where τ^z_{hyd} is the hydrostatic zenith delay "sensitivity" in units of metres per millibar of ambient atmospheric pressure.

What remains from equation (2.12) will be denoted here as the wet zenith delay and can also be integrated after specifying suitable relationships for temperature and water vapour pressure with height. Unfortunately, water vapour is rarely in hydrostatic

15

equilibrium and varies significantly throughout the troposphere, hence specifying an accurate relationship with height is difficult. However, it is common in meteorology to model the average decrease of water vapour with height (or total pressure) as an exponential function with exponent λ. From *Smith* [1966], the mixing ratio (w) of water vapour to moist air is given approximately by:

$$w = w_0 \left(\frac{P}{P_0} \right)^{\lambda} , \qquad (2.14)$$

where the zero subscript indicates surface (i.e. mean-sea-level) values. However,

$w = \left(\frac{M_w}{M} \right) \left(\frac{e}{P} \right)$, $w_0 = \left(\frac{M_w}{M} \right) \left(\frac{e_0}{P_0} \right)$ and by substitution and re-arrangement we can

obtain:

$$e = e_0 \left(\frac{P}{P_0} \right)^{\lambda+1} , \qquad (2.15)$$

which provides a relationship for the average decrease in water vapour pressure with height. Separating the two zenith wet delay components in equation (2.12) we have:

$$d_{wet}^{z} = 10^{-6} k_2' \int_{r_0}^{r_1} \frac{e}{T} dr + 10^{-6} k_3 \int_{r_0}^{r_1} \frac{e}{T^2} dr . \qquad (2.16)$$

By specifying a linear lapse rate (positive) for temperature (β), the temperature throughout the troposphere is represented as:

$$T = T_0 \left(\frac{P}{P_0} \right)^{\frac{R_d \beta}{g}} , \qquad (2.17)$$

which, when combined with equation (2.15), allows for the integration of equation (2.16). The formulation given by *Askne and Nordius* [1987] is:

$$d^z_{wet} = \frac{10^{-6} k'_2 R_d}{g_m(\lambda + 1)} \cdot e + \frac{10^{-6} k_3 R_d}{g_m(\lambda + 1 - \beta R_d / g_m)} \cdot \frac{e}{T},$$

(2.18)

which we will choose to write as:

$$d^z_{wet} = \frac{10^{-6}(T_m k'_2 + k_3) R_d}{g_m \lambda' - \beta R_d} \cdot \frac{e}{T},$$

$$= \tau^z_{wet} \cdot \frac{e}{T}$$

(2.19)

where the mean temperature of the water vapour $T_m = T\left(1 - \dfrac{\beta R_d}{g_m \lambda'}\right)$, $\lambda' = \lambda + 1$ and τ^z_{wet}

is the wet zenith delay "sensitivity" in units of kelvin metres per millibar of water vapour

pressure.

2.2.2 Mapping Functions

Mapping functions in geodesy are generally derived from one of two approaches. The

older and less reliable functions use various approximations of Snell's law of refraction for

a spherically symmetric medium with uniform refractivity [*Janes et al.*, 1991]:

$$\sec \zeta(r) \approx \sec z(r) = \frac{1}{\sqrt{\left[1 - \left(\dfrac{r_0^2}{r^2}\right) \sin^2 z_0\right]}} \cdot$$

(2.20)

where $z(r)$ is the unrefracted zenith angle at the antenna position r. The remaining terms

have been defined in equation (2.5). In general, many of these functions also ignore the

effect of ray bending and are poor performers at elevation angles less than 15°. In

addition, those that do attempt to model the bending are also limited by the

approximations required to solve the integrals of equation (2.7). A comprehensive review

of the performance of all the currently available mapping functions is provided by *Mendes and Langley* [1994] and *Mendes* [1999].

It has been found that mapping functions expressed as a continued fraction are a better approximation to atmospheric profiles at low elevation angles, while retaining the necessary accuracy toward the zenith. The general form is known as the Marini mapping function:

$$m(E) = \frac{d_{trop}}{d_{trop}^z} = \cfrac{1}{\sin E + \cfrac{a}{\sin E + \cfrac{b}{\sin E + c}}} \qquad (2.21)$$

where E is the unrefracted elevation angle of the satellite and a, b, and c are coefficients to describe a particular atmospheric profile. It is possible to evaluate these from expressions for various types of atmospheric layer [*Marini*, 1972; *Marini and Murray*, 1973], however it has become common to empirically fit these coefficients to ray-traced radiosonde or other profile data. In this way it is also possible to take into account the effect of ray bending and the separation of the hydrostatic and wet delays. These coefficients can also be derived in terms of atmospheric parameters and position and time information.

2.2.3 Providing Meteorological Information

In geodetic use, zenith delay models and mapping functions are often provided with values of surface meteorological parameters recorded "on-site" to derive the tropospheric delays. This concept can be extended by using equations to scale surface parameter values

to an aircraft's height. As the primary driving parameters of the tropospheric delays it is natural to choose total pressure (P_0), temperature (T_0) and water vapour pressure (e_0) at sea-level. The vertical profiles of these parameters are then specified through the temperature lapse rate (β) and the parameter that represents the average decrease of water vapour (λ).

The temperature lapse rate is assumed linear with height (H):

$$T = T_0 - \beta \cdot H,\qquad(2.22)$$

which, coupled with the condition of hydrostatic equilibrium and application of the perfect gas law, yields the standard expression (see Appendix A1):

$$P = P_0 \left(\frac{T}{T_0} \right)^{\frac{g}{R_d \beta}},\qquad(2.23)$$

which substituted into equation (2.15) gives:

$$e = e_0 \left(\frac{T}{T_0} \right)^{\frac{\lambda' g}{R_d \beta}},\qquad(2.24)$$

where surface gravity is represented by g. From these equations we can derive the following expressions to scale the sea-level values to the user's height. Substituting equation (2.22) into equation (2.23) gives:

$$P = P_0 \left(1 - \frac{\beta H}{T_0} \right)^{\frac{g}{R_d \beta}},\qquad(2.25)$$
$$\equiv P_0 \cdot \kappa_{hyd} \{T_0, \beta\}$$

where κ_{hyd} is the hydrostatic delay scaling factor (as a function of T_0 and β). Combining

equation (2.22) and equation (2.24) gives:

$$\frac{e}{T} = \frac{e_0}{T_0}\left(1 - \frac{\beta H}{T_0}\right)^{\frac{\lambda' g}{R_d \beta} - 1}.$$

$$\equiv \frac{e_0}{T_0} \cdot \kappa_{wet}\{T_0, \beta, \lambda'\}$$

(2.26)

where κ_{wet} is the wet delay scaling factor (as a function of T_0, β and λ').

Combining equations (2.25) and (2.26) with (2.13) and (2.19) allows the zenith delays to be formulated as:

$$d_{hyd}^z = \tau_{hyd}^z \cdot \kappa_{hyd} \cdot P_0 \quad,$$

(2.27)

$$d_{wet}^z = \tau_{wet}^z \cdot \kappa_{wet} \cdot \frac{e_0}{T_0} \quad.$$

(2.28)

Specifically, for the airborne environment, we can see that the hydrostatic delay is dependent upon the surface pressure and the temperature profile. The wet delay is dependent upon the surface values of temperature and water vapour pressure and both the temperature profile and the water vapour profile.

Theoretically, all the models represented here are limited to use below the tropopause. In isothermic layers the scaling functions κ_{hyd} and κ_{wet} are not valid and must be replaced. The new functions are then dependent upon the temperature and pressures at the base of the isothermic layer.

These five meteorological parameters of pressure (P_0), temperature (T_0), and partial pressure of water vapour (e_0) at sea-level, coupled with the temperature lapse rate (β) and

water vapour "lapse rate" (λ) provide a simple, yet comprehensive method for modelling the neutral atmosphere for the purposes of determining the tropospheric delay.

Previous researchers have pointed out the strong correlation of height bias in GPS position solutions and tropospheric delay error (e.g. *Tiemeyer et al*. [1994] and *Shi and Cannon* [1995]). An intuitive understanding of this can be gleaned from considering the hydrostatic delay. Equation (2.13) shows its fundamental dependence on the atmospheric pressure at the GPS antenna which is conversely dependent, by equations (2.22) and (2.23), on height. Therefore, any attempt to treat the atmosphere at altitude as if it were equivalent to conditions at the earth's surface, or to ignore the tropospheric effect altogether, will introduce a bias inversely proportional to the height above sea-level. The important point for GPS air navigation is that for an aircraft undergoing descent, such as during a landing approach, the tropospheric delay must be determined at every epoch for which a position solution is computed.

2.3 Original Models for Navigation Use

Much of the early tropospheric delay work of the type undertaken at CRPL and later applied to GPS was based on deriving simplified solutions of equations (2.7) or (2.9) based on ray-traced radiosonde data. The ray trace equations can be derived from equation (2.2) through Snell's Law of refraction. Radiosonde data provided the measurements of the ambient atmospheric conditions necessary to derive the refractivity.

The original model of this type designed specifically for GPS is the Altshuler model [*Altshuler and Kalaghan*, 1974]. For the purposes of WAAS, the algorithms that make up this model were simplified to produce the initially proposed WAAS model [*DeCleene*, 1995]. In addition to these two models, there is a similar model recommended by the North Atlantic Treaty Organisation (NATO) in its GPS Standards Document [*NATO*, 1993].

The NATO model uses a three-stage equation to represent three distinct atmospheric layers as an approximation to equation (2.9): from 0 to 1 km, between 1 and 9 km and from 9 km and above. Although not stated in the reference for this model [*NATO*, 1993], this model is derived directly from the Central Radio Propagation Laboratory Reference Atmosphere-1958 (CRPL RA-1958) (see *Bean and Thayer* [1959]). Atmospheric refractivity is represented as decreasing linearly in the first kilometre above the earth's surface, then exponentially to a constant value of 105 N units at 9 km and exponentially from there on upwards (see Appendix A2.3).

The CRPL RA-1958 was originally derived from radiosonde data from what was then extensive balloon launches around the United States (45 sites for the 0–1 km part of the model, 13 sites for 1–9 km and rocket data for heights greater than 9 km; see *Bean and Thayer* [1959] for more details). Similarly, the Altshuler model was also derived from ray tracing through CRPL profiles, including RA-1958, using seasonal world-wide surface refractivity data. With the initially proposed WAAS model being derived from the Altshuler model, all three of these models appear to have a similar provenance. Theoretically, all three models are specified with the same mean global surface refractivity

value of 324.8 N units, although the Altshuler and WAAS models adjust this in an attempt to account for seasonal and latitude dependence.

These three models all deal with the total zenith delay; that is, none attempt to consider the separate contribution of different atmospheric gases. In the NATO formulation, the zenith delay is mapped to the observed elevation angle by the *Chao* [1972] "dry" mapping function. The elevation angle dependence in the Altshuler model is effected through a seven coefficient polynomial, whereas the initially proposed WAAS model uses a modified form of the elevation angle cosecant as its mapping function.

Because the NATO model is specified with a constant value of surface refractivity, only the user's height is required to evaluate its atmospheric profile. The Altshuler and WAAS models require the height for the same reason, but they also require the user's latitude and time (season for Altshuler, day-of-year for WAAS) in an attempt to model the variation in surface refractivity. The algorithms for these models are provided in Appendix A2.

CHAPTER THREE
DEVELOPMENT OF UNB MODELS

This chapter will proceed with the chronological development of the tropospheric models assembled during this research. The first tests of the models were undertaken with sets of GPS and meteorological data simultaneously recorded during extensive aircraft flights from St. John's, Newfoundland.

3.1 Rationale For UNB1

As the basis for an accurate model of the tropospheric delay, the choice of zenith delay components is important because their errors will be magnified to lower elevation angles by the mapping functions. The hydrostatic and wet zenith delays of *Saastamoinen* [1972], which can be derived from equations (2.13) and (2.19) with the refractivity constants of *Smith and Weintraub* [1953] and "standard" lapse rate constants, are the most accurate zenith delay models available when provided with adequate meteorological measurements (*Janes et al.* [1991]; *Mendes and Langley* [1995]). Hence they are a logical choice for a standard model.

Because they inherently magnify any zenith delay errors, it is obviously an advantage for mapping functions to have a near-zero bias. This beneficial feature is one of several shown by the functions derived by *Niell* [1996]. These functions are a normalised form of equation (2.21) and parameterised in terms of position information (latitude and height) and time (day-of-year) only. Although they require no user input of meteorological

information, they have been shown to work as well as, if not better than, other mapping functions that do (see e.g., *Mendes and Langley* [1994]; *Niell* [1996]; *Mendes*, [1999]). The coefficients for the functions are derived from ray-traces of the 1966 U.S. Standard Atmosphere Supplements [*Dubin et al.*, 1966] which provide climate data for 15°, 30°, 45°, 60° and 75° latitudes for the January and July extremes of winter and summer conditions in the northern hemisphere. The southern hemisphere is assumed equivalent and anti-symmetric in time.

For initial testing purposes, it was possible to make this composite model equivalent to the three navigation models with regards to the meteorological input. Using the same refractivity constants as Saastamoinen and setting pressure and temperature to the 1976 Standard Atmosphere [*Dubin et al.*, 1976] values of 1013.25 mbar and 288.15 K, a water vapour pressure of 11.7 mbar can be derived to equal the total surface refractivity of 324.8 N units, the value used by the other models. The standard atmosphere lapse rate of 6.5 K/km was used as was a lambda value of 3 – again to be consistent with the Saastamoinen zenith wet delay which uses these values. This composite model, denoted as UNB1, is summarised in Table 3.1.

Table 3.1. Meteorological parameters for the UNB1 model.

P_0 (mbar)	T_0 (kelvin)	e_0 (mbar)	β (K/km)	λ (n/a)
1013.25	288.15	11.7	6.5	3

3.2 Initial Tests With GPS Flight Data

It was decided to test the UNB1 model against the navigation-type models using GPS data recorded at an aircraft in flight. These test are conducted in what we might call the position domain — i.e. we see the effect of using different tropospheric delay models on the computed position of the aircraft.

3.2.1 Flight Data Description

The flight data processed in this study was collected by the National Research Council (NRC), Canada, at and around St. John's, Newfoundland, in March 1995 using their heavily instrumented Convair-580 aircraft [*Phillips*, 1995]. The campaign (denoted *Frizzle '95*) was primarily conducted between the latitudes of 45°N and 52°N and longitudes 57°W to 47°W (see Figure 3.1). The main objective of the campaign was to investigate the effects of freezing precipitation on aircraft dynamics and in particular:

- to study stratiform drizzle formation, particularly over sea ice;
- to study drizzle formation from frontal lifting;
- to measure ice accretion and test measurement systems;
- to test a de-icing scheme;
- and to study the change in aircraft performance with ice accretion.

Most of the twelve flights were over several hours long and consisted of many horizontal and vertical profiles through cloud layers up to heights of approximately 7 km (see Table 3.2). Frontal zones and temperature inversions are often associated with

potential causes of freezing precipitation and along with the geographic location and unpredictable weather conditions it was expected that this data set would provide a good test of the tropospheric delay models.
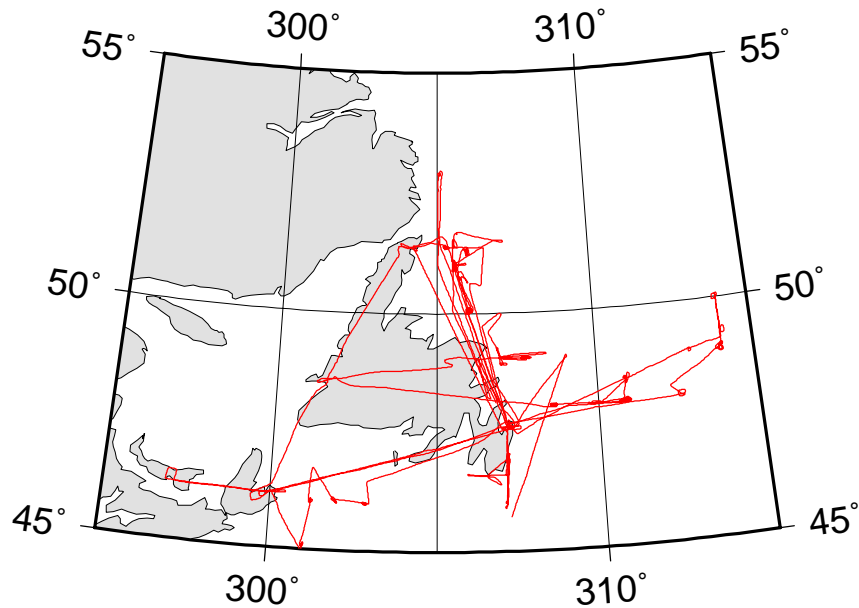
Figure 3.1. Aircraft tracks of Frizzle'95 flight tests.

The GPS data consists of 0.5 Hz dual-frequency measurements simultaneously recorded by Ashtech Z-12 receivers located onboard the aircraft and at a ground reference station in St. John's. Meteorological data was also recorded at both the ground station and the aircraft. The meteorological data is available at one minute intervals at the reference station and every second at the aircraft. Due to technical reasons, meteorological data was only recorded between take-off and touch-down, although GPS data generally exists before and after the aircraft starts and finishes taxiing on the ground.

Table 3.2. Frizzle '95 Flight Data Summary.

Date (March, 1995)	Flight Code	Duration[†] (hours)	Maximum Height (km)	Maximum Distance from Reference Station (km)
03	F503	1.70	5.4	210
06	F504	4.93	6.8	810
07	F505	4.74	6.0	565
08	F506	3.25	6.2	501
09	F507	3.32	3.1	434
10	F508	2.92	6.1	471
13	F509	3.19	6.1	189
14	F510	4.95	6.8	449
15	F511	3.56	6.4	497
17	F512	4.42	6.1	465
18	F513	4.81	3.0	625
22	F516	4.13	4.3	618

[†]Duration refers to the flight time for which GPS and meteorological data exists simultaneously.

3.2.2 Data Processing Techniques

The nature of the flights imposed a particular methodology of data processing. All of the flights included data when the aircraft was over 100 km from the reference station and on several days the maximum distance was over 600 km. This made it impractical to use the carrier phase data with our then-current software because of the increasing difficulty in correctly resolving cycle slips and integer ambiguities for new (low elevation) satellites at distances in excess of several tens of kilometres — a problem that is exacerbated when using less accurate tropospheric delay models [*Mendes et al.*, 1995].

For example, the influence of different tropospheric delay models on carrier phase ambiguity resolution is two-fold. Not only can the ambiguities be incorrectly resolved, but also at different epochs, if an "on-the-fly" (OTF) technique is employed. Hence, any

differencing of solutions to examine the impact of using a different tropospheric delay model can be complicated by spurious jumps and biases due to incorrect integer ambiguities. To avoid these problems, it is possible to use the synthetic P-code pseudorange measurements (hereafter called, simply, P-code measurements) that are available. These are still precise (compared to C/A code), low-noise measurements and they have allowed for all the collected flight data to be used.

To reduce the influence of satellite position errors, precise International GPS Service (IGS) orbits were used. The elevation mask angle was set to five degrees to allow for the examination of the effects of low elevation angle measurements, where tropospheric delay mis-modelling is often severe.

The original intention to use the ionosphere-free linear combination (P3) to remove the ionospheric delay was deemed impractical due to data gaps in the P-code measurements. These occurred at both receivers when satellites were at low elevation angles, where it seems that the Ashtech receivers had problems tracking the P-code signals near to the horizon. When using the ionosphere-free combination, satellites are temporarily removed from the solution causing spikes in the Position Dilution of Precision (PDOP) indicator and consequent jumps in the solutions. (Note: the PDOP values referred to here represent the combined satellite geometry at the two stations, not at the aircraft alone as is usually the case.) These jumps are exaggerated in the solution differences because they are at low elevation angles where the tropospheric delay may be poorly modelled. While these jumps do not affect our results statistically, they can be confusing. Using the precise L1 pseudorange measurements (P1) and substituting C/A code measurements when necessary

generally gave more consistent PDOP values and is inherently less noisy. Any residual ionospheric influence not removed by the single differencing undertaken during the processing is almost certainly removed when different position solutions are differenced.

The data was processed with the Kinematic and Rapid Static (KARS) software developed by Dr. Gerald Mader at the National Geodetic Survey, National Oceanic and Atmospheric Administration, U.S.A. [*Mader*, 1996], and subsequently heavily modified at UNB. The pseudorange processing is undertaken using single-difference observables and performs an independent least-squares position solution for each epoch of data (see e.g., *Hofmann–Wellenhof et al.* [1992] for a brief overview of this technique).

3.2.3 Testing Methodology

To provide a reference with which to compare the impact of the different tropospheric delay models, a "benchmark", or "tropospheric truth", solution was computed for each day. The benchmark solutions use the Saastamoinen/Niell combination to model the tropospheric delay but with inputs from the meteorological data recorded at the aircraft and the ground station. The solution for each flight was then sequentially re-computed replacing only the aircraft data tropospheric delay model. To examine the impact of a particular model, the solutions were differenced with the benchmark solutions.

Without an independent way of computing the positions of the aircraft, this test of *relative* accuracy is the best possible, based on superior models and the provision of real-time meteorological data at the aircraft, which is almost certainly the most that can be done in a real application of WADGPS. Hence, these tests will also identify which

model's meteorological parameters replicate the real-time data, and therefore the atmosphere, most closely, but with the differences computed in the position domain for emphasis.

The *absolute* accuracy of this "truth system" could only be improved if the meteorological data was used to construct zenith delay models and mapping functions specific for each day or flight portion. This would be an extremely large undertaking and was not practicably possible when these tests were undertaken. The only other alternative would be to use a different mapping function in the benchmark solution. However, all the modern mapping functions (Niell, Herring and Ifadis) perform approximately equally [*Mendes*, 1999] and do not affect any of the results if used in the benchmark solution.

3.2.4 UNB1 Results (All data)

Statistics were computed for the solution differences of each day and for all the days. The mean, standard deviation and range (peak to peak) of the differences in latitude, longitude and height were derived to quantify any overall bias and variation from the benchmark solutions. The statistics for all the data are presented in Table 3.3.

Table 3.3. Position difference statistics for navigation-type models.
Units are metres. (All data, ~46 hours over 12 flights.)

	Altshuler			WAAS			NATO			UNB1		
	Range	Mean	S.D.	Range	Mean	S.D.	Range	Mean	S.D.	Range	Mean	S.D.
Latitude	0.95	0.01	0.07	0.91	0.00	0.06	0.56	0.01	0.05	0.26	0.00	0.02
Longitude	0.51	-0.01	0.04	0.65	0.01	0.04	0.29	-0.01	0.03	0.17	0.00	0.02
Height	1.75	0.10	0.24	1.98	-0.26	0.24	1.24	0.24	0.16	1.12	0.08	0.13

As expected there are low biases in the latitude and longitude components of position for all the models, however the UNB1 solutions show a consistently smaller variation than the other three. In addition, the range of horizontal position error of all three navigation models is large compared to the vertical error. For example, the latitude error range is approximately 54% of the height range for Altshuler compared to 23% for UNB1. The variations of the position differences, as represented by the standard deviation, are larger for Altshuler and the initially proposed WAAS model. The general trends are clearly represented by Table 3.3.

The largest effects are seen in the height differences. The NATO and WAAS solutions have means of similar magnitude, but opposite sign. Altshuler and UNB1 have similar means, however the variation from the benchmark solution, as represented by the standard deviation, are much smaller for UNB1 indicating that on average this model causes the smallest variations from the benchmark solution.

3.2.5 UNB1 Results (Flight F508 only; 2.9 hours)

To get a better understanding of the performance of each model, we can study an individual flight. Because it represents the worst case for the height component we will analyse the results from flight F508 (March 10) more closely. Figure 3.2 shows the differences in latitude, longitude and height for each model's solution with reference to the benchmark solution. The latitude and longitude plots use the same scale, while the height difference is represented on a larger scale (approximately 5 times larger) to accommodate the greater variation seen in the height component.
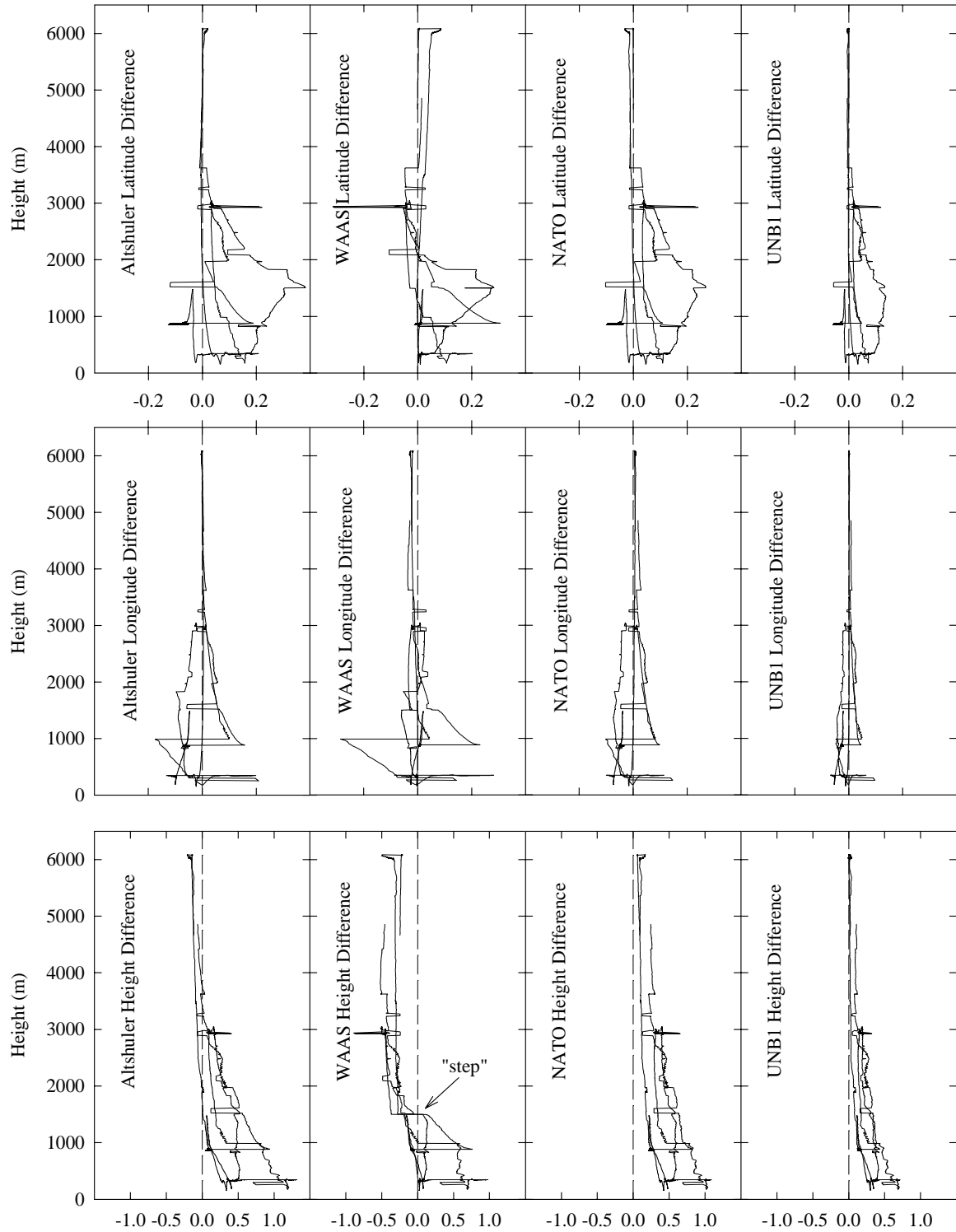
Figure 3.2. Solution differences (in metres) plotted against altitude for flight F508.

This figure shows the generally poorer performance of the Altshuler and initially proposed WAAS models with height as compared to the UNB1 and NATO models. An important point to be made is that there is a "step" visible in the WAAS solution height differences at 1500 metres; this appears in all the solutions computed with this model. In contrast, the NATO and UNB1 models perform better and more consistently at all altitudes, although a diverging trend is visible at very low altitudes (below approximately 1 km). The Altshuler model performance is generally not as good as the others. In the worst case, it is possible to have an error of 1.32 m in height by using the Altshuler model. The worst case for the initially proposed WAAS and NATO models is approximately one metre. Similar plots for all the flight data are presented in Appendix B1. Compared with solutions computed with the initially proposed WAAS model, those computed with UNB1 generally show a two-fold improvement in variance at altitudes below 1000 metres.

All of the solutions suffer to some extent from large steps and jumps. By considering Figure 3.3, where the solution differences are plotted against time, we can see that these are correlated with changes in the PDOP value. This indicates the influence of rising and setting satellites on the modelling of the tropospheric delay. These plots show that at low elevation angles, the position errors increase until the satellite sets below the elevation mask angle (e.g. at approximately 118 minutes) whereupon the solution improves. When a new satellite rises (e.g. at approximately 12 minutes) an error is introduced into the solution and it jumps away from the benchmark solution. As the satellite continues to rise the error decreases and the solution improves. The jumps between 100 and 120 minutes are complicated by the fact that satellites are both rising and setting at the same time and

34

the solutions also suffer from data gaps. It should be noted that the largest latitude difference in the WAAS solution is due to a PDOP spike, however there are differences of a similar magnitude that are not. Despite the problems of these jumps they are present in all the solutions and yet are much less severe in the UNB1 solutions. Therefore, given the good performance of the Niell functions, these large trends are almost certainly related to mapping function errors in the other tested models. Similar plots to Figure 3.3 for each flight can be found in Appendix B2.
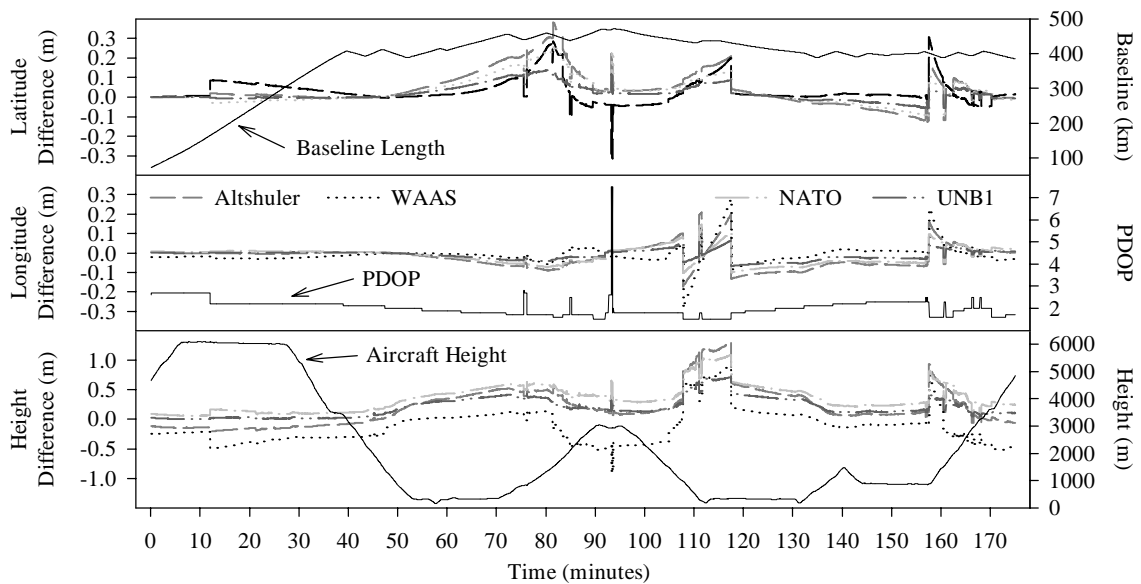
Figure 3.3. Solution differences plotted against time for flight F508.

3.2.6 Preliminary Conclusions

From this initial investigation, it was apparent that the initially proposed WAAS model performed somewhat poorly. Solutions computed using the proposed WAAS model with the aircraft data have a step at a height of 1500 metres. This is due to a discontinuity in the formulation of the algorithm. Otherwise above 1500 metres it models the rate of

change of the delay in the atmosphere reasonably well. Close examination of the NATO algorithm reveals discontinuities between the layers of that model also. However, they do not appear to show up in the solution differences.

An important error source in the tested models is in the mapping functions. These are significant in Altshuler and the proposed WAAS models; the NATO model performs slightly better because of its use of the Chao mapping function. Because the same mapping functions are used in both the UNB1 and the benchmark solutions, the errors seen in these differences are the errors in the zenith delays mapped to the lower elevation angles.

The UNB1 model performs best overall. It consistently shows the smallest bias and variation in the solutions computed using it. The improvement over solutions computed with the WAAS model is approximately two-fold. The comparatively elegant formulation of the algorithms is seen to be an advantage. For example, the delay algorithms are continuous with height and do not model the atmosphere in distinct layers as the NATO or initially proposed WAAS models do. The complex polynomials comprising the Altshuler model do not appear to model the change of the atmosphere with height with sufficient accuracy.

From these preliminary tests we can begin to appreciate the fact that the high variation in the atmospheric profile is likely to be the limiting factor in reducing the tropospheric delay errors for airborne navigation using GPS. However, the use of standard geodetic-type zenith delay models and mapping functions, coupled with suitable sea-level

meteorological values performs better than the navigation-type tropospheric delay models. At least some of the improvement is due to the better modelling of the change of the atmosphere with height.

3.3 Evolution of the UNB2, UNB3 and UNB4 Models

This section will deal with the introduction of further UNB models designed to improve upon the performance of UNB1. Aircraft navigation systems typically require the greatest accuracy at low altitudes and this has influenced the evolution of the UNB-proposed tropospheric delay model.

3.3.1 Rationale For UNB2

Because of its use of algorithms based on the physics of the atmosphere, any significant improvement over the performance of UNB1 (without estimating the delays through the use of the GPS data itself) can only come through improving the meteorological values used to drive the algorithms. These "improved" values would have to better represent the atmosphere, if only in an average sense, for a greater variety of times and places. From research through some general atmospheric texts (e.g. *Peixoto and Oort* [1992]), it is obvious that in a "first-order" sense there exists a latitudinal (or zonal) variation of the atmosphere as a whole. Hence it was apparent that an attempt should be made to provide average annual latitudinal values of the five meteorological parameters in the model.

As was mentioned earlier, due to the stochastic nature of water vapour, the lambda parameter is only ever representative of the average decrease in water vapour in a column of air. Even if derived from real-time measurements it is only accurate for those space and time scales over which it was derived (see e.g., *Schwarz* [1968] and *Smith* [1968]). However, the water vapour profile does exhibit a latitudinal trend over the atmosphere as a whole and zenith delay models with constant values for lambda have been shown to perform poorly at high latitudes (see e.g., *Ifadis* [1986]).

A literature search provided: sea-level pressure values from *Trenberth* [1981]; average zonal temperature and lapse rates derived from a model of the global temperature structure in *Fleming et al.* [1988]; and average zonal water vapour and its lapse rate derived from *Peixoto and Oort* [1983]. The parameter values of this model are listed in Table 3.4. The UNB1 algorithm was modified with these parameters and designated as UNB2.

With the introduction of this model, the opportunity was taken to update the zenith delay algorithms to those of *Davis et al.* [1985] and *Askne and Nordius* [1987]. These are essentially refinements of Saastamoinen's algorithms, using more up-to-date values of the refractivity constants k_1, k_2 and k_3 (see equation (2.13) and equation (2.19)) from *Thayer* [1974]. The difference in the zenith delays caused by these changes is at the millimetre level for the wet delay and less for the hydrostatic delay.

Table 3.4. Meteorological parameters for the UNB2 model.

Lat. (deg)	P_0 (mbar)	T_0 (kelvin)	e_0 (mbar)	β (K/km)	λ (n/a)
80	1015.0	259.8	2.6	3.88	2.24
70	1013.1	266.1	4.0	4.49	2.55
60	1012.4	274.9	6.4	5.31	2.96
50	1014.5	281.8	9.2	5.86	3.18
40	1016.6	288.7	13.8	6.20	3.52
30	1016.1	294.8	19.6	6.23	3.42
20	1013.2	298.7	25.1	6.18	3.29
10	1010.7	300.5	28.6	6.18	3.33
0	1010.3	300.5	28.3	6.16	3.21
−10	1011.6	300.0	26.7	6.14	3.23
−20	1014.8	297.6	22.3	6.10	3.41
−30	1017.7	293.5	17.4	6.20	3.30
−40	1014.8	287.6	12.4	6.19	3.46
−50	1003.2	280.4	8.2	5.91	3.22
−60	988.5	274.9	5.3	5.71	3.00
−70	987.5	271.0	3.5	5.57	3.45

3.3.2 Rationale For UNB3

As we will see shortly, UNB2 represents an improvement over UNB1, however its make up is rather *ad hoc* and its coverage only extends from 80°N to 70°S because of the incomplete coverage of some of the data from which it was derived. At the same time it was thought that an improvement might be gained by introducing a temporal variation. It was therefore decided to apply the concepts used by the Niell mapping functions to a zenith delay model. These functions represent the annual variation of the atmosphere as a sinusoidal function of the day-of-year. Given the proven performance of the Niell

mapping functions, it was thought that a troposphere model derived from the same data would be useful.

Table 3.5. Meteorological parameters for the UNB3 model.

Lat. (deg)	Average				
	P_0 (mbar)	T_0 (kelvin)	e_0 (mbar)	β (K/km)	λ (n/a)
15	1013.25	299.65	26.31	6.30	2.77
30	1017.25	294.15	21.79	6.05	3.15
45	1015.75	283.15	11.66	5.58	2.57
60	1011.75	272.15	6.78	5.39	1.81
75	1013.00	263.65	4.11	4.53	1.55
Lat. (deg)	Amplitude				
	P_0 (mbar)	T_0 (kelvin)	e_0 (mbar)	β (K/km)	λ (n/a)
15	0.00	0.00	0.00	0.00	0.00
30	−3.75	7.00	8.85	0.25	0.33
45	−2.25	11.00	7.24	0.32	0.46
60	−1.75	15.00	5.36	0.81	0.74
75	−0.50	14.50	3.39	0.62	0.30

To this end, the temperature and humidity profiles contained in the 1966 U.S. Standard Atmosphere Supplements were used to derive values for the five meteorological parameters. For each latitude in the Standard, the average values of the five parameters and their amplitudes were calculated from the January and June profiles. To compute the value of the required parameter, linear interpolation of the average and amplitude values is required between latitudes in the range $15° < |\phi| < 75°$. At the spatial limits of the model, that is for latitudes $|\phi| \leq 15°$ and $|\phi| \geq 75°$, the values given for 15° and 75° are used. The amplitudes are used to interpolate temporally over a year using a sine function

of the day-of-year in the same way as the hydrostatic and wet mapping functions. To maintain the consistency with the Niell functions, day-of-year 28 is also used for the phase offset of the temporal variation. This model is described in Table 3.5 and is designated UNB3.

3.3.3 Rationale For UNB4

Following the construction of these two models, they were tested in the same way as the navigation models (see Section 3.4). Both showed a potential improvement at low altitudes where it is most needed. However, it was felt that to maintain a consistent performance throughout the total altitude range of our flight profiles, UNB3 could be improved upon. Because it represents a more logical flow of topics, we will discuss these modifications before discussing the testing of all the UNB models.

By considering equations (2.25) and (2.26) we can see that the reliability of the models is dependent on the behaviour of the temperature profile. To improve a model's overall performance — that is to keep a certain consistency at all heights — the temperature profile must be considered in a different manner than previously. The existence of any temperature inversion in the atmospheric boundary layer will degrade the accuracy of the hydrostatic scaling factor κ_{hyd}.

Because its impact on the wet delay is comparatively small, a "surface" temperature can be extrapolated down from the tropopause where the seasonal variation of temperature is less than at the surface. In addition to this, it is largely accepted that above

the boundary layer the lapse rate has a minimal variation across all latitudes [*Smith,* 1963], therefore at the same time we can choose to use a constant lapse rate of 6.5 K/km. These changes have been applied to UNB3 to arrive at UNB4 (see Table 3.6).

Table 3.6. Meteorological parameters for the UNB4 model.

Lat. (deg)	Average				
	P_0 (mbar)	T_0 (kelvin)	e_0 (mbar)	β (K/km)	λ (n/a)
15	1013.25	301.70	26.31	6.50	2.77
30	1017.25	298.65	21.79	6.50	3.15
45	1015.75	292.40	11.66	6.50	2.57
60	1011.75	281.35	6.78	6.50	1.81
75	1013.00	278.90	4.11	6.50	1.55
Lat. (deg)	Amplitude				
	P_0 (mbar)	T_0 (kelvin)	e_0 (mbar)	β (K/km)	λ (n/a)
15	0.00	0.00	0.00	0.00	0.00
30	−3.75	4.50	8.85	0.00	0.33
45	−2.25	7.75	7.24	0.00	0.46
60	−1.75	8.80	5.36	0.00	0.74
75	−0.50	9.00	3.39	0.00	0.30

In this way the greatest difference between UNB3 and UNB4 in surface temperature is for the January 75° atmosphere. The difference is approximately 20 K, however the water vapour pressure is so low that the lambda parameter has the greatest impact on the wet delay error. The actual differences for the wet zenith delay between the two models is approximately one millimetre, but an inherent uncertainty of $\lambda' = 2.25 \pm 1$ would contribute a potential bias of approximately 6 mm in the zenith delay for these conditions.

For the sake of computational efficiency and simplicity it is possible to simplify the wet zenith delay expression (equation 2.19) a little. Following *Davis et al.* [1985], the refractivity constants k_2' and k_3 can be combined by specifying a global value for the mean temperature (T_m). Choosing 260 ± 20 K we can derive $k_3' = T_m k_2' + k_3 = (3.82 \pm 0.04) \times 10^5$ K^2/mbar. This approximation accounts for a difference of less than 1 mm of zenith wet delay under most conditions.

3.4 Results Of Testing UNB Models With GPS Flight Data

These three further UNB models were subjected to the same tests with the GPS flight data as before. Table 3.7 represents a statistical evaluation of the performance of the models. The range, mean and standard deviation of the position differences from the benchmark solution (see Section 3.2.3) for all of the particular models solutions are provided. From Table 3.7, it would appear that UNB3 performs poorly compared to UNB2 and UNB4 which have smaller mean biases in the height component.

Table 3.7. Position difference statistics for UNB models (1).
Units are metres. (All data, ~46 hours over 12 flights.)

	UNB1			UNB2			UNB3			UNB4		
	Range	Mean	S.D.	Range	Mean	S.D.	Range	Mean	S.D.	Range	Mean	S.D.
Latitude	0.26	0.00	0.02	0.22	0.00	0.02	0.28	0.00	0.02	0.19	0.00	0.02
Longitude	0.17	0.00	0.02	0.12	0.00	0.01	0.16	0.00	0.01	0.12	0.00	0.01
Height	1.12	0.08	0.13	1.02	0.01	0.12	1.01	-0.06	0.13	0.91	0.02	0.11

Unfortunately these statistics alone do not represent the true performance of each model. An inspection of model performance with height reveals why. If we consider Figure 3.4, which represents the differences from the benchmark solution in the height component for flight F511 of March 15, it can be seen that the UNB3 model has removed the bias at low altitudes only to introduce one at higher altitudes. Similar plots to Figure 3.4 with the latitude and longitude differences, as well as the height differences, can be found in Appendix B3.
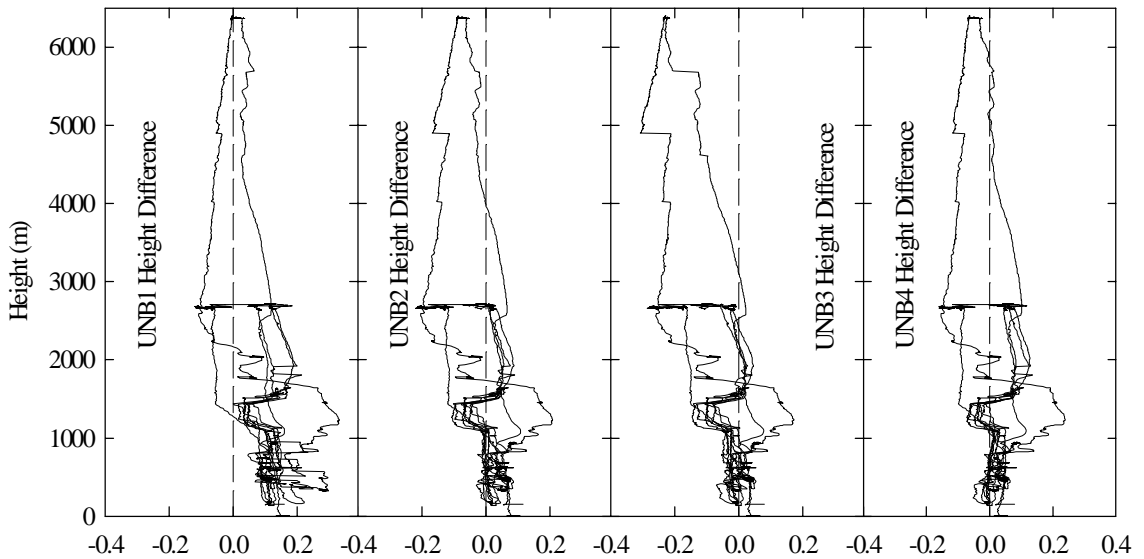

Figure 3.4. Height differences (in metres) plotted against altitude for flight F511.

By only considering the results below a height of one kilometre, we perceive a slightly different overall picture. Table 3.8 shows the improved performance of UNB3 at low altitudes. The standard deviation of the solution differences is the same and the bias is lower compared to UNB4. As can clearly be seen from Figure 3.5, UNB3 represents more closely the temperature profile at low altitudes. However, because of temperature inversions, it is less accurate above the boundary layer. Figure 3.6 indicates the reason for

44

the improved performance of UNB3 and UNB4 at low altitudes — their more accurate

representation of the water vapour profile as recorded at the aircraft. Similar plots of the

temperature, pressure and water vapour pressure profiles recorded on all the flights can be

found in Appendix B4. The reference station coordinates were used as an approximation

to the aircraft coordinates on all these plots for the sake of computational simplicity.

Table 3.8. Position difference statistics for UNB models (2).
Units are metres. (Only data from less than 1000 m altitude above mean-sea-level.)

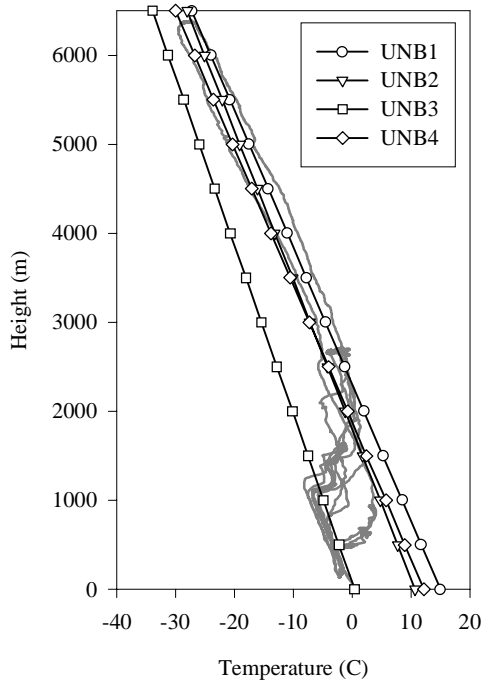|	UNB1			UNB2			UNB3			UNB4		
	Range	Mean	S.D.	Range	Mean	S.D.	Range	Mean	S.D.	Range	Mean	S.D.
Latitude	0.26	0.00	0.03	0.20	0.00	0.02	0.22	0.00	0.02	0.17	0.00	0.02
Longitude	0.17	-0.01	0.02	0.11	0.00	0.01	0.10	0.00	0.01	0.09	0.00	0.01
Height	0.85	0.19	0.12	0.74	0.10	0.11	0.73	0.05	0.10	0.67	0.07	0.10

Figure 3.5. Temperature profile recorded at the aircraft for flight F511. Profiles for the UNB models at the reference station are superimposed.
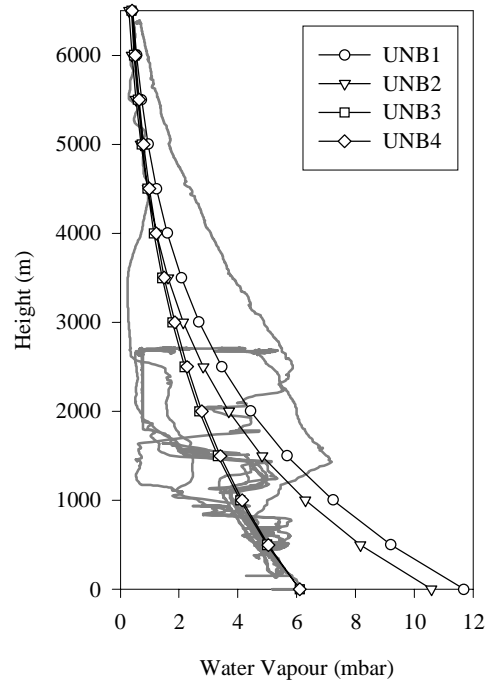
Figure 3.6. Water vapour profile recorded at the aircraft for flight F511. Profiles for the UNB models at the reference station are superimposed.

45

Considering the statistics pertaining to UNB4, they indicate that, taken over the whole flight path, the UNB4 model provides the best solution of the four models tested here. The values for the model's performance below one kilometre are approximately equal to UNB3. The 2 cm difference in the mean of the height component is probably due to the difference in temperature profile between the two models and the refractivity approximation in UNB4. This difference is almost certainly within the inherent uncertainty of the wet delay.

The statistics of Tables 3.8 and 3.7, coupled with an examination of Figure 3.4, Figure 3.5 and Figure 3.6, confirm our consideration of the impact of the temperature profile in Section 3.3.3. That is, a significant variation in the actual temperature profile away from a constant linear lapse rate indirectly introduces a bias into the tropospheric delay determination through the hydrostatic delay. This generally occurs above the first few kilometres where the bias in the wet delay is dominant.

3.5 Conclusions Of GPS Flight Data Tests

Considering the small spatial and temporal extent represented by our GPS data set, the 1966 Standard Atmosphere Supplements appear to represent the real atmosphere in the vicinity of Newfoundland in March 1995 more closely than global average or latitudinal average parameters. From this data alone however, it is not possible to draw any conclusions regarding the global or hemispheric performance of these models. For example, it is often assumed that the southern hemisphere is a mirror of the northern

hemisphere. However, UNB2 shows (Table 3.4) that there are significant differences in the average sea-level pressure in the southern hemisphere from northern hemisphere values at the same latitude. Hence the provision of an annual variation to the temperature and water vapour profiles of that model may provide an improvement over UNB3.

While we are able in many cases to remove much of the bias seen at low altitudes, large variations can still be seen within the solution differences. This is primarily due to the large variation of water vapour pressure and it is likely that this will provide the ultimate limiting factor in aircraft positioning. As we have seen with UNB3 and UNB4 however, it is possible to significantly improve the determination of the tropospheric delay near the surface for airborne navigation.

These results show that errors in the hydrostatic delay have the potential to increase in height when scaling a sea-level pressure value. The primary error source would be the existence of a temperature inversion in the atmosphere. However, the resulting error in the zenith delay is only significant if the inversion is close to the surface and the tropospheric delay model is being used a long way above it. Therefore care must be taken in the application of these models if an accurate tropospheric delay is required above the atmospheric boundary layer (which will likely not be required in WAAS, for example).

For the range of meteorological conditions experienced during the St. John's flights, it has been shown that the tropospheric delay models UNB3 and UNB4 improve the mean vertical position accuracy by one order of magnitude while reducing the variance by half, compared to the initially proposed WAAS model.

CHAPTER FOUR
TESTING WITH RAY-TRACED RADIOSONDE DATA

This chapter details the comparisons of the tropospheric delay models with ray-traced radiosonde data. The rationale for these tests is presented along with a brief overview of how this truth source is provided before proceeding with the results.

4.1 Rationale For Radiosonde Tests

Because of the inherent variation of the atmosphere we are limited in the scope of the conclusions we can make from the GPS results presented so far. To be able to validate the improvement that we see from the UNB models we need to understand their performance under a wider variety of climatic conditions than that experienced near St. John's. To do this we can turn to another truth source that describes the atmospheric effect on the GPS signals. This is ray-traced balloon launched radiosonde data. Launches of these instruments take place at hundreds of sites around the globe at least twice a day (usually at 0000 and 1200 UTC).

These new tests make use of data recorded throughout 1992 at thirteen stations in the Northern Hemisphere. Most of the sites are located in Canada or the United States (see Table 4.1 for a list of the sites and Figure 4.1 for a map of their locations). Taken together, they represent several varied climates from the tropics through the mid latitudes (including high altitude stations) to the arctic region.

Table 4.1. Radiosonde stations.

| Station	Latitude (°N)	Longitude (°W)	Orthometric Height (m)	Geoid Height (m)	Number of Profiles
Alert	82.50	62.33	66	17	720
Kotzebue	66.87	162.63	5	5	687
Iqaluit	63.75	68.55	21	−12	711
Whitehorse	60.72	135.07	704	7	719
Landvetter	57.67	347.70	155	40	713
The Pas	53.97	101.10	273	−28	723
St. John's	47.67	52.75	140	14	713
Denver	39.77	104.88	1611	−17	753
Grand Jnc.	39.12	108.53	1472	−17	758
Oakland	37.75	122.22	6	−25	740
Nashville	36.25	86.57	180	−49	745
San Juan	18.43	66.00	3	−17	675
Guam	13.55	215.17	111	50	736
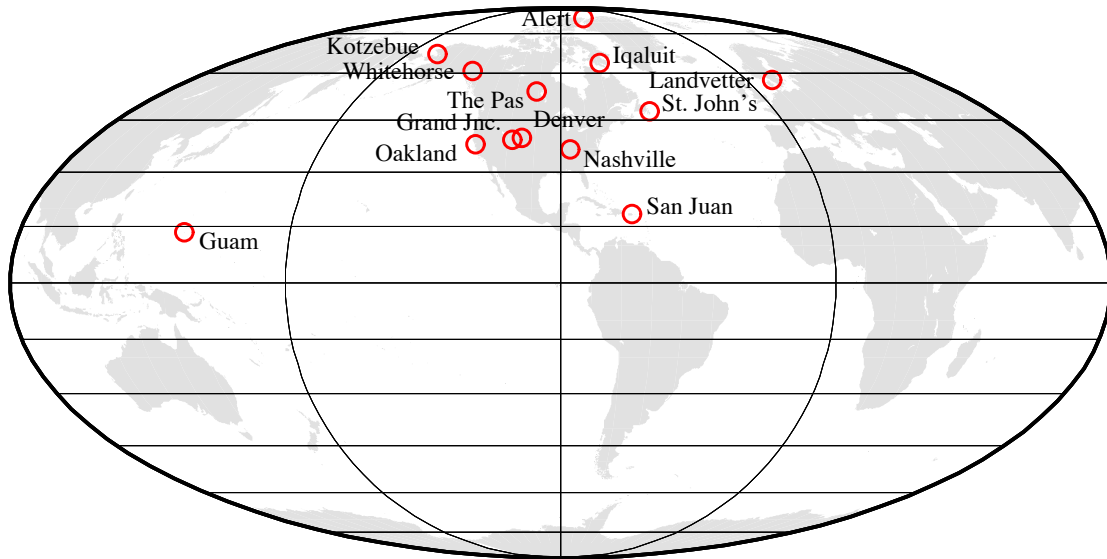
Figure 4.1. Location of radiosonde launch stations.

4.2 Principles Of Ray-Tracing

Given a profile of atmospheric refractivity (e.g. derived from a radiosonde or a standard atmosphere), it is possible to solve the equations for signal delay and path bending described in Chapter Two. The assumption of spherical symmetry allows the application of Snell's Law for spherical stratification and the numerical integration of the refraction profile. Simple formulae to do this are given by *Weisbrod and Anderson* [1959] and *Thayer* [1967]. Derivations of similar formulae and direct application to formulating mapping functions are given by *Davis* [1986] and *Ifadis* [1986].

4.3 Limitations Of Ray-Tracing

The first limitation we must consider is in the recording of the meteorological data. Unfortunately, the instrument errors in recording pressure, temperature and relative humidity vary widely among different radiosonde devices. Typical values are quoted in Table 4.2. In addition, the same refractivity constants that are used in the derivation of the tropospheric delay models are also used to construct the refractivity profile. However, with ray-tracing it is possible to use the compressibility factors to slightly improve the final accuracy.

We must also consider how well the radiosonde profile represents the actual atmosphere. For example, it is assumed that the profile recorded by the balloon is strictly vertical. In actual fact, the balloon can drift horizontally for many tens of kilometres before bursting. Hence, true zenith parameters are not recorded, however we must

assume that the radiosonde data still adequately represents the atmospheric column above the launch point.   In addition, the balloon almost always bursts at an altitude of approximately 30 km, well below the "top" of the neutral atmosphere.   However, due to the exponential decrease of pressure, the bulk of the atmosphere has been sampled by this point and a standard profile is suitable for the remainder of the ray-tracing.

**Table 4.2. Typical radiosonde
accuracies quoted by *Bisagni* [1989].**

Measurement	Accuracy
Barometric pressure	±2 mbar
Temperature	±0.4 K
Relative Humidity	±4 %

We must also assume that the vertical profile above the launch point is representative of the whole atmosphere around this point. For example, when tracing a ray at 5 degrees elevation angle, the point on the surface directly below the pierce point at the top of the neutral atmosphere will be over 400 km away from the launch point. Unless there is data from balloon launches clustered closely together or some other data source, there is no way to account for horizontal gradients in the atmosphere. Hence, we continue to assume that the atmosphere is azimuthally homogeneous and symmetrical around the launch point. All of these limitations apply equally to mapping functions, and no currently specified functions model azimuthal variations, although some attempts have been made (see e.g., *Gardner* [1977]; *Davis et al.* [1993]; *Coster et al.* [1997]; *Chen and Herring* [1997]).

Despite these qualifications, the radiosonde data represents the best available way of testing tropospheric delay models and surface parameter models. Unfortunately there is scant reference in the literature to the accuracy of ray-traced radiosonde data. *Niell et al.* [1996] suggest up to 4 cm for a particular campaign they carried out, although the generally accepted view [*Mendes*, 1996] is that the zenith delay derived from radiosonde measurements is accurate to one-or-two centimetres. Because of the inherent variation of the atmosphere and its limited sampling by the radiosonde data, plus problems of ray-tracing at low elevation angles, this error almost certainly increases toward the horizon.

There is one case where this data is limited in a way that is beneficial for our tests. All our models are specified with sea-level meteorological values plus lapse rates to scale them to the correct height. These scaling relationships are derived for the atmosphere, however much of the time they will be scaling "through the earth" to the above-surface altitude of the aircraft. Fortunately our ray-trace profiles start at surface heights ranging from a few metres to approximately 1.6 km above sea level. Therefore we should be able to examine whether our scaling relationships are valid for the atmosphere when the earth's surface is high above sea-level.

4.4 Test Methodology

The delays derived from the ray-trace data were compared to the delays predicted by the tropospheric delay models driven by their time and location parameters. The most important of the location parameters is the altitude input. For our purposes we have a

choice of two: the orthometric height above the geoid (essentially the height above mean-sea-level) or ellipsoid height.

The specifications for the WAAS system indicate the use of the ellipsoid height as an input parameter. For most cases this should not pose a problem because the WGS84 ellipsoid (GRS80) is a very close fit to the global geoid. However the worst case difference is approximately 100 m and from Table 4.1 we can see that three of our stations have geoid heights of approximately 50 m. Hence we should be able to see the potential impact of using ellipsoid height instead of the "true" orthometric height.

The orthometric height is specified in the ray-trace files and so is immediately available. Fortunately there is a simple algorithm available to interpolate the height of the geoid above the ellipsoid given latitude and longitude (see e.g., *NATO* [1993]). This enables us to derive an approximate ellipsoid height. The interpolation algorithm is the same one as specified in the WAAS specification document for interpolating the Ionospheric Grid Point Delays [*FAA*, 1996].

The ray-trace computations have been undertaken by V. de B. Mendes. From each radiosonde profile the tropospheric delay at the zenith, and at elevation angles of thirty, twenty, fifteen, ten and five degrees have been computed. These delay values have been compared against those predicted by the delay models. The differences were taken and various statistics were computed. The results are presented in the next section.

4.5 Results

A graphical presentation of the residuals from the comparison with the ray-trace data is presented in Figure 4.2. Each tropospheric delay model is represented by six frequency polygons representing the residuals for the six tested elevation angles. Although superimposed on the same axes, the drastically different distributions for each angle allow for easy identification. The narrowest, highly peaked polygon pertains to the zenith delay, while the flattest polygon is that for the five degree elevation angle. Similar plots for all the stations can be found in Appendix B5.

Figure 4.2 shows the general trends characteristic for all the stations, and indicates the large bias in the initially proposed WAAS model at five degrees elevation angle. In general, the plots for the UNB models and UNB3/4 in particular are more symmetric and centred closer to zero, although there are exceptions (e.g. Oakland). For a more comprehensive round-up we can consider the following tables: Table 4.3, Table 4.4 and Table 4.5, which give respectively the mean, standard deviation and range of the residuals for each station and for all the stations. The results presented in these tables were obtained using the ellipsoid height. Table 4.6, Table 4.7 and Table 4.8 show the same statistics computed using the orthometric height.
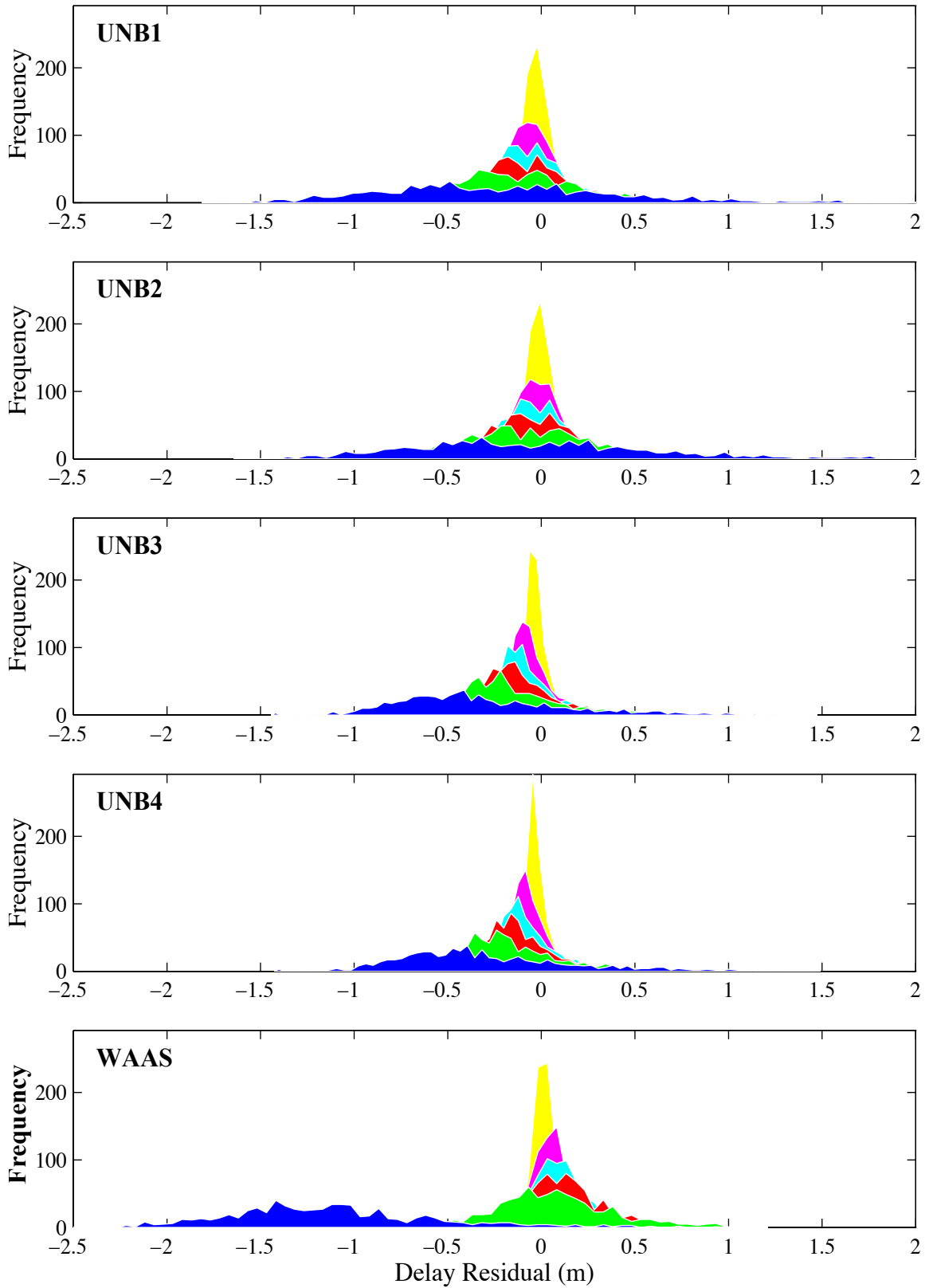
Figure 4.2. Frequency distributions of model prediction residuals for St. John's.

Table 4.3. Mean model error (delay in metres) per station and elevation angle. (Ellipsoid height.)

MEAN	E°	UNB1	UNB2	UNB3	UNB4	WAAS
Alert	90	-0.08	0.00	-0.03	-0.03	0.04
	10	-0.44	0.00	-0.15	-0.15	0.24
	5	-0.82	0.02	-0.27	-0.27	-0.76
Kotzebue	90	-0.06	0.00	-0.03	-0.03	0.02
	10	-0.36	0.01	-0.15	-0.14	0.12
	5	-0.67	0.02	-0.28	-0.26	-1.03
Iqaluit	90	-0.08	-0.03	-0.05	-0.05	0.00
	10	-0.47	-0.13	-0.28	-0.27	-0.03
	5	-0.86	-0.23	-0.51	-0.49	-1.30
Whitehorse	90	-0.03	0.01	-0.01	-0.01	0.03
	10	-0.19	0.08	-0.05	-0.08	0.15
	5	-0.37	0.15	-0.10	-0.15	-0.86
Landvetter	90	-0.02	0.03	0.00	0.00	0.05
	10	-0.09	0.16	0.01	0.01	0.24
	5	-0.19	0.28	0.00	0.00	-0.82
The Pas	90	-0.04	-0.01	-0.03	-0.03	0.01
	10	-0.22	-0.03	-0.18	-0.18	0.05
	5	-0.42	-0.05	-0.34	-0.34	-1.14
St. John's	90	-0.02	0.00	-0.03	-0.02	0.02
	10	-0.09	0.00	-0.14	-0.14	0.11
	5	-0.16	0.01	-0.26	-0.25	-1.07
Denver	90	0.02	0.01	-0.01	-0.02	0.10
	10	0.10	0.08	-0.04	-0.09	0.53
	5	0.19	0.15	-0.07	-0.16	-0.03
Grand Jnc.	90	0.02	0.01	-0.01	-0.02	0.06
	10	0.11	0.07	-0.05	-0.09	0.30
	5	0.21	0.14	-0.09	-0.17	-0.50
Oakland	90	-0.01	-0.03	-0.06	-0.06	0.01
	10	-0.04	-0.17	-0.36	-0.34	0.05
	5	-0.07	-0.32	-0.68	-0.64	-1.25
Nashville	90	0.03	0.01	-0.03	-0.03	0.05
	10	0.20	0.03	-0.17	-0.16	0.24
	5	0.38	0.07	-0.32	-0.30	-0.86
San Juan	90	0.13	0.02	-0.01	-0.01	0.11
	10	0.76	0.11	-0.05	-0.03	0.58
	5	1.45	0.21	-0.09	-0.06	-0.27
Guam	90	0.18	0.06	0.03	0.03	0.13
	10	0.99	0.33	0.15	0.16	0.73
	5	1.86	0.60	0.27	0.28	0.02
All	90	0.00	0.01	-0.02	-0.02	0.05
	10	0.02	0.04	-0.11	-0.12	0.26
	5	0.04	0.08	-0.21	-0.22	-0.76

Table 4.4. Standard deviation of model error (delay in metres) per station and elevation angle. (Ellipsoid height.)

S.D.	E°	UNB1	UNB2	UNB3	UNB4	WAAS
	90	0.03	0.03	0.03	0.03	0.02
Alert	10	0.17	0.17	0.15	0.14	0.13
	5	0.32	0.32	0.27	0.26	0.23
	90	0.05	0.05	0.04	0.03	0.04
Kotzebue	10	0.26	0.26	0.19	0.19	0.20
	5	0.48	0.48	0.35	0.35	0.36
	90	0.04	0.04	0.03	0.03	0.03
Iqaluit	10	0.24	0.24	0.16	0.16	0.18
	5	0.44	0.44	0.29	0.28	0.31
	90	0.04	0.04	0.03	0.03	0.03
Whitehorse	10	0.22	0.22	0.15	0.15	0.15
	5	0.41	0.41	0.28	0.28	0.27
	90	0.05	0.05	0.04	0.04	0.04
Landvetter	10	0.25	0.25	0.24	0.24	0.22
	5	0.47	0.47	0.44	0.43	0.40
	90	0.04	0.04	0.03	0.03	0.03
The Pas	10	0.21	0.21	0.15	0.15	0.16
	5	0.40	0.40	0.28	0.28	0.29
	90	0.06	0.06	0.05	0.05	0.06
St. John's	10	0.35	0.35	0.25	0.25	0.31
	5	0.65	0.65	0.47	0.47	0.55
	90	0.04	0.04	0.03	0.03	0.04
Denver	10	0.25	0.25	0.16	0.17	0.19
	5	0.46	0.46	0.30	0.31	0.35
	90	0.04	0.04	0.03	0.03	0.03
Grand Jnc.	10	0.20	0.20	0.15	0.15	0.16
	5	0.37	0.37	0.27	0.28	0.29
	90	0.03	0.03	0.04	0.04	0.03
Oakland	10	0.19	0.19	0.24	0.24	0.18
	5	0.36	0.36	0.45	0.45	0.34
	90	0.08	0.08	0.06	0.06	0.07
Nashville	10	0.44	0.44	0.32	0.32	0.40
	5	0.83	0.83	0.59	0.59	0.74
	90	0.04	0.04	0.04	0.04	0.04
San Juan	10	0.24	0.24	0.22	0.22	0.23
	5	0.46	0.46	0.42	0.42	0.44
	90	0.06	0.06	0.06	0.06	0.05
Guam	10	0.32	0.32	0.32	0.32	0.31
	5	0.60	0.60	0.60	0.60	0.58
	90	0.09	0.05	0.04	0.04	0.06
All	10	0.49	0.29	0.25	0.25	0.32
	5	0.93	0.55	0.46	0.46	0.60

Table 4.5. Range of model error (delay in metres) per station and elevation angle. (Ellipsoid height.)

RANGE	E°	UNB1	UNB2	UNB3	UNB4	WAAS
	90	0.21	0.21	0.15	0.15	0.16
Alert	10	1.17	1.17	0.82	0.83	0.87
	5	2.19	2.19	1.50	1.50	1.50
	90	0.22	0.23	0.18	0.18	0.19
Kotzebue	10	1.24	1.24	0.99	0.99	1.09
	5	2.31	2.31	1.80	1.79	1.95
	90	0.26	0.25	0.18	0.18	0.22
Iqaluit	10	1.43	1.42	1.00	1.00	1.20
	5	2.64	2.65	1.82	1.82	2.12
	90	0.20	0.20	0.17	0.17	0.18
Whitehorse	10	1.16	1.16	0.94	0.97	0.97
	5	2.16	2.16	1.76	1.80	1.75
	90	0.27	0.27	0.23	0.23	0.24
Landvetter	10	1.52	1.52	1.26	1.26	1.32
	5	2.81	2.81	2.27	2.26	2.37
	90	0.19	0.19	0.17	0.17	0.17
The Pas	10	1.06	1.07	0.94	0.94	0.94
	5	2.00	2.00	1.76	1.76	1.73
	90	0.37	0.38	0.28	0.29	0.34
St. John's	10	2.09	2.09	1.57	1.57	1.91
	5	3.89	3.90	2.91	2.92	3.50
	90	0.21	0.21	0.18	0.19	0.20
Denver	10	1.19	1.19	1.03	1.04	1.12
	5	2.23	2.24	1.95	1.95	2.08
	90	0.19	0.19	0.18	0.17	0.18
Grand Jnc.	10	1.07	1.06	0.97	0.97	1.00
	5	1.99	1.99	1.80	1.81	1.84
	90	0.24	0.24	0.23	0.23	0.22
Oakland	10	1.32	1.32	1.29	1.29	1.22
	5	2.48	2.48	2.44	2.44	2.24
	90	0.33	0.33	0.26	0.25	0.31
Nashville	10	1.88	1.88	1.46	1.46	1.74
	5	3.53	3.53	2.72	2.72	3.22
	90	0.21	0.21	0.20	0.20	0.21
Juan	10	1.20	1.19	1.12	1.12	1.14
	5	2.24	2.25	2.10	2.10	2.15
	90	0.22	0.22	0.22	0.22	0.22
Guam	10	1.28	1.28	1.28	1.28	1.23
	5	2.41	2.40	2.41	2.41	2.31
	90	0.50	0.38	0.29	0.30	0.37
All	10	2.81	2.09	1.66	1.65	2.04
	5	5.24	3.90	3.14	3.13	3.84

Table 4.6. Mean model error (delay in metres) per station and elevation angle. (Orthometric height.)

MEAN	E°	UNB1	UNB2	UNB3	UNB4	WAAS
Alert	90	-0.08	-0.01	-0.03	-0.03	0.04
	10	-0.47	-0.03	-0.18	-0.18	0.21
	5	-0.88	-0.03	-0.33	-0.32	-0.81
Kotzebue	90	-0.07	0.00	-0.03	-0.03	0.02
	10	-0.37	0.00	-0.16	-0.15	0.11
	5	-0.69	0.00	-0.29	-0.27	-1.05
Iqaluit	90	-0.08	-0.02	-0.05	-0.05	0.00
	10	-0.44	-0.11	-0.26	-0.25	-0.01
	5	-0.82	-0.19	-0.47	-0.46	-1.26
Whitehorse	90	-0.04	0.01	-0.01	-0.02	0.03
	10	-0.21	0.07	-0.06	-0.09	0.14
	5	-0.39	0.13	-0.12	-0.17	-0.88
Landvetter	90	-0.03	0.02	-0.01	-0.01	0.03
	10	-0.16	0.09	-0.06	-0.06	0.17
	5	-0.32	0.16	-0.13	-0.13	-0.95
The Pas	90	-0.03	0.00	-0.02	-0.02	0.02
	10	-0.17	0.02	-0.13	-0.14	0.10
	5	-0.33	0.04	-0.25	-0.26	-1.06
St. John's	90	-0.02	-0.01	-0.03	-0.03	0.02
	10	-0.11	-0.03	-0.17	-0.16	0.09
	5	-0.21	-0.04	-0.31	-0.30	-1.12
Denver	90	0.02	0.02	0.00	-0.01	0.10
	10	0.13	0.10	-0.01	-0.06	0.56
	5	0.24	0.19	-0.02	-0.12	0.02
Grand Jnc.	90	0.02	0.02	0.00	-0.01	0.06
	10	0.13	0.10	-0.02	-0.07	0.33
	5	0.25	0.18	-0.04	-0.13	-0.45
Oakland	90	0.00	-0.02	-0.05	-0.05	0.02
	10	0.01	-0.12	-0.31	-0.29	0.09
	5	0.01	-0.24	-0.59	-0.56	-1.17
Nashville	90	0.05	0.02	-0.01	-0.01	0.06
	10	0.28	0.12	-0.08	-0.07	0.32
	5	0.54	0.23	-0.15	-0.13	-0.70
Juan	90	0.15	0.04	0.01	0.01	0.12
	10	0.84	0.20	0.05	0.06	0.66
	5	1.60	0.37	0.08	0.10	-0.13
Guam	90	0.16	0.04	0.01	0.01	0.12
	10	0.90	0.23	0.05	0.05	0.64
	5	1.70	0.42	0.08	0.09	-0.15
All	90	0.00	0.01	-0.02	-0.02	0.05
	10	0.03	0.05	-0.10	-0.11	0.26
	5	0.06	0.10	-0.19	-0.20	-0.74

Table 4.7. Standard deviation of model error (delay in metres) per station and elevation angle. (Orthometric height.)

S.D.	E°	UNB1	UNB2	UNB3	UNB4	WAAS
Alert	90	0.03	0.03	0.03	0.03	0.02
	10	0.17	0.17	0.15	0.14	0.13
	5	0.32	0.32	0.27	0.26	0.23
Kotzebue	90	0.05	0.05	0.04	0.03	0.04
	10	0.26	0.26	0.19	0.19	0.20
	5	0.48	0.48	0.35	0.35	0.36
Iqaluit	90	0.04	0.04	0.03	0.03	0.03
	10	0.24	0.24	0.16	0.16	0.18
	5	0.44	0.44	0.29	0.28	0.31
Whitehorse	90	0.04	0.04	0.03	0.03	0.03
	10	0.22	0.22	0.15	0.15	0.15
	5	0.41	0.41	0.28	0.28	0.27
Landvetter	90	0.05	0.05	0.04	0.04	0.04
	10	0.25	0.25	0.24	0.24	0.22
	5	0.47	0.47	0.44	0.44	0.40
The Pas	90	0.04	0.04	0.03	0.03	0.03
	10	0.21	0.21	0.15	0.15	0.16
	5	0.40	0.40	0.28	0.28	0.28
St. John's	90	0.06	0.06	0.05	0.05	0.06
	10	0.35	0.35	0.25	0.25	0.31
	5	0.65	0.65	0.47	0.47	0.55
Denver	90	0.04	0.04	0.03	0.03	0.04
	10	0.25	0.25	0.16	0.17	0.19
	5	0.46	0.46	0.30	0.31	0.35
Grand Jnc.	90	0.04	0.04	0.03	0.03	0.03
	10	0.20	0.20	0.15	0.15	0.16
	5	0.37	0.37	0.27	0.28	0.29
Oakland	90	0.03	0.03	0.04	0.04	0.03
	10	0.19	0.19	0.24	0.24	0.18
	5	0.36	0.36	0.45	0.45	0.34
Nashville	90	0.08	0.08	0.06	0.06	0.07
	10	0.44	0.44	0.32	0.32	0.40
	5	0.83	0.83	0.60	0.60	0.74
Juan	90	0.04	0.04	0.04	0.04	0.04
	10	0.24	0.24	0.22	0.22	0.23
	5	0.46	0.46	0.42	0.42	0.44
Guam	90	0.06	0.06	0.06	0.06	0.05
	10	0.32	0.32	0.32	0.32	0.31
	5	0.60	0.60	0.60	0.60	0.58
All	90	0.09	0.05	0.04	0.04	0.06
	10	0.49	0.29	0.24	0.24	0.32
	5	0.93	0.53	0.45	0.44	0.59

Table 4.8. Range of model error (delay in metres) per station and elevation angle. (Orthometric height.)

RANGE	E°	UNB1	UNB2	UNB3	UNB4	WAAS
Alert	90	0.21	0.21	0.15	0.15	0.16
	10	1.17	1.17	0.82	0.82	0.87
	5	2.19	2.19	1.50	1.50	1.50
Kotzebue	90	0.22	0.23	0.19	0.18	0.19
	10	1.24	1.25	0.99	0.99	1.09
	5	2.31	2.31	1.80	1.80	1.95
Iqaluit	90	0.25	0.26	0.18	0.17	0.21
	10	1.42	1.42	0.99	0.99	1.20
	5	2.64	2.65	1.82	1.82	2.12
Whitehorse	90	0.20	0.21	0.17	0.17	0.18
	10	1.15	1.16	0.94	0.97	0.97
	5	2.16	2.16	1.75	1.80	1.75
Landvetter	90	0.27	0.27	0.23	0.23	0.24
	10	1.52	1.52	1.27	1.26	1.33
	5	2.82	2.81	2.28	2.27	2.37
The Pas	90	0.19	0.19	0.17	0.17	0.17
	10	1.07	1.06	0.94	0.94	0.93
	5	2.00	2.00	1.76	1.76	1.73
St. John's	90	0.38	0.37	0.28	0.28	0.34
	10	2.09	2.09	1.57	1.57	1.92
	5	3.89	3.89	2.91	2.91	3.49
Denver	90	0.21	0.21	0.18	0.18	0.20
	10	1.19	1.19	1.04	1.03	1.12
	5	2.23	2.23	1.95	1.96	2.08
Grand Jnc.	90	0.19	0.19	0.17	0.18	0.18
	10	1.06	1.06	0.97	0.97	1.00
	5	2.00	2.00	1.80	1.81	1.84
Oakland	90	0.24	0.23	0.23	0.23	0.22
	10	1.32	1.33	1.28	1.28	1.21
	5	2.49	2.49	2.43	2.43	2.23
Nashville	90	0.34	0.34	0.26	0.26	0.31
	10	1.87	1.88	1.45	1.45	1.74
	5	3.54	3.53	2.73	2.73	3.22
Juan	90	0.21	0.21	0.20	0.19	0.20
	10	1.20	1.19	1.12	1.12	1.15
	5	2.24	2.25	2.10	2.10	2.14
Guam	90	0.23	0.23	0.22	0.23	0.22
	10	1.28	1.28	1.28	1.28	1.23
	5	2.41	2.41	2.41	2.40	2.31
All	90	0.48	0.38	0.28	0.28	0.37
	10	2.69	2.12	1.58	1.57	2.07
	5	5.04	3.94	3.00	2.99	3.93

Considering the impact of the two heights first, it is clear that there is a slight overall improvement in UNB3 and UNB4 from using the orthometric height. The high geoid stations of Nashville and Guam show a lower mean error, while Landvetter is degraded. The range of the errors at each of these stations is generally smaller by a few centimetres, however the total range error shown by UNB4 has been reduced by over 10 cm at 5 degrees elevation angle.

Curiously, the overall performance of UNB1 and UNB2 is slightly worse when using the orthometric height. We must consider, though, the complicated application of height through the scaling factors κ_{hyd} and κ_{wet}. It may be the case that for a few sites the use of ellipsoid height compensates slightly, in an average sense, for biases in the surface meteorological values. However, should the atmosphere be accurately modelled by the five parameters of our models, then the use of an ellipsoid height would impose a bias in the tropospheric delay, therefore the use of orthometric heights is preferred.

For similar reasons, it is always possible to find a station where one UNB model is better. For an example from this data, it would appear that on average, UNB2 models the atmosphere at St. John's better than UNB3 or UNB4 (although at the same time with a larger standard deviation and range). This is the danger of using only our GPS data to draw all of our conclusions. Taking all the radiosonde stations together should better reveal the performances of the models.

Examining the statistics representing all the data, it is clear that each subsequent UNB model is an improvement over the previous one and all are an improvement over the

initially proposed WAAS model with regard to their mean error. UNB1 and UNB2 may

have larger standard deviations than WAAS, but their mean is always smaller. The WAAS

model does make some attempt to model the annual variation of the atmosphere and hence

shows a smaller scatter in the residuals.   The bias in WAAS however, is large and

inconsistent through changing elevation angles; between 10 and 5 degrees the sign of the

bias has changed. These trends are clearly revealed in Figure 4.3, which presents the mean

and standard deviation of the combined residuals for all stations.
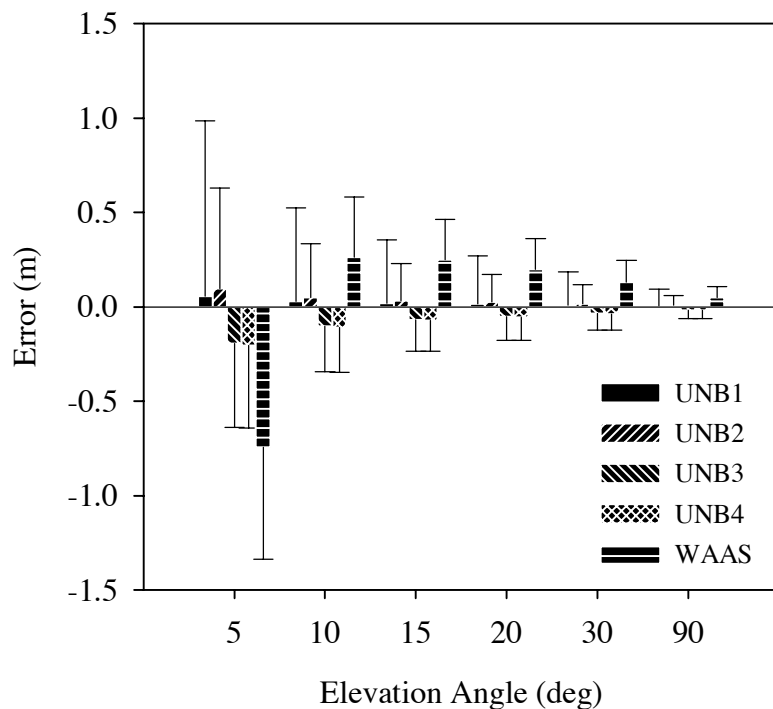
**Figure 4.3. Bar chart of model residual bias and dispersion for all stations.
For each elevation angle the mean error is represented by a solid bar extended by
one standard deviation. (Orthometric height.)**

A major problem with this data is that the residuals are not normally distributed. In

general they are highly skewed and leptokurtic. This has been seen before in these kinds

of tests but not commented on (see *Marini and Murray* [1973]). We will do so now

because it presents some problems when defining extreme error bounds for the delay models. Figure 4.4 shows the distribution of the normalised zenith residuals from all stations on a Gaussian plot. If the residuals were normally distributed they would be close to the diagonal line. As can clearly be seen they are not, and diverge significantly at the tails of the distribution.
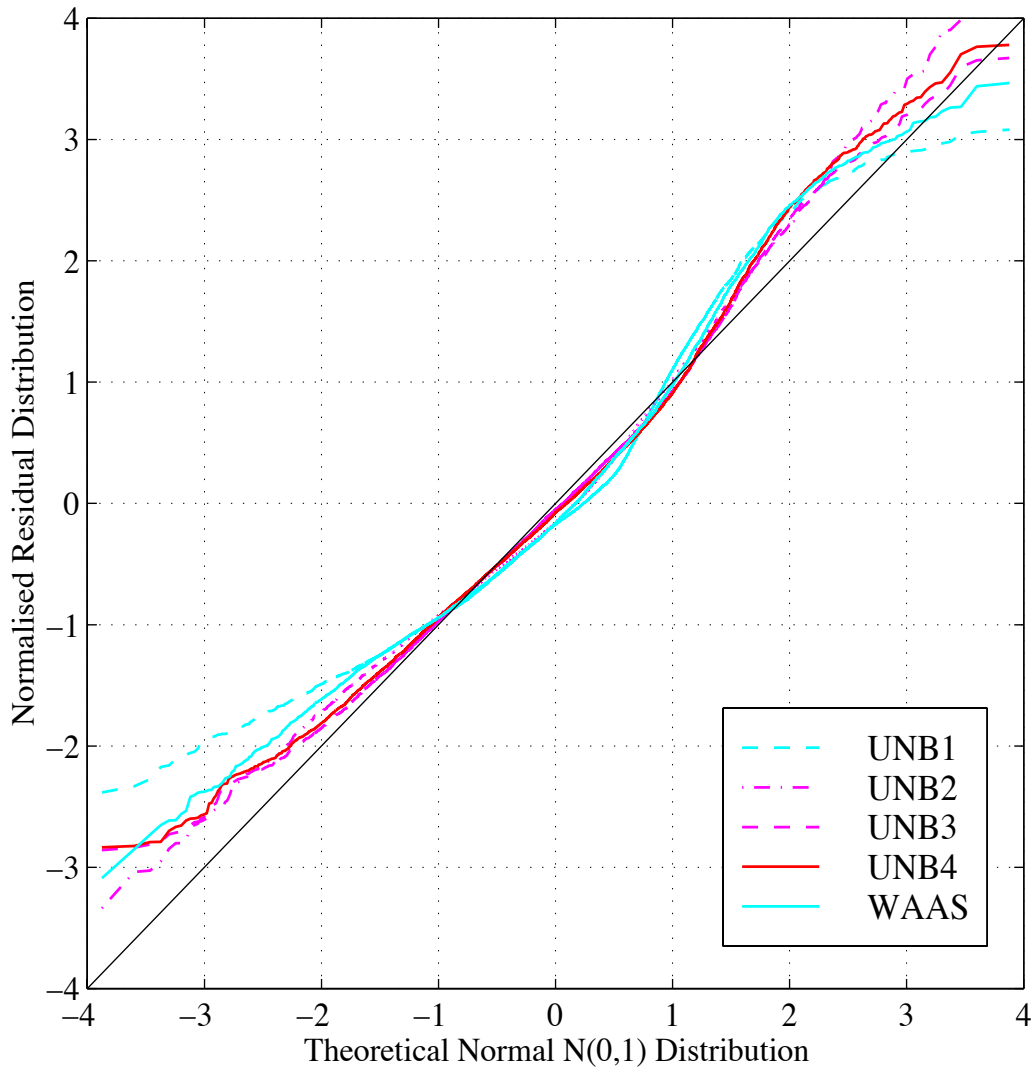
Figure 4.4. Gaussian plot of ray-traced zenith residuals.

The particular distribution of the residuals may be due to the fact that the sample of the atmosphere does not represent the full range of atmospheric conditions. The data contains diurnal changes recorded by the 0000 and 1200 UTC launches. These changes will primarily be seen in the temperature and water vapour content and hence the wet delay. These two parameters undergo large diurnal changes which are not modelled (and would almost certainly be impossible to model globally).

Table 4.9 represents the overall mean zenith delay error split into the constituent components. It indicates that the slight bias remaining in UNB3 and UNB4 appears to be due to the water vapour component of the delay. Therefore, it might be possible to improve both of these models by improving the water vapour profile representation. As Table 4.10 shows, the bias could be largely due to the lambda and e_0 parameters.

Table 4.9. Mean and standard deviation (metres) of hydrostatic and wet zenith delay differences of UNB models and all ray-trace data.

	Hydrostatic		Wet	
	Mean	S.D.	Mean	S.D.
UNB1	0.001	0.020	0.004	0.085
UNB2	0.000	0.019	0.009	0.049
UNB3	0.001	0.019	–0.019	0.042
UNB4	–0.002	0.019	–0.018	0.042

Table 4.10. Mean and standard deviation of atmospheric parameter differences determined from the UNB models and all ray-trace data.
(Temperature lapse rates were not provided with the ray-trace data; lambda values were estimated by inverting the wet zenith delays.)

	UNB1		UNB2		UNB3		UNB4	
	Mean	S.D.	Mean	S.D.	Mean	S.D.	Mean	S.D.
P_0 (mbar)	0.50	8.58	-0.05	8.33	0.37	8.36	-0.73	8.38
T_0 (kelvin)	-6.70	17.12	-1.28	11.30	-0.11	8.03	-8.12	10.12
e_0 (mbar)	-0.05	8.64	-0.26	4.02	-1.02	3.30	-1.04	3.30
λ (n/a)	-0.38	1.23	-0.51	1.13	0.29	1.12	0.29	1.12

All-in-all, there is a lot of scatter inherent in the sampled radiosonde data that is not well represented by the tropospheric delay models. Only if real-time values of the meteorological parameters are input can some of these variations be accommodated. It is interesting to note that even if this is done the residuals are not normally distributed; but they are more symmetric. This is shown by Table 4.11 which summarises the UNB and WAAS models and includes statistics for the Saastamoinen zenith delay/Niell mapping function combination using the surface meteorological values from the radiosonde data. This model is denoted SAAN and represents the tropospheric delay model of the "benchmark" solutions for the GPS data sets discussed in Chapter Three.

Hence, the best that can be hoped for is a tropospheric delay model that gives high symmetry in the residuals (positive and negative errors equally likely). This is again given by UNB3 and UNB4 which have roughly equal maximum and minimum residuals and a skewness of approximately 0.4 and 0.5 respectively.

Table 4.11. Extended statistical summary of UNB, WAAS and SAAN models differenced with respect to ray-traced data at sampled elevation angles. (Units are metres except skewness and kurtosis; see below.)

UNB1	RANGE	MEAN	S.D.	MIN	MAX	SKEW[†]	KURT[‡]
90	0.48	0.00	0.09	-0.20	0.28	0.78	3.09
30	0.96	0.01	0.18	-0.41	0.55	0.78	3.10
20	1.39	0.01	0.26	-0.59	0.80	0.78	3.10
15	1.83	0.02	0.34	-0.78	1.05	0.79	3.10
10	2.70	0.03	0.49	-1.14	1.55	0.79	3.10
5	5.04	0.06	0.93	-2.12	2.92	0.81	3.11
UNB2	RANGE	MEAN	S.D.	MIN	MAX	SKEW	KURT
90	0.38	0.01	0.05	-0.16	0.22	0.58	3.40
30	0.75	0.02	0.10	-0.32	0.43	0.58	3.40
20	1.10	0.02	0.15	-0.47	0.63	0.58	3.40
15	1.44	0.03	0.19	-0.61	0.83	0.59	3.40
10	2.12	0.05	0.29	-0.90	1.22	0.59	3.40
5	3.94	0.10	0.53	-1.64	2.30	0.61	3.40
UNB3	RANGE	MEAN	S.D.	MIN	MAX	SKEW	KURT
90	0.28	-0.02	0.04	-0.14	0.14	0.40	3.28
30	0.56	-0.04	0.09	-0.28	0.28	0.40	3.28
20	0.82	-0.05	0.12	-0.41	0.41	0.40	3.28
15	1.07	-0.07	0.16	-0.54	0.53	0.40	3.29
10	1.58	-0.10	0.24	-0.80	0.78	0.40	3.30
5	3.00	-0.19	0.45	-1.53	1.47	0.40	3.34
UNB4	RANGE	MEAN	S.D.	MIN	MAX	SKEW	KURT
90	0.28	-0.02	0.04	-0.14	0.14	0.53	3.46
30	0.56	-0.04	0.08	-0.28	0.28	0.53	3.46
20	0.82	-0.06	0.12	-0.41	0.41	0.53	3.46
15	1.07	-0.07	0.16	-0.53	0.54	0.53	3.47
10	1.57	-0.11	0.24	-0.78	0.79	0.53	3.48
5	2.98	-0.20	0.44	-1.50	1.49	0.53	3.52
WAAS	RANGE	MEAN	S.D.	MIN	MAX	SKEW	KURT
90	0.37	0.05	0.06	-0.13	0.25	0.68	3.27
30	0.74	0.13	0.11	-0.22	0.53	0.70	3.31
20	1.08	0.20	0.16	-0.31	0.77	0.71	3.32
15	1.42	0.25	0.22	-0.42	1.00	0.70	3.31
10	2.07	0.26	0.32	-0.71	1.36	0.69	3.27
5	3.93	-0.74	0.59	-2.54	1.39	0.58	2.97
SAAN	RANGE	MEAN	S.D.	MIN	MAX	SKEW	KURT
90	0.33	0.01	0.03	-0.12	0.20	0.22	5.01
30	0.65	0.01	0.05	-0.24	0.41	0.22	5.01
20	0.95	0.02	0.08	-0.36	0.59	0.21	5.01
15	1.25	0.02	0.10	-0.47	0.78	0.20	5.01
10	1.84	0.03	0.15	-0.69	1.15	0.18	5.00
5	3.49	0.06	0.29	-1.31	2.17	0.07	4.94

[†]Skewness indicates the symmetry of the residuals. The Normal distribution is symmetric with a skewness value of zero. [‡]Kurtosis indicates the shape of the residuals. The Normal distribution has a value = 3; a flat - platykurtic - distribution is < 3, a pointed - leptokurtic - distribution > 3.

67

In considering the maximum possible error of the tropospheric delay models, given that our residuals are not normally distributed, it is more prudent to examine the maximum and minimum residuals explicitly. Figure 4.5 represents the maximum and minimum of the residuals for all the data from Table 4.11. It is clear that the maximum error incurred by using UNB3 and UNB4 is almost equally the same in a positive or negative sense. In contrast, UNB1 and UNB2 and especially the initially proposed WAAS model are skewed with respect to their error range.
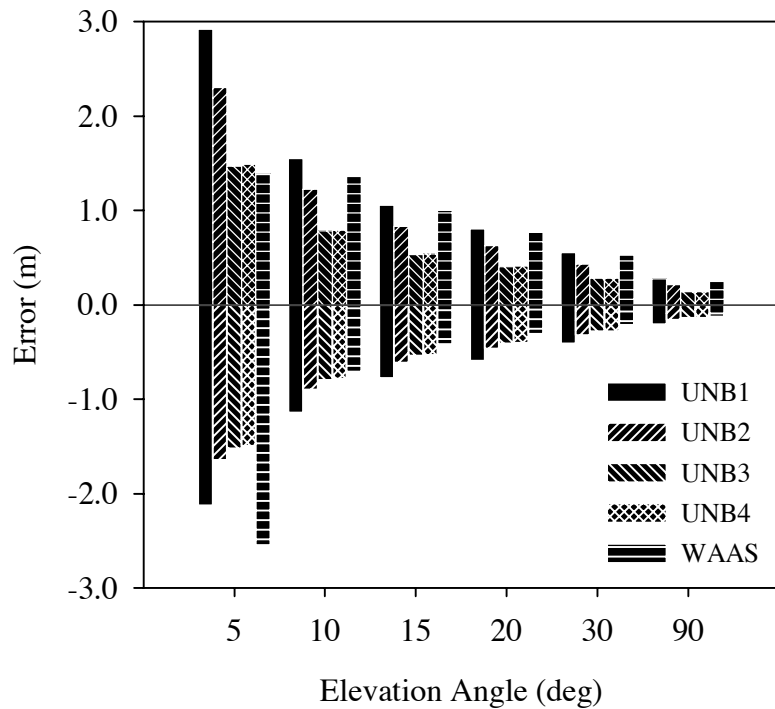
Figure 4.5. Bar chart of maxima and minima model residuals.
For each elevation angle, bars indicate total range. (Orthometric height.)

4.6 Conclusions From Ray-Traced Radiosonde Data

In summary, our statistics from the analysis of ray-trace data describe the following trends. The mean error shows the overall performance of each model. The standard deviation indicates how well the models deal with the annual and diurnal variation in the atmosphere. The initially proposed WAAS model often has comparable standard deviations to the UNB models solely because it makes an attempt to model the annual variation. The residual mean shows that its delays are biased however.

Concerning the temperature profile and how this represents the change in pressure "through the earth" for high altitude stations, the statistics for Denver and Grand Junction indicate that there does not appear to be a problem. This is fortunate as the only other solution would be the provision of a terrain model of orthometric height. This would almost certainly be unrealistic for a WADGPS, including WAAS.

Considering the worst-case errors from this ray-trace data, the maximum and minimum statistics show that the range of the tropospheric delay errors for UNB3 and UNB4 is smaller than that for the initially proposed WAAS model and almost symmetrical. These statistics show that for the worst case at five degrees elevation angle, the UNB3 and UNB4 models removed approximately one metre more of the tropospheric delay than the initially proposed WAAS model.

CHAPTER FIVE
THE TROPOSPHERIC ERROR BOUND FOR GPS MEASUREMENTS

This chapter of the thesis attempts to bring together the conclusions of the previous two chapters and to quantify the error bounds of the tropospheric delay models. To help in this task, further information regarding theoretical atmospheric extremes is introduced.

5.1 Summary of Tests Undertaken

From the investigations described in the previous chapters it can be seen that the models designated as UNB3 and UNB4 limit the maximum tropospheric range delay error to approximately 1.5 m for a satellite at five degrees elevation angle. This compares to approximately 2.5 m for the initially proposed WAAS model. At this point the results should be qualified by providing statistical error bounds for the tropospheric range errors. Unfortunately, as we saw in Chapter Four, the residuals from our radiosonde data are not normally distributed and we should therefore be reluctant to quote extreme error bounds statistically (i.e. $3.3\sigma = 99.9\%$ as required for WAAS, for example). However, if the radiosonde data accurately represents the full variation of the atmosphere then we might be justified in saying that we have derived the 100% error bound (in the maximum and minimum values). Table 5.1 gives the full range of conditions represented by our ray-trace data. As can be seen this represents a wide variation, but we must ask the question: are they the largest that could be encountered?

Table 5.1. Meteorological limits of the radiosonde data.

Parameter	Minimum	maximum
Sea-level Pressure (mbar)	954.6	1059.7
Surface Temperature (°C)	–44.1	36.7
Surface Water Vapour Pressure (mbar)	0.0	33.7

5.2 Consideration of Meteorological Extremes

This section will present some numerical examples of weather extremes that might invalidate the position solution computed with the tropospheric delay models. Following the previous methodology of defining the tropospheric delay as dependent upon two main atmospheric constituents: the gases in hydrostatic equilibrium and water vapour, we will deal with potential weather extremes separately also.

5.2.1 The Hydrostatic Component

For the hydrostatic portion of the tropospheric delay, the only major problem that might invalidate our ray-trace results is the absence of extreme high or low sea-level pressures in the data sample. Examples of such conditions might be the common polar lows.

A typical sea-level hydrostatic zenith delay value is 2.30 m, corresponding to 1010 mbar (the average value given by the UNB models); a hypothetical low pressure of 900 mbar would give a hydrostatic zenith delay of approximately 2.05 m, a high of 1083.8 mbar (the highest ever recorded) a delay of 2.47 m. Assuming for the moment no error in the wet component, this typical hydrostatic zenith delay would have a potential error range of –0.25 m to +0.17 m at the zenith. Using an approximate mapping function

value of 10.1, this translates into –2.53 m to +1.72 m at five degrees elevation angle. Table 5.2 summarises these errors and attempts to show their influence on aircraft position. (Note that the results in Table 5.2 and Table 5.3 are slightly different from those in *Collins and Langley*, [1997]) due to a numerical computation error.) A negative height bias indicates that the computed position is higher than the true position.

Table 5.2. Influence of extreme pressure conditions on tropospheric delay and position determination.

Pressure Extreme	Error at Zenith	Error at 5 degrees	Height Bias[†]
low, 900 mbar	–0.25 m	–2.53 m	–2.50 m
high, 1084 mbar	+0.17 m	+1.72 m	+1.70 m

[†]This height bias is computed for a four satellite constellation: 1 at the user's zenith, 3 equidistantly spaced around the user's horizon at five degrees elevation angle.

The satellite constellation used for Table 5.2 is rather arbitrary because of the inherent difficulty in taking account of the varying geometry of the GPS constellation. The pattern of satellites chosen however, maximises the impact of a tropospheric delay error on the computed position. Worse constellation geometry's, in terms of VDOP, can be chosen, however these always involve satellites that are clustered at high elevation angles where the delay error is smaller and hence, the impact on the position bias is less.

5.2.2 The Wet Component

The wet delay provides far more complications. As we have discussed in Section 3.3.1, the concentration of water vapour in the atmosphere is usually highly variable and difficult to model accurately under most circumstances. This unpredictability is the main problem in providing error bounds for the wet portion of the tropospheric delay.

The lowest extreme can be considered by assuming that the air is completely dry, but the upper boundary is harder to derive. Knowledge of the temperature profile, could in theory provide an upper limit, by assuming that the air is saturated. As a numerical example (which may not be physically feasible), we could use the highest surface temperature ever recorded (57.3°C) and a relative humidity of 100%. Coupled with an average lapse rate of $\lambda = 3$, this would give a potential range delay of 1.59 m.

A more realistic value for the upper bound however, would be based on a precipitable water content of 80 mm. (The highest precipitable water content from a large global sample of radiosonde data is 77 mm [*Petty*, 1996].) The amount of precipitable water in a column of air can be converted to the equivalent range delay through a factor which is a function of temperature. A typical value is 6.277 [*Hogg et al.*, 1981] giving 0.50 m of range delay in this case. This extreme range delay is compared to a typical "tropical" value for the zenith wet delay given by UNB3/4 (0.28 m for 15°N). The results are shown in Table 5.3 in a similar fashion to the hydrostatic extremes (the average five degree mapping function value used is 10.7). The lower bound is taken to be a dry atmosphere in the same region. This value may also be unrealistic, but a *nearly* dry atmosphere will give results of a similar magnitude.

Table 5.3. Influence of extreme humidity conditions on tropospheric delay and position determination.

Humidity Extreme	Error at Zenith	Error at 5 degrees	Height Bias[†]
low, 0 mm PW	–0.28 m	–3.00 m	–2.98 m
high, 80 mm PW	+0.22 m	+2.38 m	+2.37 m

[†]This height bias is computed for a four satellite constellation: 1 at the user's zenith, 3 equidistantly spaced around the user's horizon at five degrees elevation.

Unfortunately, these kinds of conditions are likely to affect the performance of the mapping functions also. However to examine their performance under these conditions it would be necessary to ray-trace the theoretical profile to consider the impact at low elevation angles. Such extremes, should they exist, would almost certainly be very localised and to ray-trace at five degrees as if they represented the whole atmosphere could be unrealistic.

5.2.3 General Considerations

The theoretical extremes of the hydrostatic and wet delay error show that even though the nominal contribution of the water vapour to the tropospheric delay is small (~5%), because of its highly variable nature, it can cause a range error of the same magnitude as the hydrostatic gases. Whether these two conditions will occur concurrently is something that could be answered by future work. If they do, then the total height bias caused by mis-modelling the tropospheric delay could approach 5 m.

The previous examples highlight the problems of discussing theoretical extremes of the tropospheric delay. Extremes such as we have described are rare and in the case of low pressure zones, very transient. High pressure zones are generally more stable and can last for longer periods; very high humidity conditions less so. A comprehensive study of these types of weather conditions is the only way to categorically understand their impact on tropospheric delay determination.

Two important points can be made regarding the previous discussion. First, unless real-time input values are provided or corrections are estimated from the GPS data itself,

any model will fail to adequately model the tropospheric delay under these extreme meteorological conditions. Even then, the wet delay may remain inadequately determined. Second, it is highly unlikely that such extreme conditions can be reliably predicted for the purpose of tropospheric delay modelling.

Therefore, in order to properly quantify the operation of a tropospheric delay model where specified limits must be maintained, it may be necessary to monitor the atmosphere at reference stations and indicate to the user the presence of extreme conditions. Again, the effectiveness of this sort of monitoring for the kind of localised, transient conditions that produce these extremes, requires further study.

5.3 The Error Bound

If we consider that our ray-trace data is a good representation of the average atmosphere, we can provide an error model for the tropospheric delay for the UNB models. Figure 5.1 shows the 1σ error limits computed from the fits to the ray-trace data for all the models we have tested. For comparison purposes, the oft-quoted error limits for the Altshuler model are also plotted [*Altshuler and Kalaghan*, 1974]. We can see that from this data, the error in the UNB1 model is approximately equivalent to the error in the Altshuler model with full meteorological information (AFCRL-A). However, considering that the initially proposed WAAS model is an approximation to this model and our estimate of its standard deviation is much lower, it is likely that these Altshuler curves are overly pessimistic. (Note however, they were computed from a larger data set.)
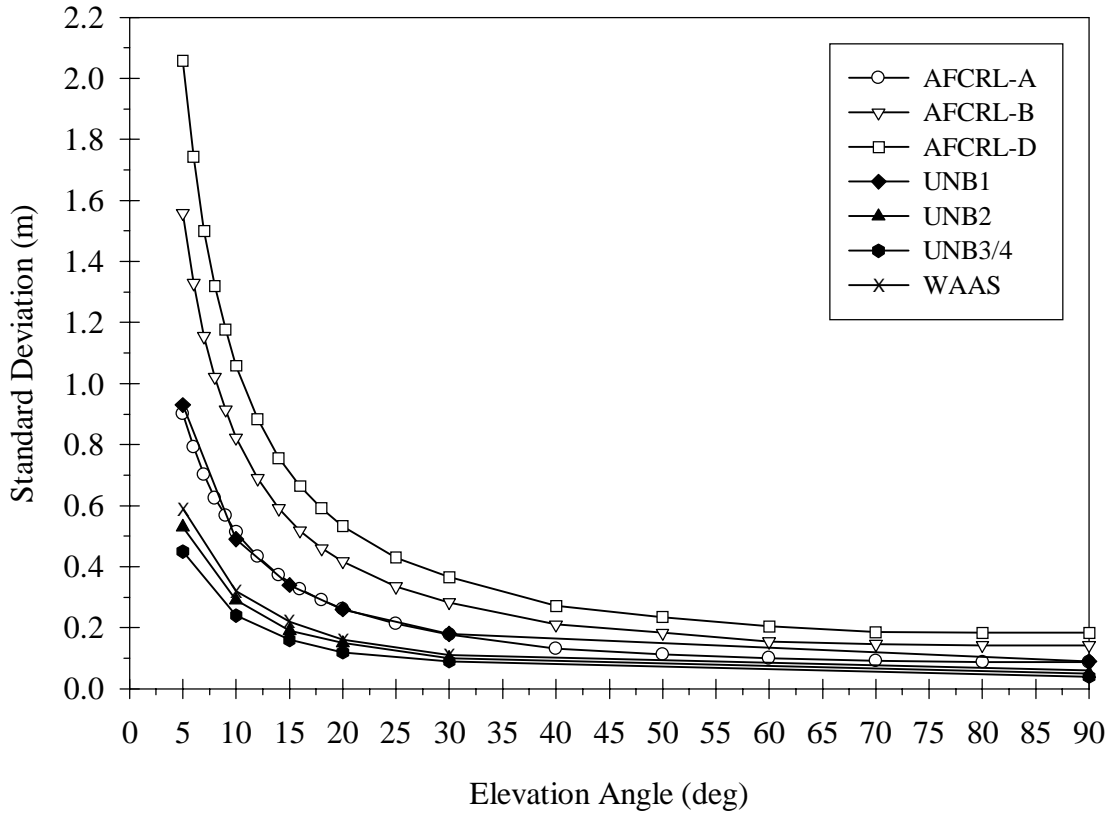
Figure 5.1. Tropospheric delay error – one standard deviation.
AFCRL curves represent quoted error for Altshuler model with: surface
meteorology (A), position and time information only (B), and mean global
refractivity only (D).

Because of the non-normality of the residuals, we are reluctant to use these sigma values to indicate higher order error bounds. However, because Figure 5.1 appears to show that the initially proposed WAAS model is only slightly less accurate than UNB3/4 we will show the total error that takes into account the inherent bias in each model. Figure 5.2 shows that the "mean plus two-sigma" error limit of the UNB3/4 model is clearly an improvement over the initially proposed WAAS model.
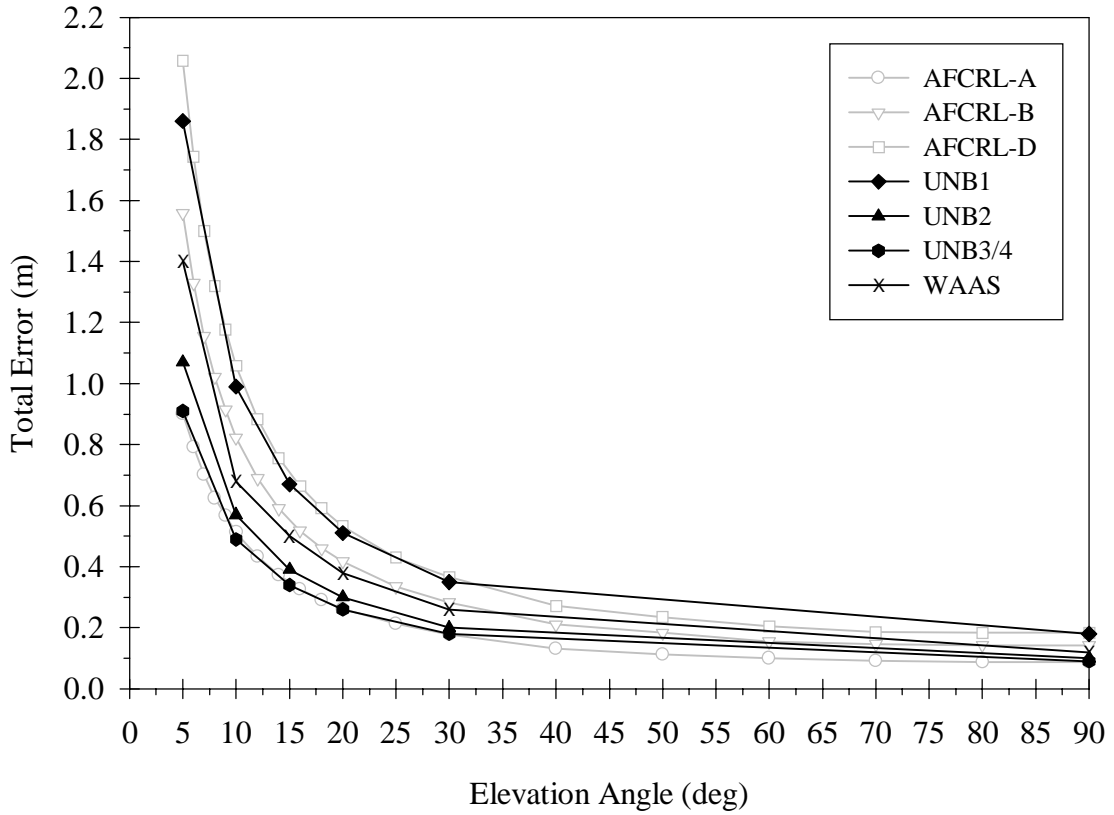
Figure 5.2. **The mean plus two sigma total error for the UNB and WAAS models. Total error equals** $\sqrt{\bar{x}^2 + (2\sigma)^2}$ **, AFCRL 1σ curves plotted in background for comparison purposes.**

CHAPTER SIX
SUMMARY, CONCLUSIONS AND RECOMMENDATIONS

6.1 Summary

The currently available navigation-type tropospheric delay models have been researched and compared with a simple composite model based on: standard equations for the hydrostatic and wet zenith delays; accurate, globally defined mapping functions; and scaling equations to map sea-level meteorological values to the height of a user's aircraft. Based on successful tests using GPS data, the meteorological data was expanded to look-up tables of sea-level data to better represent the annual variations in the atmosphere. These improvements were confirmed with an extensive set of ray-traced radiosonde data covering the Northern Hemisphere.   Finally, tropospheric delay determination under extreme conditions has been considered and the potential impact on the models estimated.

6.2 Conclusions

Through the application of physical principles such as geometric optics, the gas laws and hydrostatic equilibrium, this thesis has indicated the equations necessary for determining the electromagnetic path and bending delay due to the neutral atmosphere with specific application to navigation of an aircraft using GPS. These equations allow for the correct modelling of the change of the atmosphere and its refractivity with height. The basic requirements to drive the assembled models are tables of five meteorological and six

mapping function parameters. This research has found that the 1966 U.S. Standard Atmosphere Supplements are suitable sources for these values.

Of the models constructed, the similarity between UNB3 and UNB4 poses a problem as to which, if either, is better. The purpose of UNB4 was to try and overcome the problem of temperature inversions and their impact on the hydrostatic delay. This problem was therefore confined to the incorrect scaling of sea-level pressure to high altitudes and, as the GPS tests indicated, this was overcome for the most part. However, if the accuracy requirement of the tropospheric delay model is confined only to the region from the surface to a height of one kilometre, then the UNB3 model is the better choice.

GPS users who wish to use one of the UNB models for non-aviation applications at the Earth's surface would also probably be best served by UNB3. The difference in performance between UNB3 and UNB4 is for most purposes, insignificant. However, the processing of data recorded above any temperature inversions, even over short horizontal baselines, might benefit from the use of UNB4, especially if the resolution of carrier-phase ambiguities is required.

It should be noted that the height limit of the model's use is determined by the scaling factors κ_{hyd} and κ_{wet}. Numerically, these are functions of the sea-level temperature and lapse rate. Theoretically, the model will perform less well above the tropopause, due to the change in temperature structure. The degraded accuracy under these circumstances however, is no greater than that expected with inversion layers below the tropopause. It would be possible to extend the models to deal with the atmosphere at and above the

tropopause, however the added complexity is not worth the effort for the position accuracies required by WAAS and other WADGPS users at these heights.

6.3 Recommendations

It is recommended that where real-time meteorological measurements are unavailable, the tropospheric delay model denoted in this thesis as UNB3 be implemented in the processing of GPS data recorded at an aircraft in flight. Should meteorological data such as pressure, temperature and relative humidity be available they can be substituted for the equivalent values in the look-up table. The full definition of the algorithm and a discussion of the practical implementation of the model can be found in Appendix C, along with a discussion of the numerical weights required for the tropospheric delay in a least-squares adjustment.

Further work should be undertaken to explore extreme weather conditions and their effects on delay modelling with a more extensive set of truth data. This work should be directed at determining the frequency, duration and magnitude of extreme atmospheric conditions to determine when, where and by how much the recommended tropospheric delay model could be in error.

Should this work prove that these conditions are significant, then an assessment of optional methods to cope will be needed. This might involve ground monitoring of atmospheric conditions and broadcasts to users of a "do not use" flag. Alternatively, the

provision of real-time atmospheric parameters to the user, either from instruments on the aircraft or broadcasts of data from ground reference stations could be considered.

6.3.1 Potential Improvements

While the performance of UNB3 and UNB4 is excellent under a wide range of conditions, it is possible that improvements could be made to these models. There is an obvious bias remaining in these models and considering the results of the ray-trace tests, it seems likely that this is in the determination of the zenith wet delay and due to the lambda and surface water vapour values used. It might be possible to update these values using for example, a large radiosonde data set, to provide a better mean performance.

Alternatively, the UNB2 model could be expanded using the same principles as UNB3/4. The data sets used to derive the parameter values for UNB2 are comprehensive enough to provide an annual variation similar to UNB3/4. This data could also be ray-traced to provide mapping function coefficients to retain the homogeneous nature of the model similar to UNB3/4. The primary benefit of this would be to improve the global latitudinal resolution to 10 degrees. In addition, there could be the provision of an annual variation to the tropics, a feature present in the radiosonde data, but not represented in the 1966 U.S. Standard Atmosphere Supplements.

At the same time, research could be undertaken into the phase constant of the annual variation. This is currently fixed at day-of-year 28. However, it is likely that the mapping

functions performance could be degraded where the atmospheric variation is significantly "out-of-phase" with this value.

It should again be noted that these improvements would be confined to the values of the atmospheric parameters and the mapping function coefficients. The basic algorithms to compute the zenith delays and mapping functions are the same and therefore any "new" models or updates to the old ones can be easily implemented (see Appendix C).

Beyond these suggestions, the only other way to improve the determination of the tropospheric delay, with or without access to real-time meteorological values, would be by estimating the residual range delay remaining after the predicted delay, a common approach in high-accuracy geodetic applications of GPS. An investigation could be undertaken into the feasibility of estimating this parameter simultaneously with the position components of the user in a real-time navigation environment.

REFERENCES

Altshuler, E.E. (1971). "Corrections for tropospheric range error." AFCRL-71-0419. Air Force Cambridge Research Laboratories, Bedford, Mass., July 27, 43 pp.

Altshuler, E.E. and P.M. Kalaghan (1974). "Tropospheric range error corrections for the NAVSTAR system." AFCRL-TR-74-0198. Interim scientific report, Air Force Cambridge Research Laboratories, Bedford, Mass., April 16, 13 pp.

Altshuler, E.E. (1998). "Tropospheric range-error corrections for the Global Positioning System." *IEEE Transactions on Antennas and Propagation*, Vol. 46, pp. 643-649.

Askne, J. and H. Nordius (1987). "Estimation of tropospheric delay for microwaves from surface weather data." *Radio Science*, Vol. 22, No. 3, pp. 379-386.

Bean, B.R. and G.D. Thayer (1959). "Models of the atmospheric radio refractive index." *Proceedings of the Institute of Radio Engineers*, Vol. 47, May, pp. 740-755.

Bean, B.R. and E.J. Dutton (1966). *Radio Meteorology*. National Bureau of Standards Monograph 92, U.S. Government Printing Office, Washington, DC.

Bisagni, J.J. (1989). "Wet tropospheric range corrections for satellite altimeter-derived dynamic topographies in the western North Atlantic." *Journal of Geophysical Research*, Vol. 94, No. C3, pp. 3247-3254.

Bohn, E.V. (1968). *Introduction to Electromagnetic Fields and Waves*. Addison-Wesley, Reading, Mass.

Brunner, F.K. (1992). "Refraction, refractive index and dispersion: Some relevant history." *Refraction of Transatmospheric Signals in Geodesy*, Eds. J.C. De Munck and T.A.Th. Spoelstra. Proceedings of the Hague Symposium, May 19-22. Netherlands Geodetic Commission, Publications on Geodesy, New Series, No.36, pp. 3-9.

Chao, C.C. (1972). "A model for tropospheric calibration from daily surface and radiosonde balloon measurements." JPL Technical Memorandum 391-350, Jet Propulsion Laboratory, Pasadena, Calif.

Chen, G. and T.A. Herring (1997). "Effects of atmospheric azimuthal asymmetry on the analysis of space geodetic data." *Journal of Geophysical Research*, Vol. 102, No. B9, pp. 20,489-20,502.

Collins, J.P. and R.B. Langley (1997). "Estimating the residual tropospheric delay for airborne differential GPS positioning." *Proceedings of ION GPS-97*, The 10th International Technical Meeting of the Satellite Division of The Institute of Navigation, Kansas City, Mo., September 16-19, pp. 1197-1206.

Coster, A.J., A.E. Niell, F.S. Solheim, V.B. Mendes, P.C. Toor and R.B. Langley (1997). "The effect of gradients in the GPS estimation of tropospheric water vapour." *Proceedings of the 53rd Annual Meeting*, Institute of Navigation, Albuquerque N. Mex., June 30-July 1, pp. 107-114.

Davis, J.L., T.A. Herring, I.I. Shapiro, A.E.E. Rogers and G. Elgered (1985). "Geodesy by radio interferometry: Effects of atmospheric modeling errors on estimates of baseline length." *Radio Science*, Vol. 20, No. 6, pp. 1593-1607.

Davis, J.L. (1986). "Atmospheric propagation effects on radio interferometry." AFGL-TR-86-0243. Air Force Geophysics Laboratory, Hanscom Air Force Base, Mass., 284 pp.

Davis, J.L., G.E. Elgered, A.E. Niell, and C.E. Kuehn (1993). "Ground-based measurements of gradients in the 'wet' radio refractivity of air." *Radio Science*, Vol. 28, No. 6, pp. 1003-1018.

DeCleene, B. (1995). Personal communication. Federal Aviation Administration, May 1995.

Dixon, T.H. and S. Kornreich Wolf (1990). "Some tests of wet tropospheric calibration for the CASA UNO Global Positioning System experiment." *Geophysical Research Letters*, Vol. 17, No. 3, pp. 203-206.

Dubin, M., N. Sissenwine and S. Teweles (1966). *U.S. Standard Atmosphere Supp–lements, 1966*. U.S. Committee on Extension to the Standard Atmosphere. U.S. Government Printing Office, Washington, DC.

Dubin, M., A.R. Hull and K.S.W. Champion (1976). *U.S. Standard Atmosphere 1976*. NOAA-S/T 76-1562, NTIS AD/A035 728, National Technical Information Service, U.S. Dept. of Commerce, Springfield, Va.

Estefan, J.A. and O.J. Sovers (1994). "A comparative survey of current and proposed tropospheric refraction-delay models for DSN radio metric (*sic*) data calibration." JPL Publication 94-24, Jet Propulsion Laboratory, Pasadena, Calif.

FAA (1996). *Wide Area Augmentation System (WAAS) Specification*. FAA-E-2892A. Federal Aviation Administration, U.S. Department of Transportation, Washington, DC.

Fleming, E.L., S. Chandra, M.R. Schoeberl and J.J. Barnet (1988). *Monthly mean Global Climatology of Temperature, Wind, Geopotential Height and Pressure for 0-120 km*. NASA TM-100697. Goddard Space Flight Centre, Greenbelt, Md.

Gardner, C.S. (1977). "Correction of laser tracking data for the effects of horizontal refractivity gradients." *Applied Optics*, Vol. 16, No. 9, pp. 2427-2432.

Georgiadou, Y. and K.D. Doucet (1990). "The issue of selective availability." *GPS World*, Vol. 1, No. 5, pp. 53-56.

Herring, T.A. (1992). "Modeling atmospheric delays in the analysis of space geodetic data." *Refraction of Transatmospheric Signals in Geodesy*, Eds. J.C. De Munck and T.A.Th. Spoelstra . Proceedings of the Hague Symposium, May 19-22. Netherlands Geodetic Commission, Publications on Geodesy, New Series, No.36, pp. 157-163.

Hofmann-Wellenhof, B., H. Lichtenegger and J. Collins (1992). *GPS Theory and Practice*. Springer-Verlag, Vienna.

Hogg, D.C., F.O. Guiraud and M.T. Decker (1981). "Measurement of excess radio transmission length on Earth-space paths." *Astronomy and Astrophysics*, Vol. 95, pp. 304-307.

Ifadis, I. (1986). "The atmospheric delay of radio waves: Modeling the elevation dependence on a global scale." Technical Report 38L, Chalmers University of Technology, Göteborg, Sweden.

Janes, H.W., R.B. Langley and S.P. Newby (1991). "Analysis of tropospheric delay prediction models: Comparisons with ray-tracing and implications for GPS relative positioning." *Bulletin Géodésique*, Vol. 65, pp. 151-161.

Kee, C., B.W. Parkinson and P. Axelrad (1991). "Wide Area Differential GPS." *Navigation*, Journal of The Institute of Navigation, Vol. 38, No. 2, pp. 123-145.

Kerker, M. (1969). *The Scattering of Light and Other Electromagnetic Radiation*. Academic Press, New York.

Kline, M. and I.W. Kay (1965). *Electromagnetic Theory and Geometrical Optics*. John Wiley & Sons, Inc., New York.

Langley, R.B. (1996). "Propagation of the GPS signals." In *GPS for Geodesy*, Eds. A. Kleusberg and P.J.G. Teunissen. Lecture Notes in Earth Sciences No. 60, Springer-Verlag, New York, pp. 103-140.

Langley, R.B. (1997). "The GPS error budget." *GPS World*, Vol. 8, No. 3, pp. 51-56.

Loh, R. (1993). "FAA Wide Area Integrity and Differential GPS Program." *Proceedings of the 2nd International Symposium on Differential Satellite Navigation Systems* (DSNS 93), Amsterdam, March 29-April 2.

Loh, R. (1995). "Seamless aviation: FAA's Wide Area Augmentation System." *GPS World*, Vol. 6, No. 4, pp. 20-30.

Loh, R. (1996). "GPS Wide Area Augmentation System (WAAS)." Seminar Lecture Notes, Presented at the IEEE Position, Location and Navigation Symposium, Atlanta, Ga., April 23.

Loh, R., V. Wullschleger, B. Elrod, M. Lage and F. Haas (1995). "The U.S. Wide-Area Augmentation System (WAAS)." *Navigation*, Journal of The Institute of Navigation, Vol. 42, No. 3, pp. 435-465.

Mader, G.L. (1996). "Kinematic And Rapid Static (KARS) GPS positioning: Techniques and recent experiences." *GPS Trends in Precise Terrestrial, Airborne and Spaceborne Applications*, Eds. G. Beutler, G.W. Hein, W.G. Melbourne, G. Seeber. International Association of Geodesy Symposia No. 115, Boulder, Colo., July 3-4, 1995. Springer-Verlag, New York, pp. 170-174.

Marini, J.W. (1972). "Correction of satellite tracking data for an arbitrary tropospheric profile." *Radio Science*, Vol. 7, No. 2, pp. 223-231.

Marini, J.W. and C.W. Murray (1973). "Correction of laser range tracking data for atmospheric refraction at elevations above 10 degrees." NASA TM-X-70555. Goddard Space Flight Centre, Greenbelt, Md.

McDonald, K. D. (1991). "GPS in Civil Aviation." *GPS World*, Vol. 2, No. 8, pp. 52-59.

Mendes, V.B. (1996). Personal communication. Faculdade de Ciências da Universidade de Lisboa, Departamento de Matemática, Lisboa, Portugal.

Mendes, V.B. (1999). *Modeling the neutral-atmosphere propagation delay in radiometric space techniques*. Ph.D. dissertation, Department of Geodesy and Geomatics Engineering Technical Report No. 199, University of New Brunswick, Fredericton, New Brunswick, Canada, 353 pp.

Mendes, V.B. and R.B. Langley (1994). "A comprehensive analysis of mapping functions used in modeling tropospheric propagation delay in space geodetic data." *Proceedings of KIS94, International Symposium on Kinematic Systems in Geodesy, Geomatics and Navigation*, Banff, Canada, August 30-September 2, pp. 87-98.

Mendes, V.B. and R.B. Langley (1995). "Zenith wet tropospheric delay determination using prediction models: Accuracy analysis." *Cartografia e Cadastro*, Instituto Português de Cartografia e Cadastro, No. 2, pp. 41-47.

Mendes, V.B., J.P. Collins and R.B. Langley (1995). "The effect of tropospheric propagation delay errors in airborne GPS precise positioning." *Proceedings of ION GPS-95*, The 8th International Technical Meeting of the Satellite Division of The Institute of Navigation, Palm Springs, Calif., September 12-15, pp. 1681-1689.

NATO (1993). Standardisation Agreement (STANAG) Document 4294 EL (Edition 1), Appendix 6 to Annex A. pp. A-6-34–A-6-37. North Atlantic Treaty Organisation, Brussels, Belgium.

Niell, A.E. (1996). "Global mapping functions for the atmosphere delay at radio wavelengths." *Journal of Geophysical Research*, Vol. 101, No. B2, pp. 3227-3246.

Niell, A.E., A.J. Coster, F.S. Solheim, V.B. Mendes, P.C.P. Toor, R.B. Langley and C.A. Ruggles (1996). "Measurement of water vapour by GPS, WVR and radiosonde". *Proceedings of the 11th Working Meeting on European VLBI for Geodesy and Astronomy*, Ed. G. Elgered, Onsala, Sweden, August 23-24. Research Report No. 177, Onsala Space Observatory, Chalmers University of Technology, Göteborg, Sweden, pp. 96-101.

Owens, J.C. (1967). "Optical refractive index of air: Dependence on pressure, temperature and composition." *Applied Optics*, Vol. 6, No. 1, pp. 51-59.

Parkinson, B.W. and P.K. Enge (1995). "Differential GPS." In *Global Positioning System: Theory and Applications*, Volume II, Eds. B.W. Parkinson and J.J. Spilker Jr. American Institute of Aeronautics and Astronautics, Progress in Astronautics and Aeronautics Volume 164, Washington, DC, U.S.A., pp. 3-50.

Petty G.W. (1996). Personal communication. Associate Professor of Atmospheric Science, Department of Earth and Atmospheric Sciences, Purdue University, West Lafayette, Ind.

Peixoto, J.P. and A.H. Oort (1983). "The atmospheric branch of the hydrological cycle and climate." In *Variations in the Global Water Budget*, Eds. A. Street-Perrott, M. Beran and R. Ratcliffe. D. Reidel, Dordrecht, Holland, pp. 5-65.

Peixoto, J.P. and A.H. Oort (1992). *Physics of Climate*. American Institute of Physics, New York.

Phillips, E.H. (1995). "Canada probes role of freezing drizzle." *Aviation Week and Space Technology*, March 13, pp. 32-33.

Saastamoinen, J. (1972). "Atmospheric correction for the troposphere and stratosphere in radio ranging of satellites." In *The Use of Artificial Satellites for Geodesy*, Geophys. Monogr. Ser., Vol. 15, American Geophysical Union, Washington DC, pp. 247-251.

Salby, M.L. (1996). *Fundamentals of Atmospheric Physics*. International Geophysics Series, Vol. 61. Academic Press Inc., San Diego, Calif.

Shi, J. and M.E. Cannon (1995). "Critical error effects and analysis in carrier phase-based airborne GPS positioning over large areas." *Bulletin Géodésique*, Vol. 69, No. 4, pp. 261-273.

Schwarz, F.K. (1968). "Comments on 'Note on the relationship between total precipitable water and surface dew point'." *Journal of Applied Meteorology*, Vol. 7, June, pp. 509-510.

Smith, E.K. and S. Weintraub (1953). "The constants in the equation for atmospheric refractive index at radio frequencies." *Proceedings of the Institute of Radio Engineers*, Vol. 53, August, pp. 1035-1037.

Smith, J.W. (1963). "The vertical temperature distribution and the layer of minimum temperature." *Journal of Applied Meteorology*, Vol. 2, October, pp. 655-667.

Smith, W.L. (1966). "Note on the relationship between total precipitable water and surface dew point." *Journal of Applied Meteorology*, Vol. 5, October, pp. 726-727.

Smith, W.L. (1968). Reply. *Journal of Applied Meteorology*, Vol. 7, June, p. 510.

Thayer, G.D. (1967). "A rapid and accurate ray tracing algorithm for a horizontally stratified atmosphere." *Radio Science*, Vol. 1, No. 2, pp. 249-252.

Thayer, G.D. (1974). "An improved equation for the radio refractive index of air." *Radio Science*, Vol. 9, No. 10, pp. 803-807.

Tiemeyer, B., M.E. Cannon, G. Lachapelle and G. Schänzer (1994). "Satellite navigation for high precision aircraft navigation with emphasis on atmospheric effects." *Proceedings of PLANS'94*, IEEE Position, Location and Navigation Symposium, Las Vegas, Nev., April 11-15, pp. 394-401.

Tralli, D.M., S.M. Lichten and T.A. Herring (1992). "Comparison of Kalman filter estimates of zenith atmospheric path delays using the Global Positioning System and Very Long Baseline Interferometry." *Radio Science*, Vol. 27, No. 6, pp. 999-1007.

Trenberth, K.E. (1981). "Seasonal variations in global sea level pressure and the total mass of the atmosphere." *Journal of Geophysical Research*, Vol. 86, No. C6, pp. 5238-5246.

Ware, R, C. Rocken, F. Solheim, T. Van Hove, C. Alber and J. Johnson (1993). "Pointed water vapor radiometer corrections for accurate Global Positioning System surveying." *Geophysical Research Letters*, Vol. 20, No. 23, pp. 2635-2638.

Weisbrod, S. and L.J. Anderson (1959). "Simple methods for computing tropospheric and ionospheric refractive effects on radio waves." *Proceedings of the Institute of Radio Engineers*, Vol. 59, October, pp. 1770-1777.

APPENDIX A
MISCELLANEOUS DERIVATIONS AND ALGORITHMS

The first part of this appendix presents the full derivation of the pressure–height relationship used throughout the development of both the hydrostatic and wet zenith delays and their scaling factor equations. The second part details the algorithms of the navigation-type models tested and reported on in this thesis.

APPENDIX A1   Derivation Of Pressure–Height Relationship

If we only have access to sea-level pressure (P_0) for the computation of the hydrostatic zenith delay, we must specify a relationship to scale this value to the user's height. The fundamental relationship governing the change of atmospheric pressure with height is the vertical component of the equation of hydrostatic equilibrium:

$$\frac{dP}{dz} = -\rho g \; . \qquad\qquad (\text{A.1})$$

Combining this relationship with the ideal gas law removes the density parameter ρ:

$$\frac{dP}{dz} = -\frac{Pg}{R_d T} \; . \qquad\qquad (\text{A.2})$$

Now, by assuming a temperature lapse rate linear with height (z):

$$T = T_0 - \beta \cdot z \; , \qquad\qquad (\text{A.3})$$

we can then, ignoring for the time being the variation of g with height, integrate and rearrange,:

$$\int_{P_0}^{P} \frac{dP}{P} = -\frac{g}{R_d} \int_0^z \frac{dz}{(T_0 - \beta z)} \quad ,$$

$$\left[\ln|P| + C_1\right]_{P_0}^{P} = -\frac{g}{R_d}\left[-\frac{1}{\beta}\ln|T_0 - \beta z| + C_2\right]_0^z \quad ,$$

$$\ln(P) - \ln(P_0) = \frac{g}{R_d \beta}\left[\ln(T_0 - \beta z) - \ln(T_0)\right] \quad ,$$

then taking antilogarithms and multiplying by P_0 yields the standard expression:

$$P = P_0\left(\frac{T}{T_0}\right)^{\frac{g}{R_d \beta}} \; . \qquad\qquad (\text{A.4})$$

This equation is commonly stated in meteorology textbooks. What is less commonly stated however, is that g is the mean value for sea-level gravity and that the geometric height above sea-level (z) has been replaced with the geopotential height (Z) with units of "geopotential metres". This change is undertaken because much use is made in meteorology of surfaces of constant geopotential to simplify the representation of gravity. The differential equation relating an increase in geopotential with an increase in height is:

$$d\Phi = g dz. \qquad (A.5)$$

The absolute geopotential is obtained by integrating this equation from a reference point, usually taken to be mean-sea-level because it is almost equivalent to the constant geopotential surface of the geoid. Hence,

$$P = P_0 \left(\frac{T}{T_0} \right)^{\frac{g}{R_d \beta}}. \qquad (A.6)$$

To account for the variation of g with height, the geopotential height (in geodesy: dynamic height) is defined as:

$$Z = \frac{1}{\bar{g}_0} \int_0^z g dz,$$

$$= \frac{1}{\bar{g}_0} \Phi(z), \qquad (A.7)$$

where $\bar{g}_0$ is a reference value for the average gravity at the surface of the earth [*Salby*, 1996]. This is often taken to be 9.80665 m/s^2 (the mid-latitude value) with Z as units of length, usually geopotential metres. Hence, when height is represented in terms of geopotential height, gravity can be described by the constant $\bar{g}_0$. Taking the derivative of equation (A.7) yields:

$$dZ = \frac{1}{\bar{g}_0} d\Phi$$

$$= \frac{g}{\bar{g}_0} dz, \qquad\qquad (\text{A.8})$$

which can be used to simplify the equation for hydrostatic equilibrium. Thus equation (A.1) becomes:

$$\frac{dP}{dZ} = -\rho \bar{g}_0, \qquad\qquad (\text{A.9})$$

and it is this form of the hydrostatic equilibrium equation that is integrated to achieve equation (A.4). As previously stated, for practical purposes, the geometric height is usually substituted for the geopotential height in equation (A.4). Fortunately, at a geopotential height of 10 kilometres, for the mid-latitude conditions of the U.S. Standard Atmosphere 1976 [*Dubin et al.*, 1976], the relative error from using the geometric height is only approximately 0.16%. This amounts to less than one millibar of pressure and less than two millimetres of zenith delay. The use of geometric height is therefore justified.

APPENDIX A2 Algorithms For Original Navigation-Type Models

The complete algorithms for all three of the original navigation-type tropospheric delay models are provided in this sub-Appendix. Bringing together these models in one place is particularly useful, especially as one (Altshuler) has almost always been specified incorrectly in almost all previous publications and another (NATO) is incompletely derived in its original reference.

APPENDIX A2.1 Altshuler Model

The Altshuler model is a three function polynomial of the form:

$$d_{trop} = 0.3048 \cdot G(E) \cdot H(h) \cdot F(h, N_s) \quad metres.$$

The function $G(E)$ is a mapping function of sorts:

$$G(E) = \left(g_0 + \frac{g_1}{E} + \frac{g_2}{E^2} + \frac{g_3}{E^3} \right) \cdot \left(g_4 + g_6 \left[E - g_5 \right]^2 \right),$$

where $g_0 = 0.1556$, $g_1 = 138.8926$, $g_2 = -105.0574$, $g_3 = 31.5070$, $g_4 = 1.0$, $g_5 = 30.0$ and $g_6 = 1.0 \times 10^{-4}$. The elevation angle E is in degrees. The function can be normalised by multiplying by 2.29286 to give a "true" mapping function that equals unity at the zenith. It should be noted that in theory, this function was derived with the apparent (refracted elevation angle), however as this is unknown, the true (unrefracted) elevation angle E is usually substituted. It is unlikely that use of the apparent elevation angle would drastically improve this model's performance. A separate formula (dependent upon the atmospheric profile) would be required to compute this parameter.

The function $H(h)$ is a function of the user's height h in thousands of feet:

$$H(h) = b_0 + \frac{b_1}{(h+8.6286)} + \frac{b_2}{(h+8.6286)^2} + \frac{b_3}{(h+8.6286)^3},$$

where $b_0 = 0.00970$, $b_1 = -2.08809$, $b_2 = 122.73592$ and $b_3 = -703.82166$.

The function $F(h,N_s)$ is a function of both the user's height and the surface refractivity N_s:

$$F(h, N_s) = c_0 \cdot \left(\frac{c_1}{h+c_0} + c_2[h+c_0] + c_3 N_s - c_4 \right) \cdot \left(1 - c_5[N_s - c_6]^2 \right),$$

where $c_0 = 3.28084$, $c_1 = 6.81758$, $c_2 = 0.30480$, $c_3 = 0.00423$, $c_4 = 1.33333$, $c_5 = 1.41723 \times 10^{-6}$ and $c_6 = 315.0$. When unknown, the surface refractivity is predicted from:

$$N_s(h', L, M) = \alpha_0 + \alpha_1 h' + \alpha_2 L + \alpha_3 h's^2 + \alpha_4 Ls^2 + \alpha_5 h'c + \alpha_6 Lc,$$

where L is the latitude in degrees and h' is the user's height above sea level in feet. The constants are $\alpha_0 = 369.03$, $\alpha_1 = -0.01553$, $\alpha_2 = -0.92442$, $\alpha_3 = 0.0016$, $\alpha_4 = 0.19361$, $\alpha_5 = 0.00063$, $\alpha_6 = -0.05958$, $s = \sin(\pi M/12)$ and $c = \cos(\pi M/12)$. The M value represents the month number, but is usually specified to vary with season only: $M = 1.5$ winter; $M = 4.5$ spring; $M = 7.5$ summer; $M = 10.5$ autumn. Note that the height dependence of this equation should only be utilized on the surface, i.e. for an aircraft in flight $h' = 0$.

This model represents an attempt to convert a previous formulism to avoid the use of transcendental and trigonometric expressions [*Altshuler*, 1971; *Altshuler*, 1998]. The original algorithm may show some improvement over this one, but most likely only to a similar level of the Initial WAAS and NATO models.

APPENDIX A2.2 Initial WAAS Model

The initially proposed WAAS model is a simplification of the Altshuler model. It is described with an equation of the form:

$$d_{trop} = \frac{\tau(\delta N_s)}{\sin(E + 0.35°)} f(h),$$

where τ is primarily a function the surface refractivity N_s corrected for altitude (h), day-of-year (d) and latitude (φ):

$$\delta N_s = \delta N_h(d) + \delta N_\varphi(d)$$

$$\delta N_h(d) = 3.61 \cdot 10^{-3} \cdot h \cdot cos\left(2\pi[d - d_h]/365\right)$$

$$\delta N_\varphi(d) = \left\{-0.8225 + 0.1 \cdot cos\left(2\pi[d - d_\varphi]/365\right)\right\} \cdot |\varphi|$$

where in the northern hemisphere, $d_h = 152$, $d_\varphi = 213$ and in the southern hemisphere, $d_h = 335$, $d_\varphi = 30$. Then for a user at or below 1500 metres above sea level:

$$\tau(\delta N_s) = 2.506(1 + 0.00125 \cdot \delta N_s) \ metres$$

$$f(h) = 1 - 1.264 \cdot 10^{-4} \cdot h$$

and above 1500 metres above sea level:

$$\tau(\delta N_s) = 2.484\left(1 + 0.0015363 \cdot e^{-2.133 \cdot 10^{-4} \cdot h} \cdot \delta N_s\right) \ metres$$

$$f(h) = e^{-1.509 \cdot 10^{-4} \cdot h}$$

APPENDIX A2.3 NATO Model

The NATO model is essentially the integrated solution of the refractivity profile in the CRPL RA-1958 model. That profile is specified as a function of height in kilometres:

for $0 \le h < 1$ km, $N(h) = N_s - h \cdot \Delta N$, where $\Delta N = -7.32 e^{\left(0 \cdot 005577 N_s\right)}$,

for $1 \le h < 9$ km, $N(h) = N_1 \cdot e^{-c(h-1)}$, where $N_1 = N_s + \Delta N$ and $c = \dfrac{1}{8} \log_e\left(\dfrac{N_1}{105}\right)$,

and for $h \ge 9$ km, $N(h) = 105 \cdot e^{-0.1424(h-9)}$.

The surface refractivity, N_s ($\equiv N(h = 0)$) is specified by the user.

The NATO model is represented in the usual tropospheric delay form:

$$d_{trop} = d_{trop}^z(h) \cdot m(E),$$

where E is the (unrefracted) elevation angle and h is the user's height above sea level in kilometres. The zenith delay is considered in three parts, corresponding to the reference atmosphere. It should be noted that in the original reference for this model, the solutions for the integrals are not completely solved algebraically. They have been done so here, but certain approximations have been retained.

For a user below 1 kilometre above mean-sea-level:

$$d_{trop}^z(1) = N_s(1 - h) + \tfrac{1}{2}\Delta N\left(1 - h^2\right),$$

$$d_{trop}^z(2) = 1430,$$

$$d_{trop}^z(3) = 732,$$

where $N_s = 324.8$ is the mean global surface refractivity.

Between 1 km and 9 km:

$$d_{trop}^z(1) = 0,$$

$$d_{trop}^z(2) = \frac{N_1}{c}\left(e^{-c(h-1)} - e^{-8c}\right),$$

$$d_{trop}^z(3) = 732.$$

For a user bove 9 km:

$$d_{trop}^z(1) = 0,$$

$$d_{trop}^z(2) = 0,$$

$$d_{trop}^z(3) = \frac{105}{0.1424} \cdot e^{-0.1424(h-9)}.$$

The total zenith delay is computed with:

$$d_{trop}^z(h) = \left[d_{trop}^z(1) + d_{trop}^z(2) + d_{trop}^z(3)\right] \cdot 10^{-3} \quad metres,$$

and mapped to the required elevation angle with the Chao "dry" mapping function:

$$m(E) = \frac{1}{\sin(E) + \dfrac{0.00143}{\tan(E) + 0.0455}}.$$

APPENDIX B
PLOTS

This appendix presents a comprehensive series of plots for all the GPS and ray-trace data used in this study. An example of each plot has been used previously to describe the tests undertaken with the tropospheric delay models.

APPENDIX B1 Navigation-Type Models:

Solution Position Differences With Respect To Height

The following plots are of the same type as Figure 3.2, that is the position differences (in metres) of the solutions computed using the navigation-type tropospheric delay models with respect to the position solutions of the benchmark solution. For the purposes of providing insight into the performance of the models, the differences are plotted against the aircraft height.
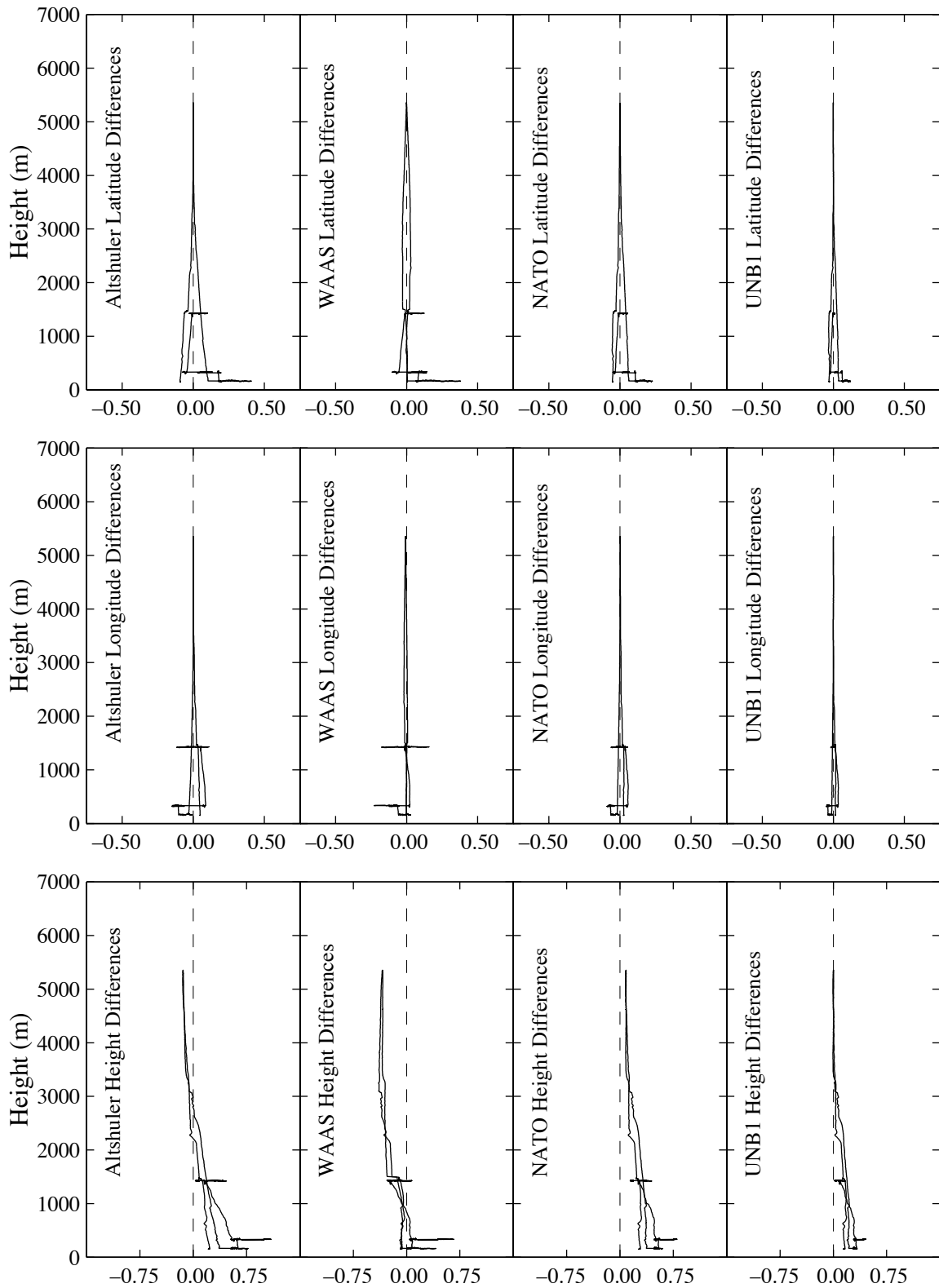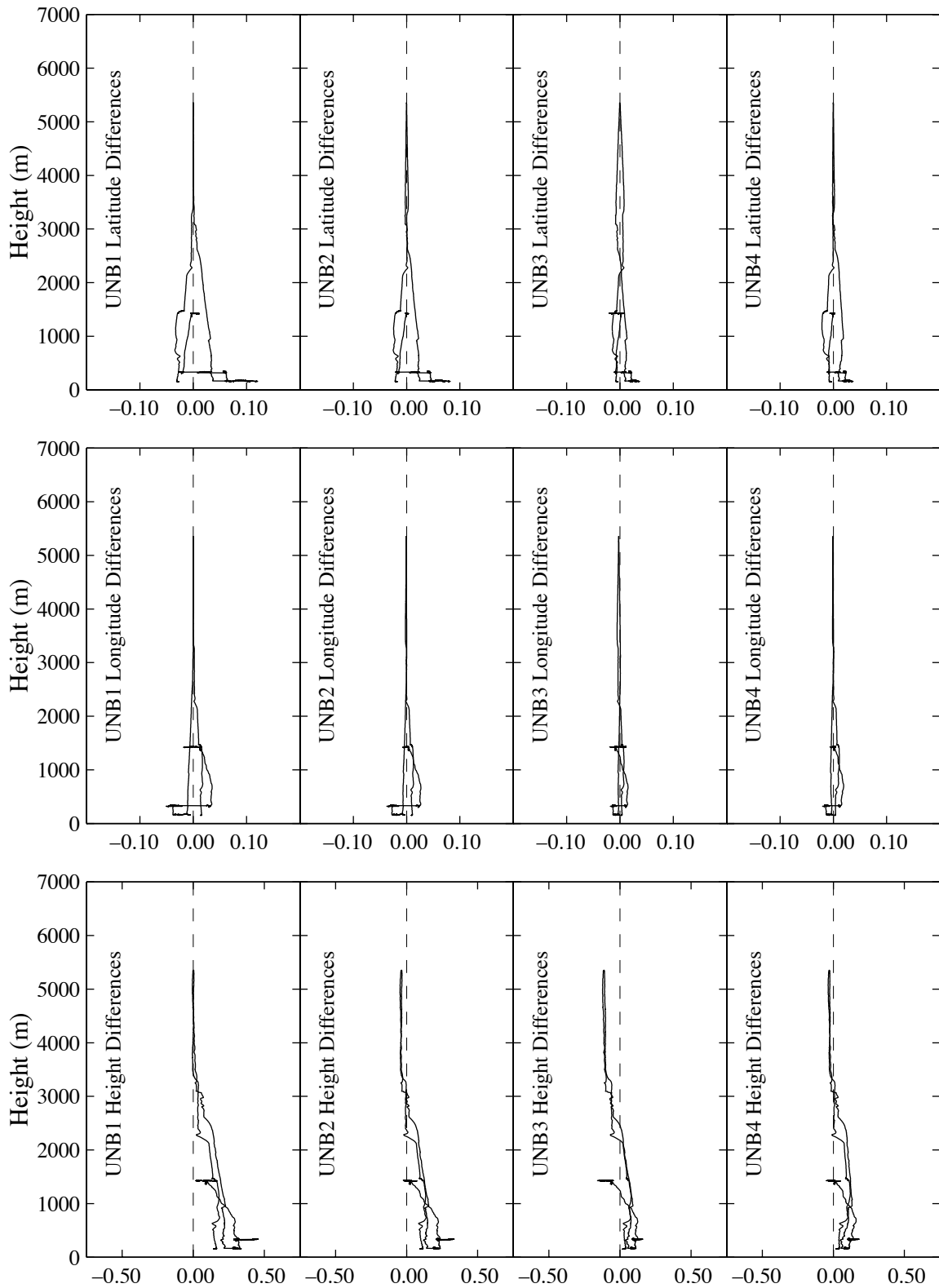
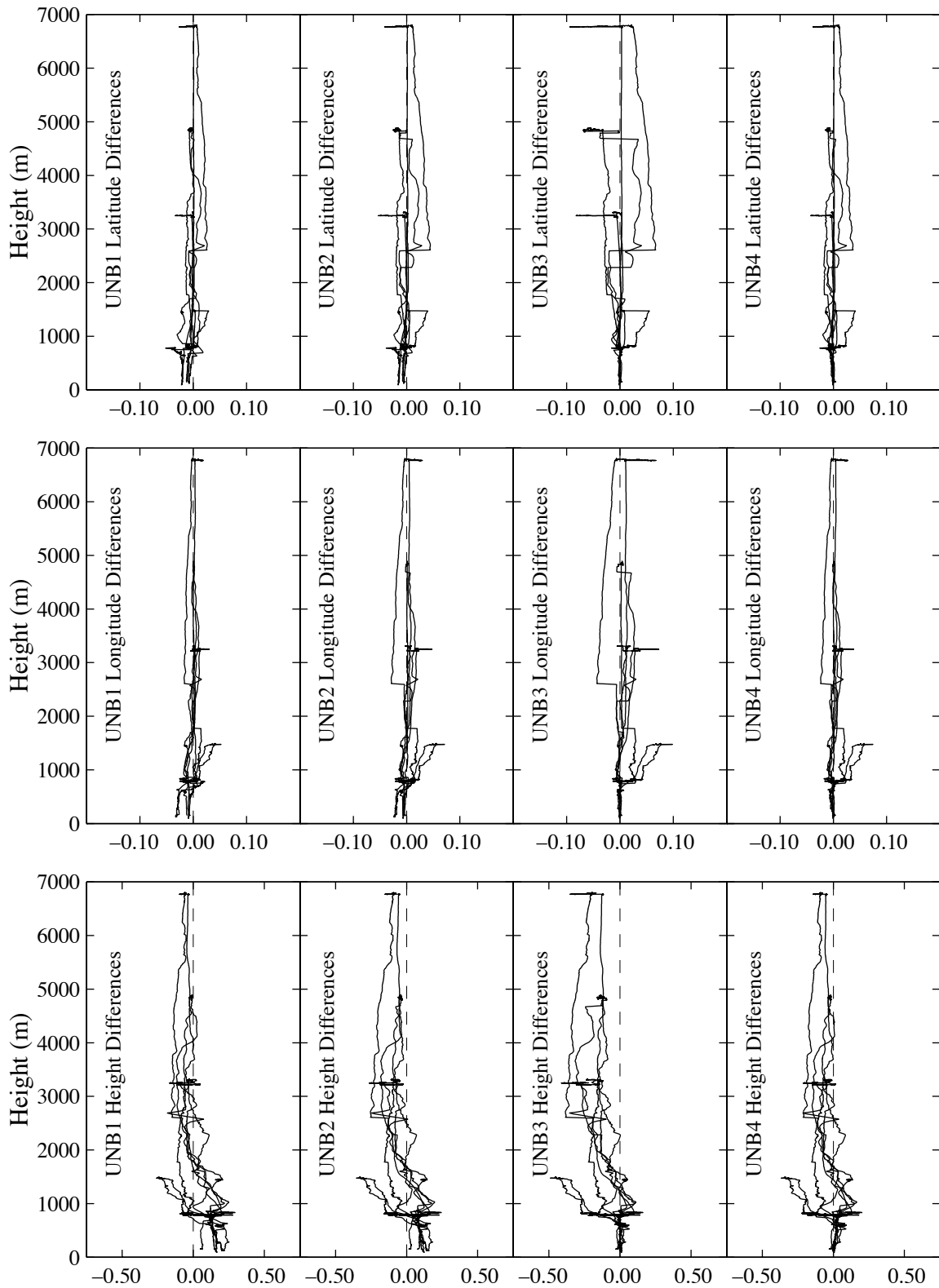**Figure B1.1. Solution Differences for Flight F503, March 03, 1995.**

100
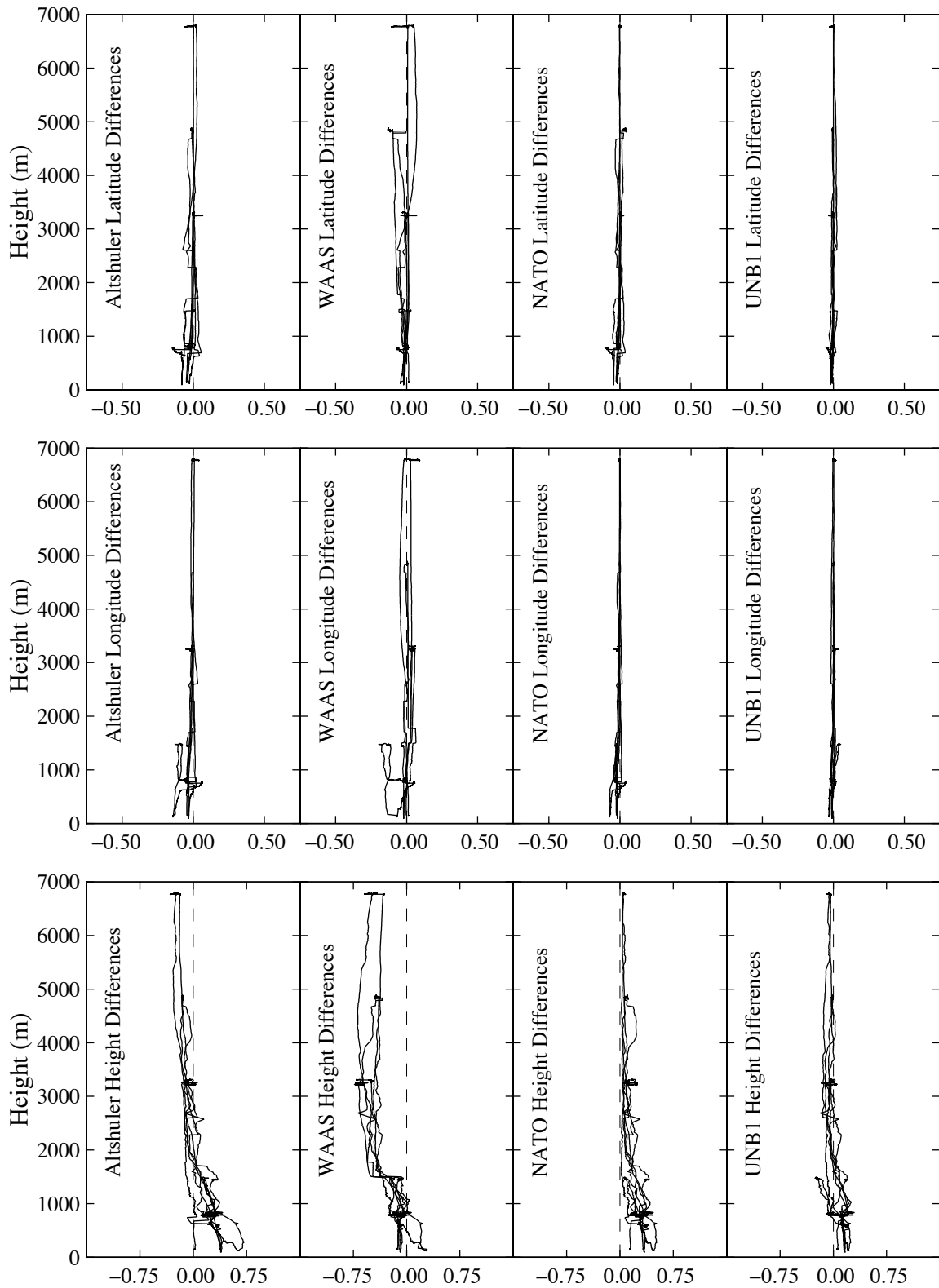
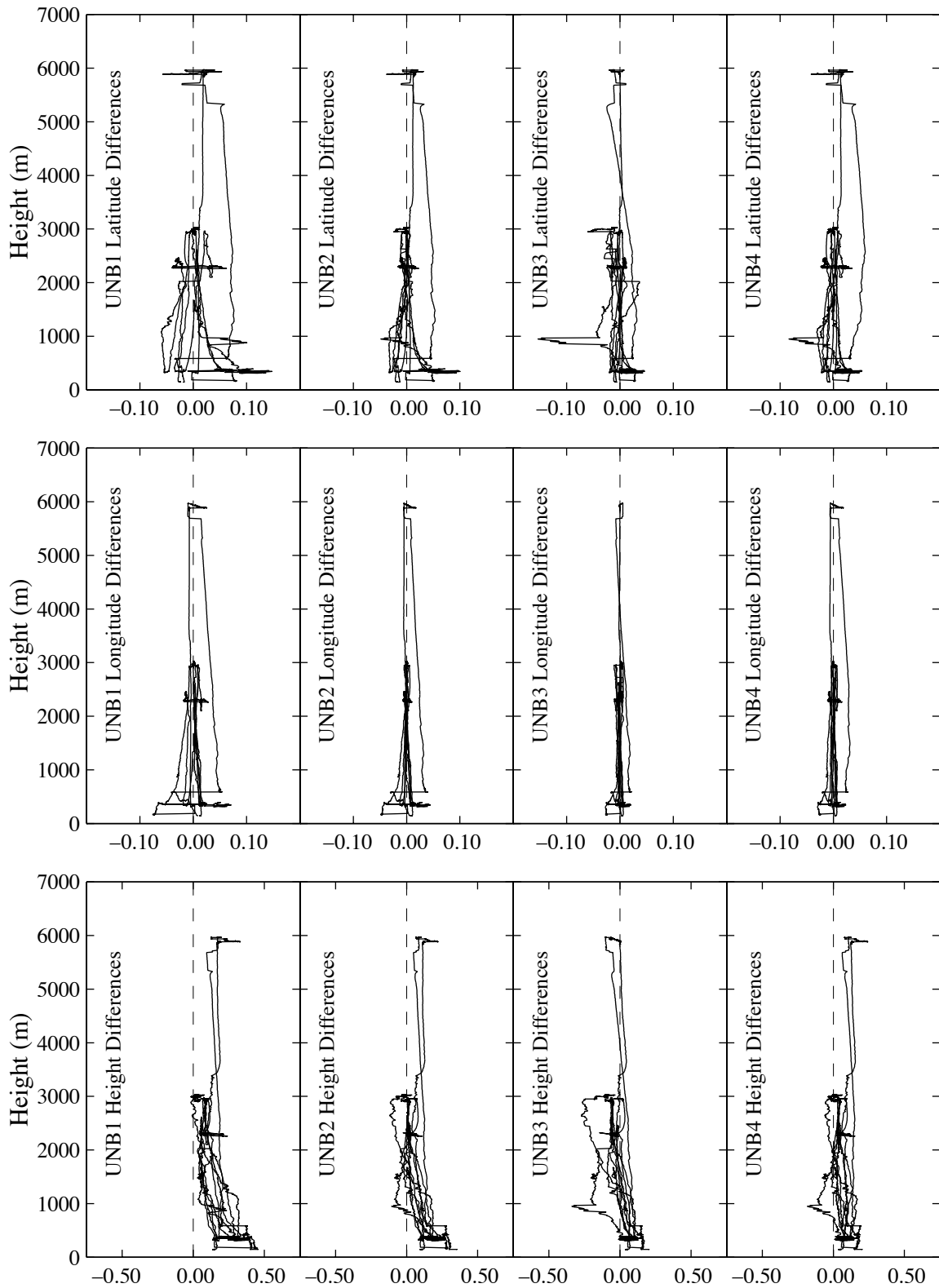**Figure B1.2. Solution Differences for Flight F504, March 06, 1995.**
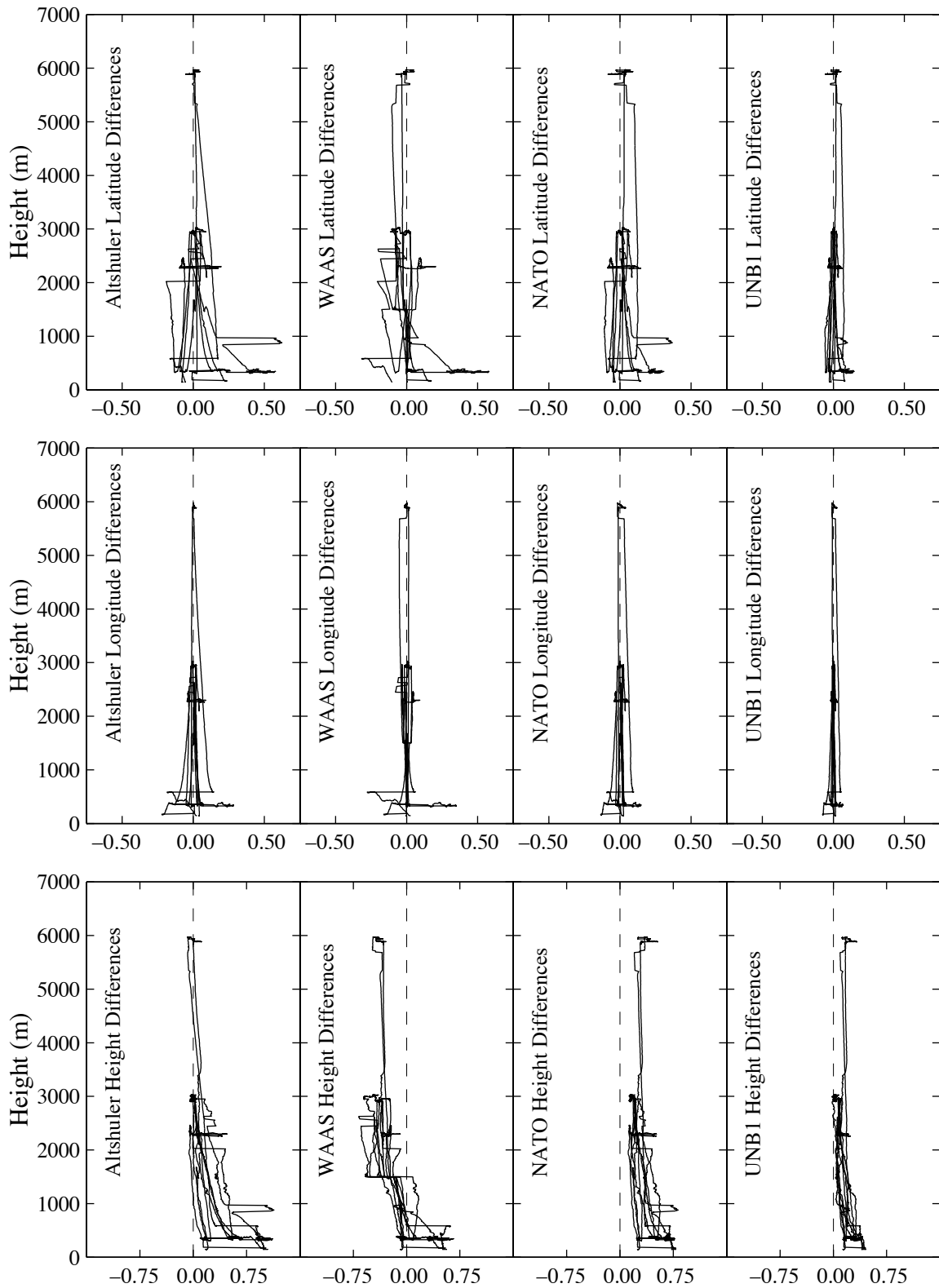
Figure B1.3. Solution Differences for Flight F505, March 07, 1995.
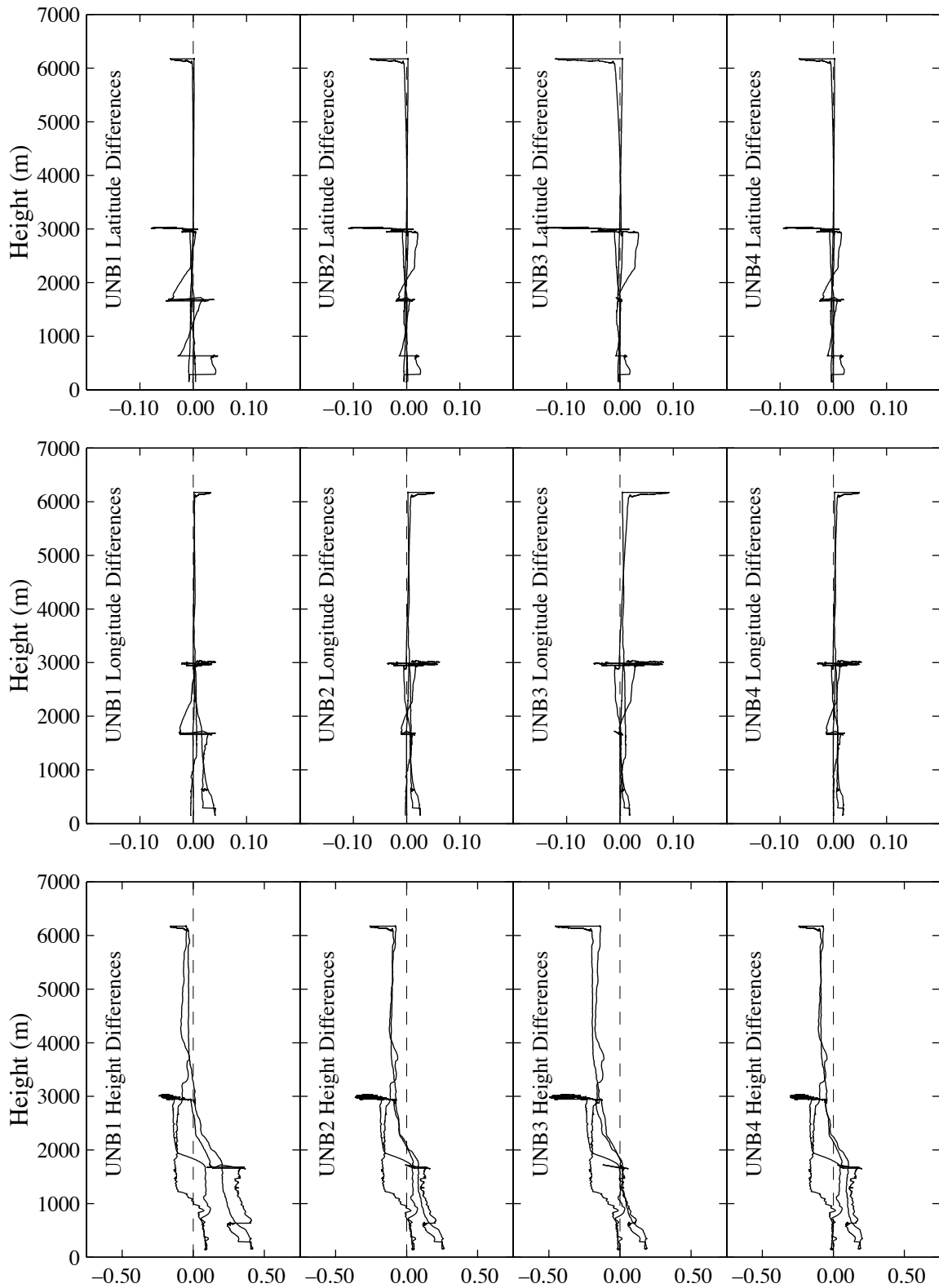
102
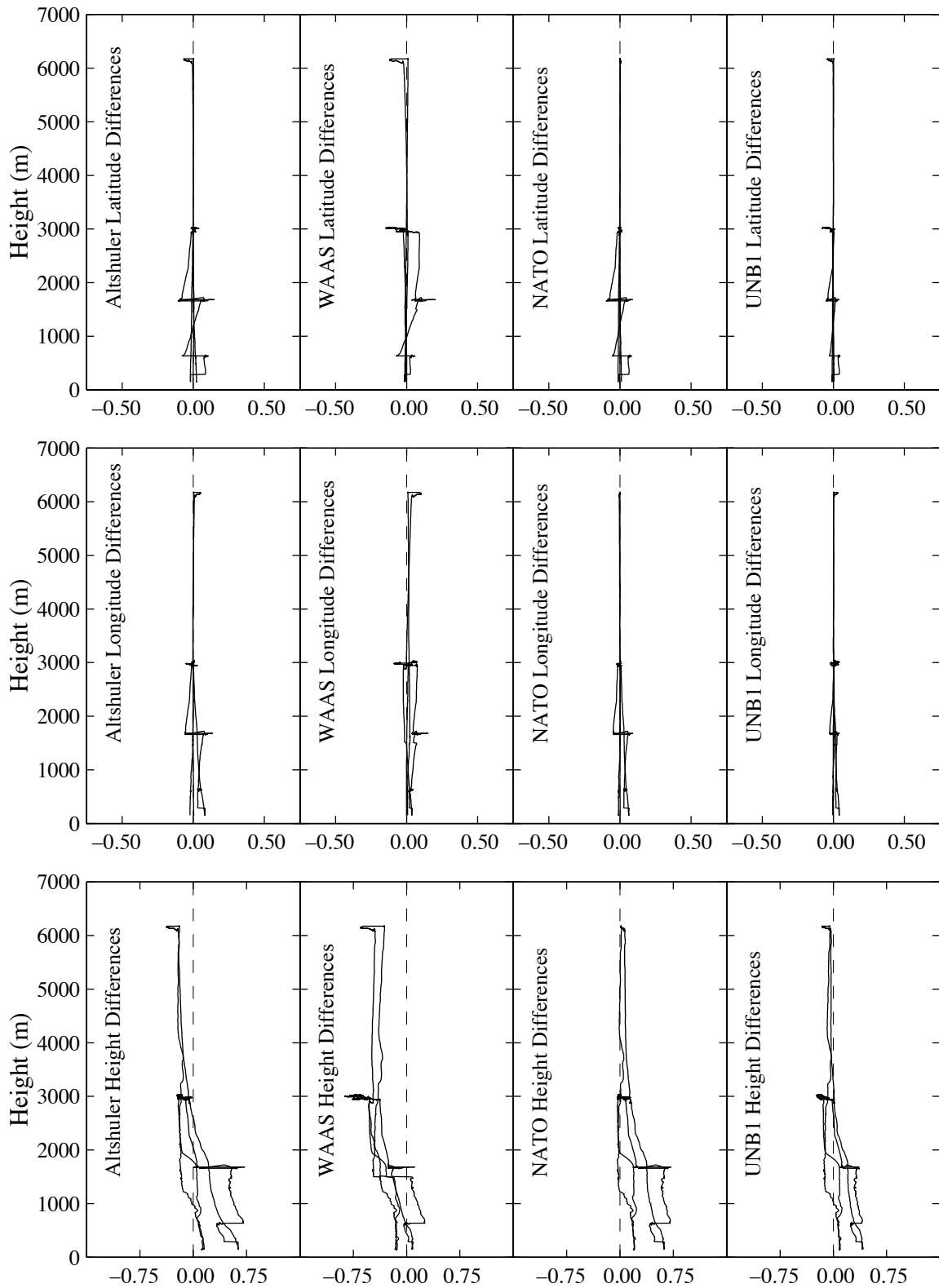
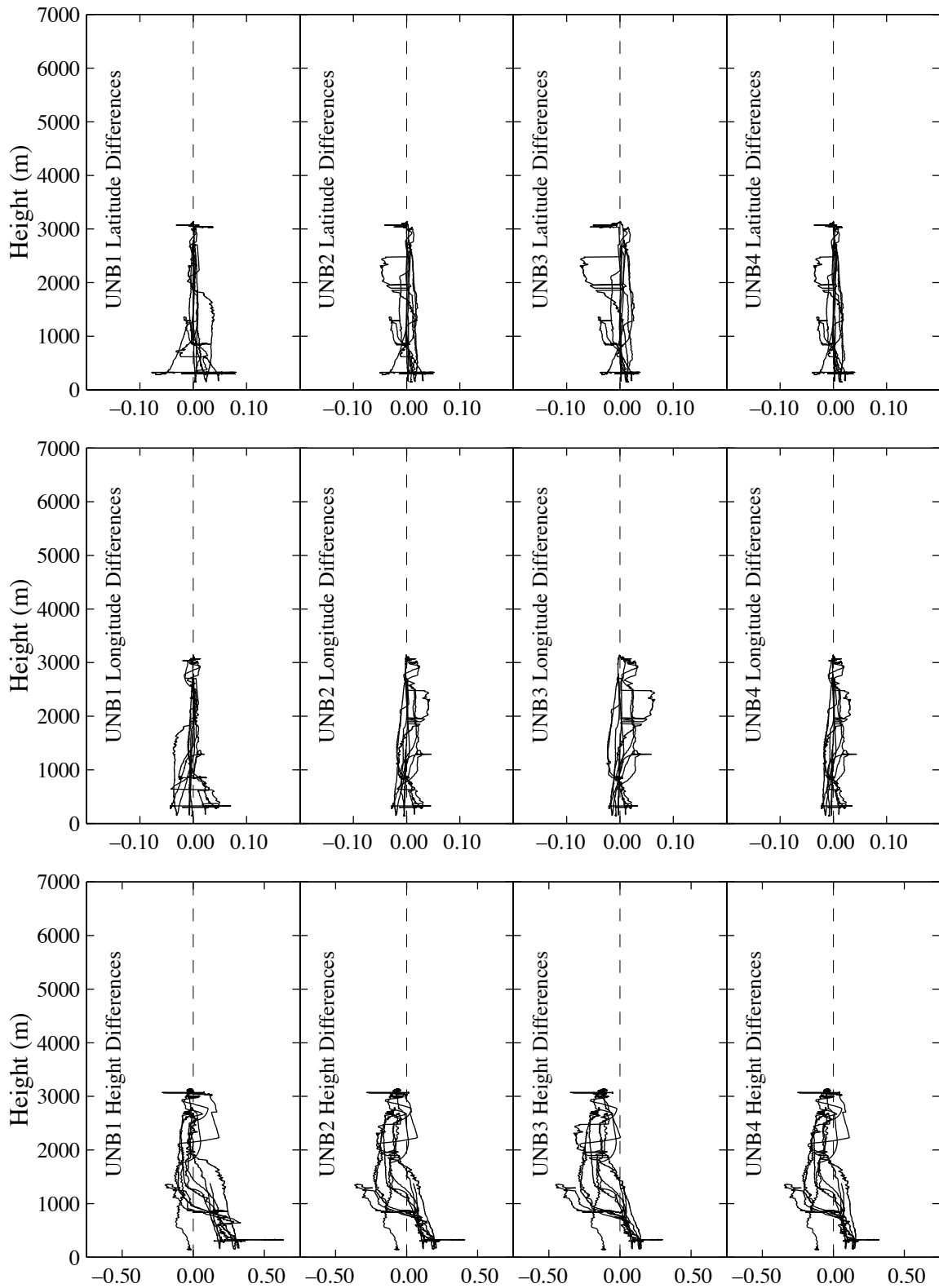**Figure B1.4. Solution Differences for Flight F506, March 08, 1995.**
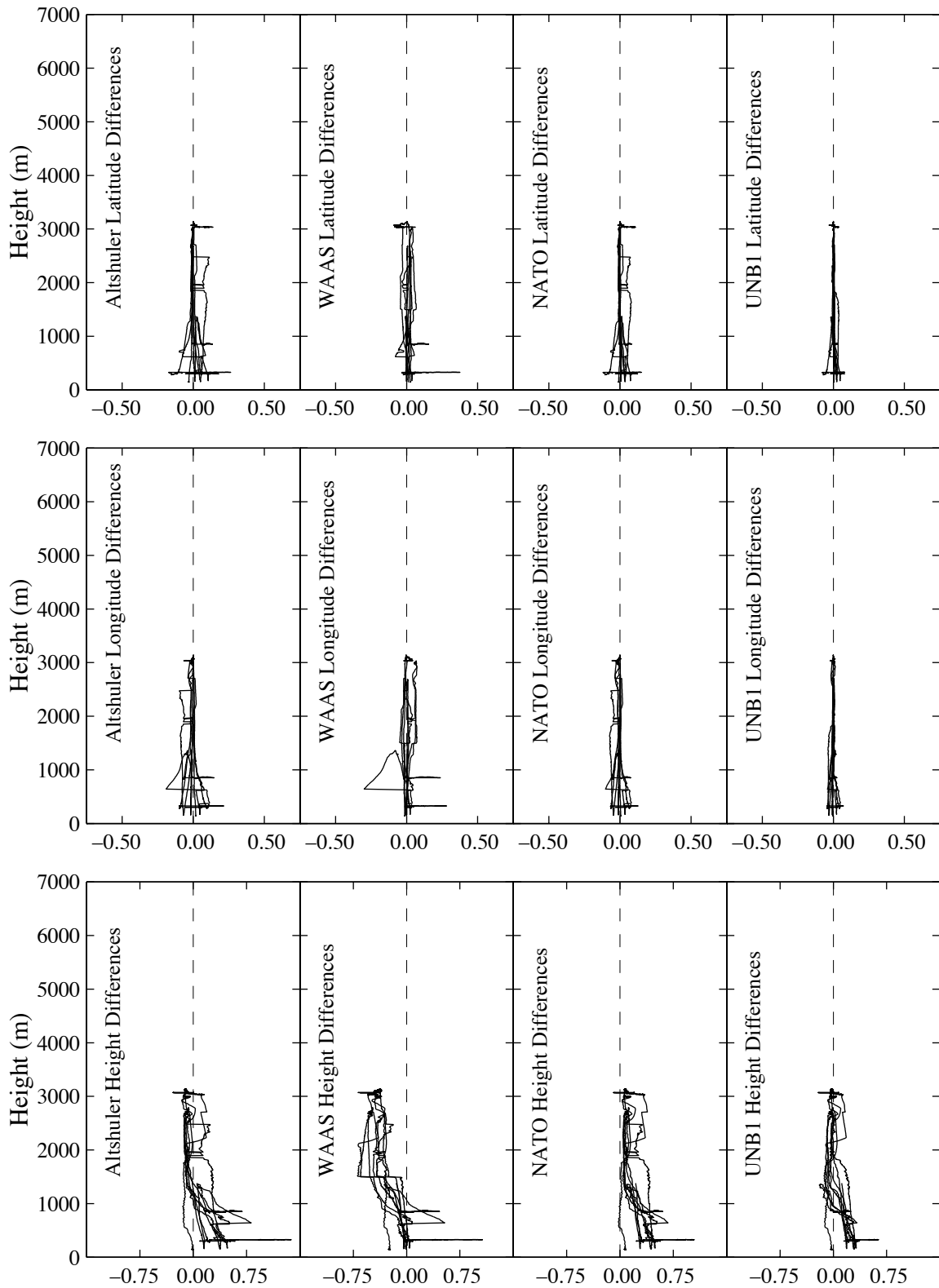
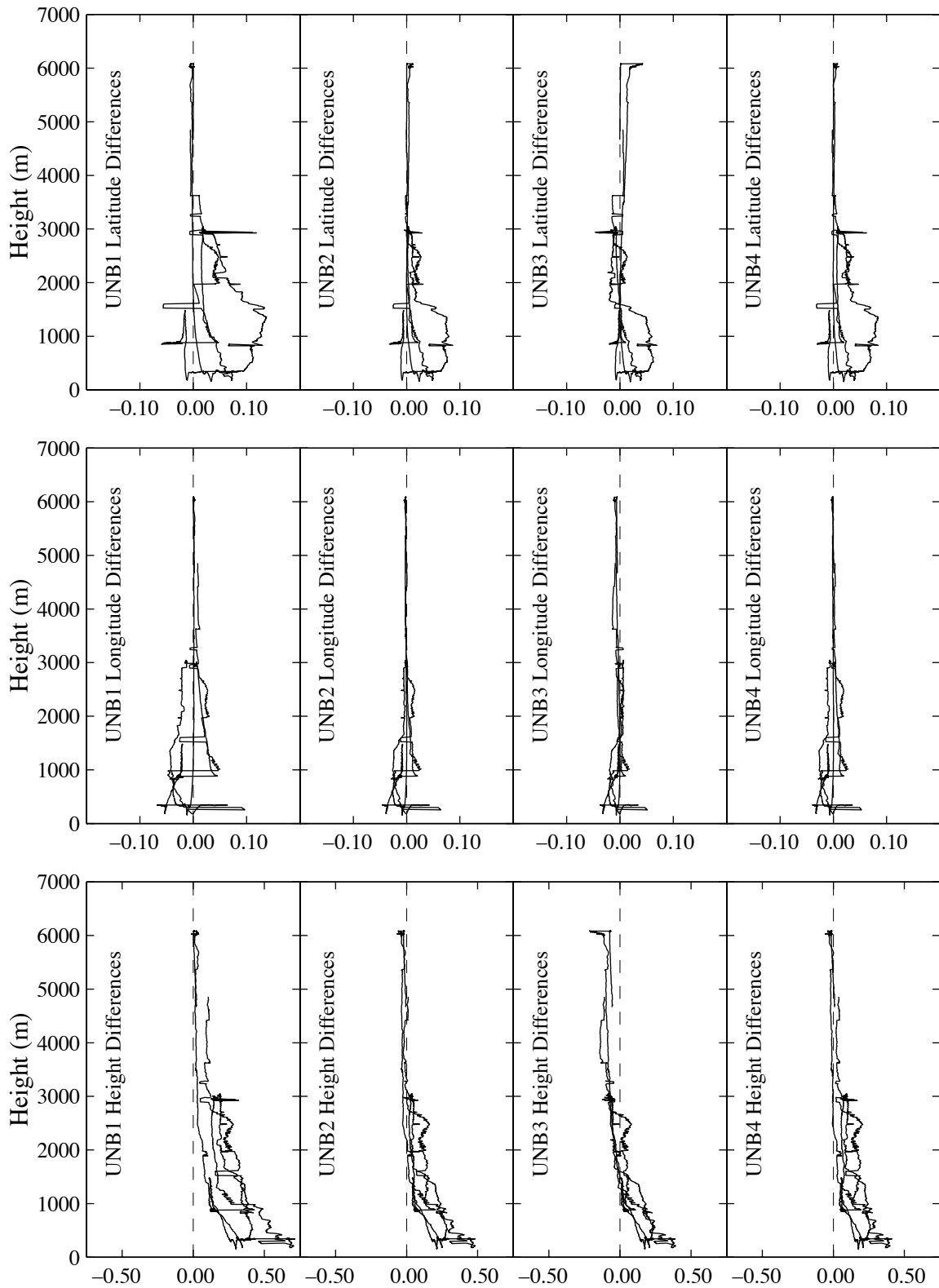**Figure B1.5. Solution Differences for Flight F507, March 09, 1995.**
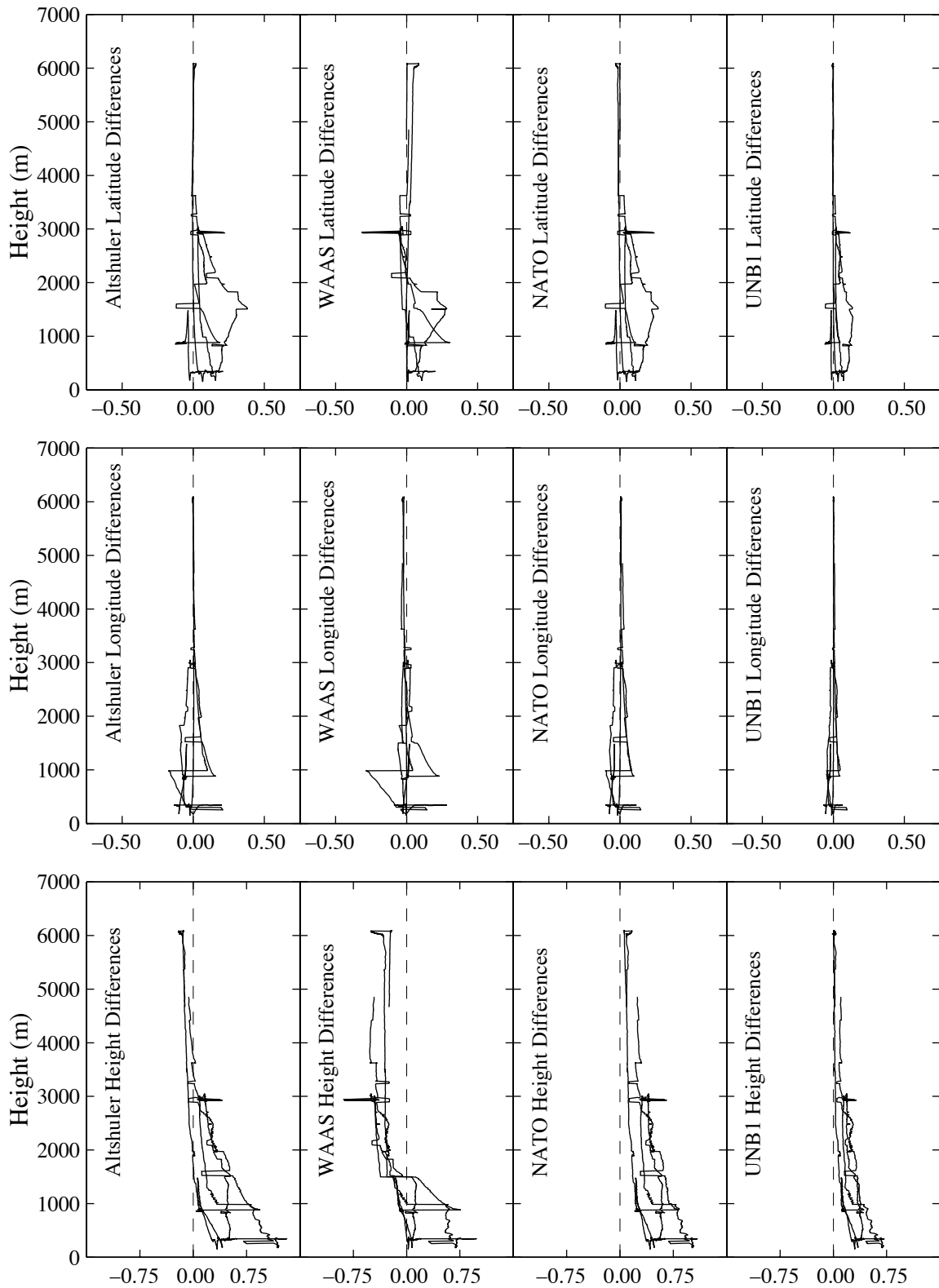
Figure B1.6. Solution Differences for Flight F508, March 10, 1995.
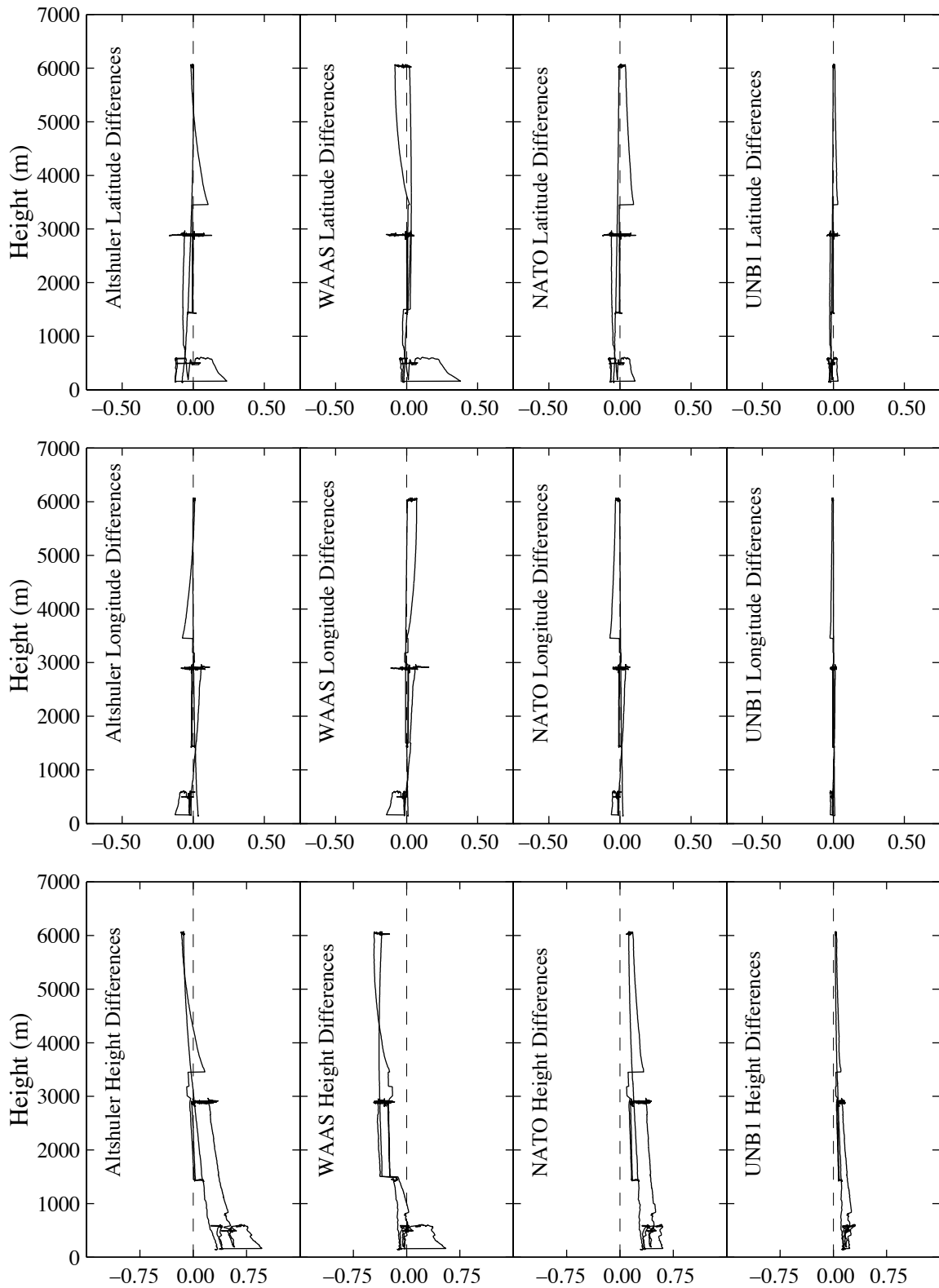
Figure B1.7. Solution Differences for Flight F509, March 13, 1995.
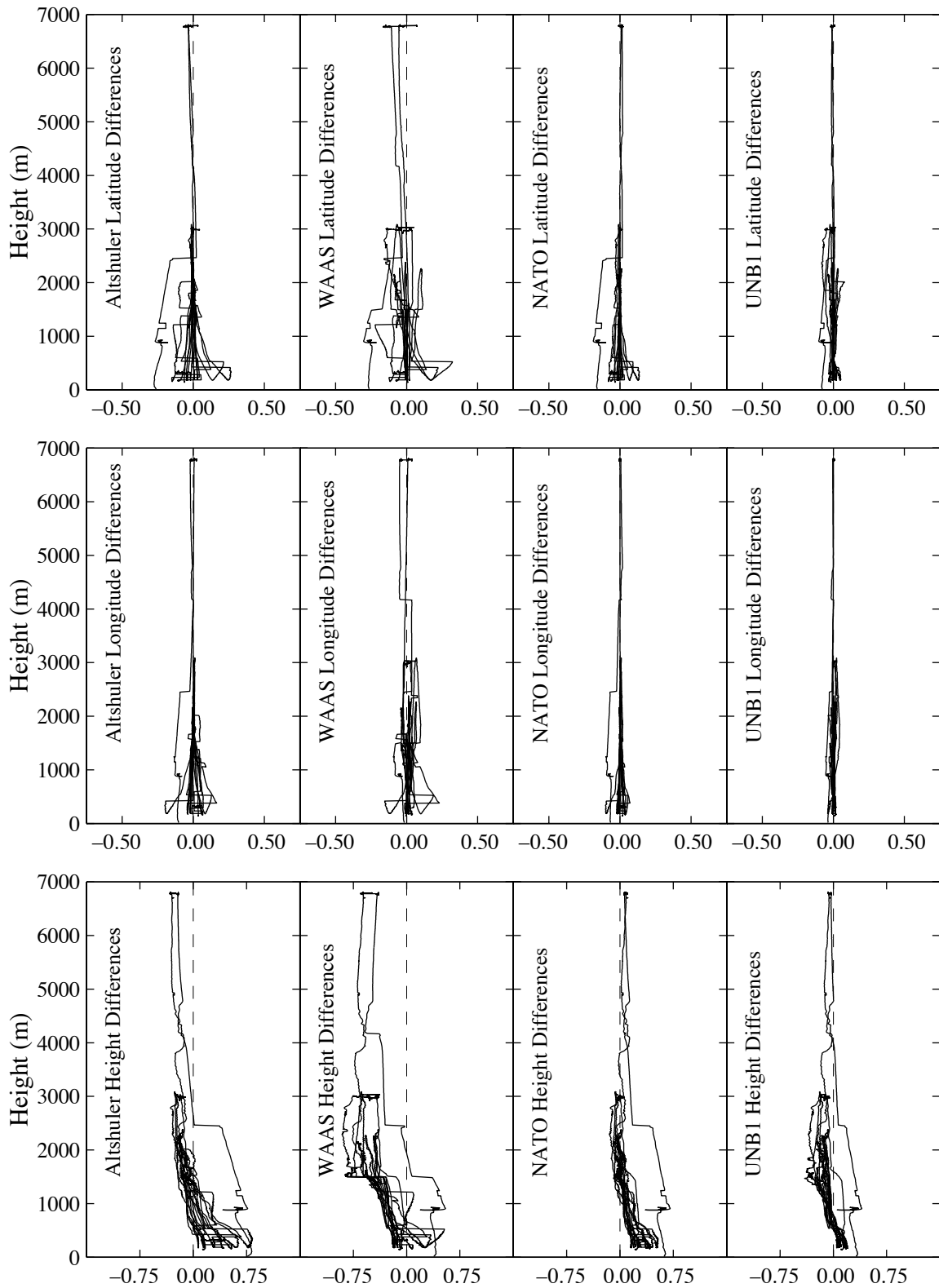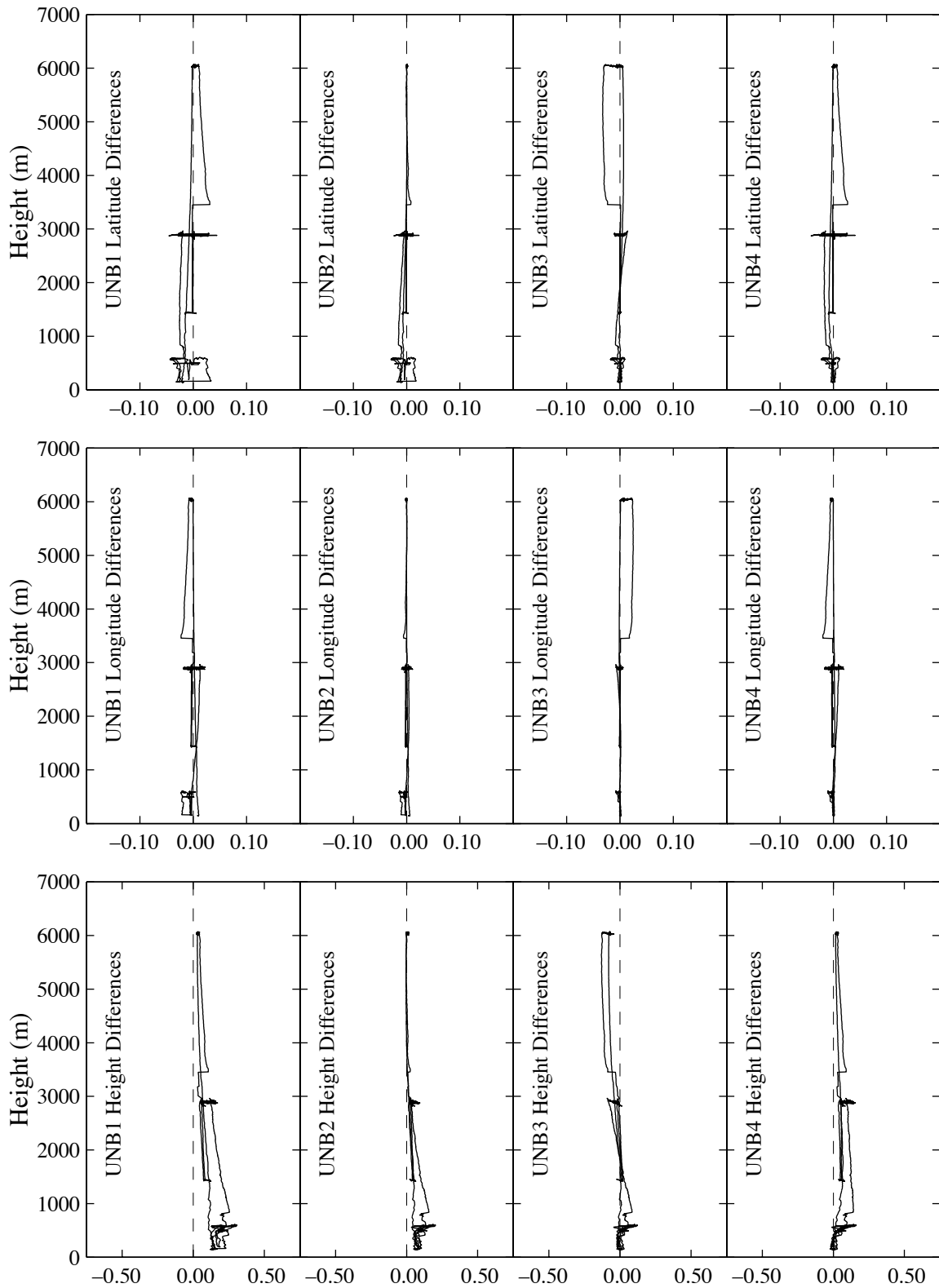
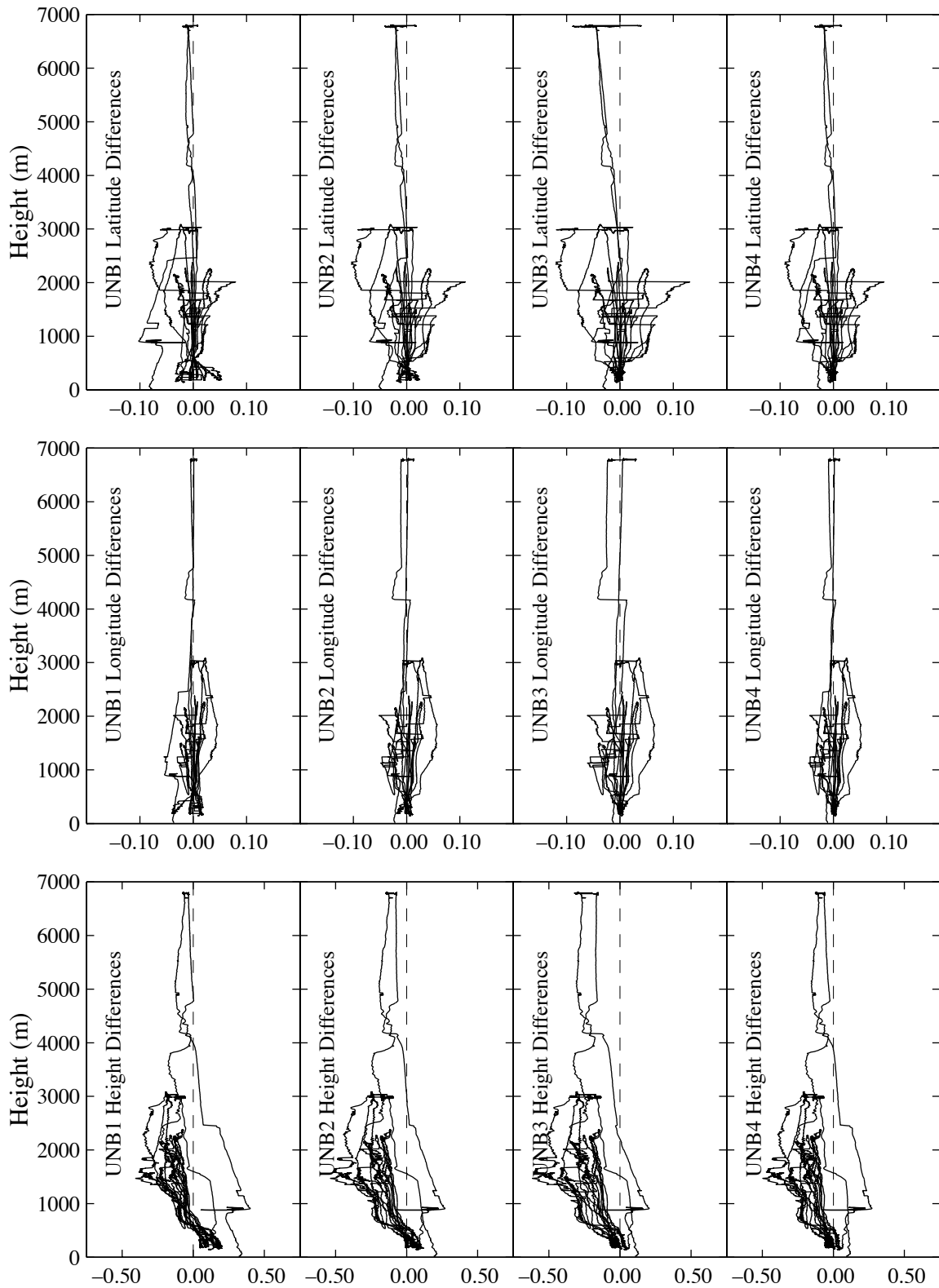**Figure B1.8. Solution Differences for Flight F510, March 14, 1995.**

107
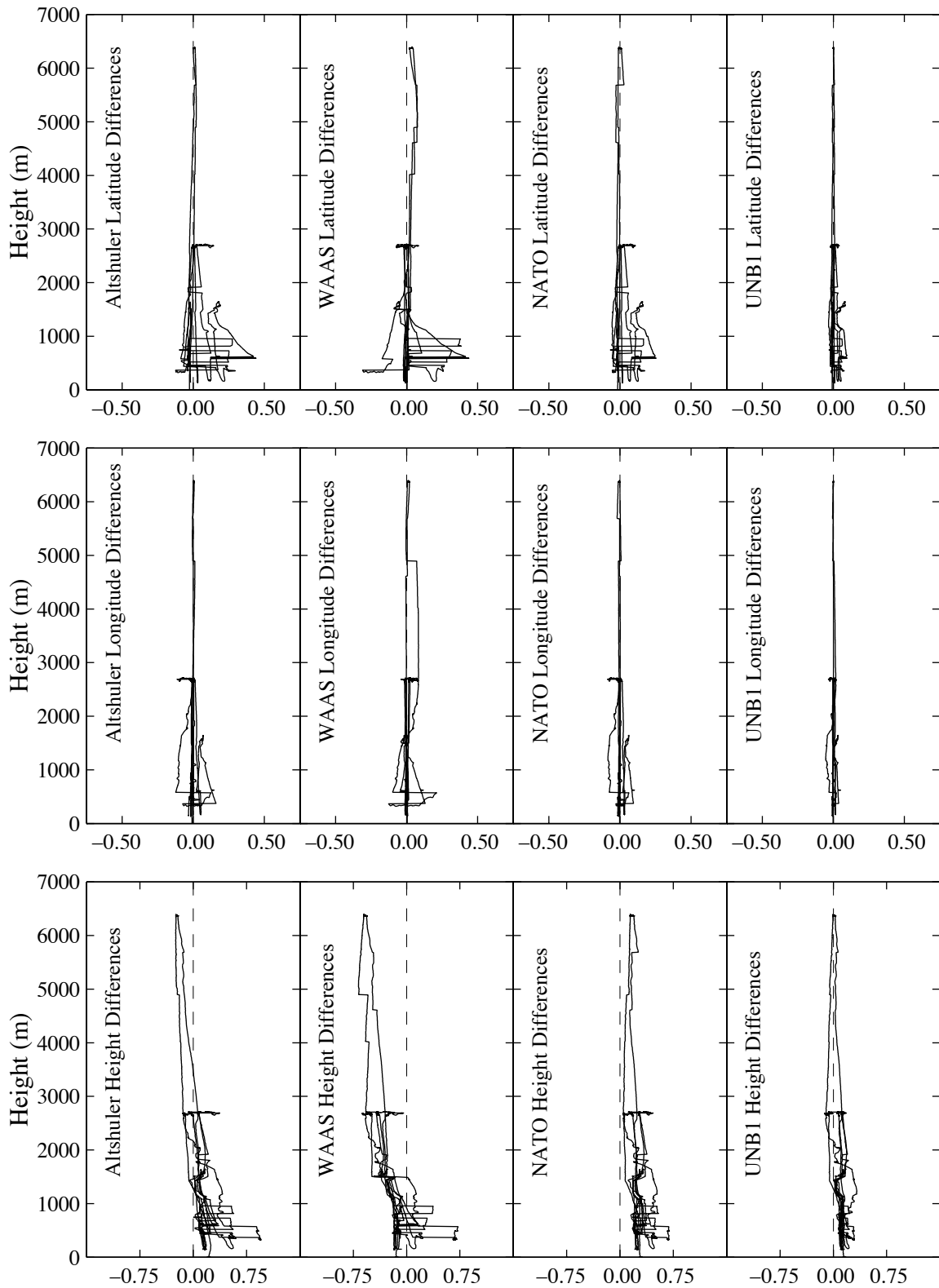
Figure B1.9. Solution Differences for Flight F511, March 15, 1995.

108
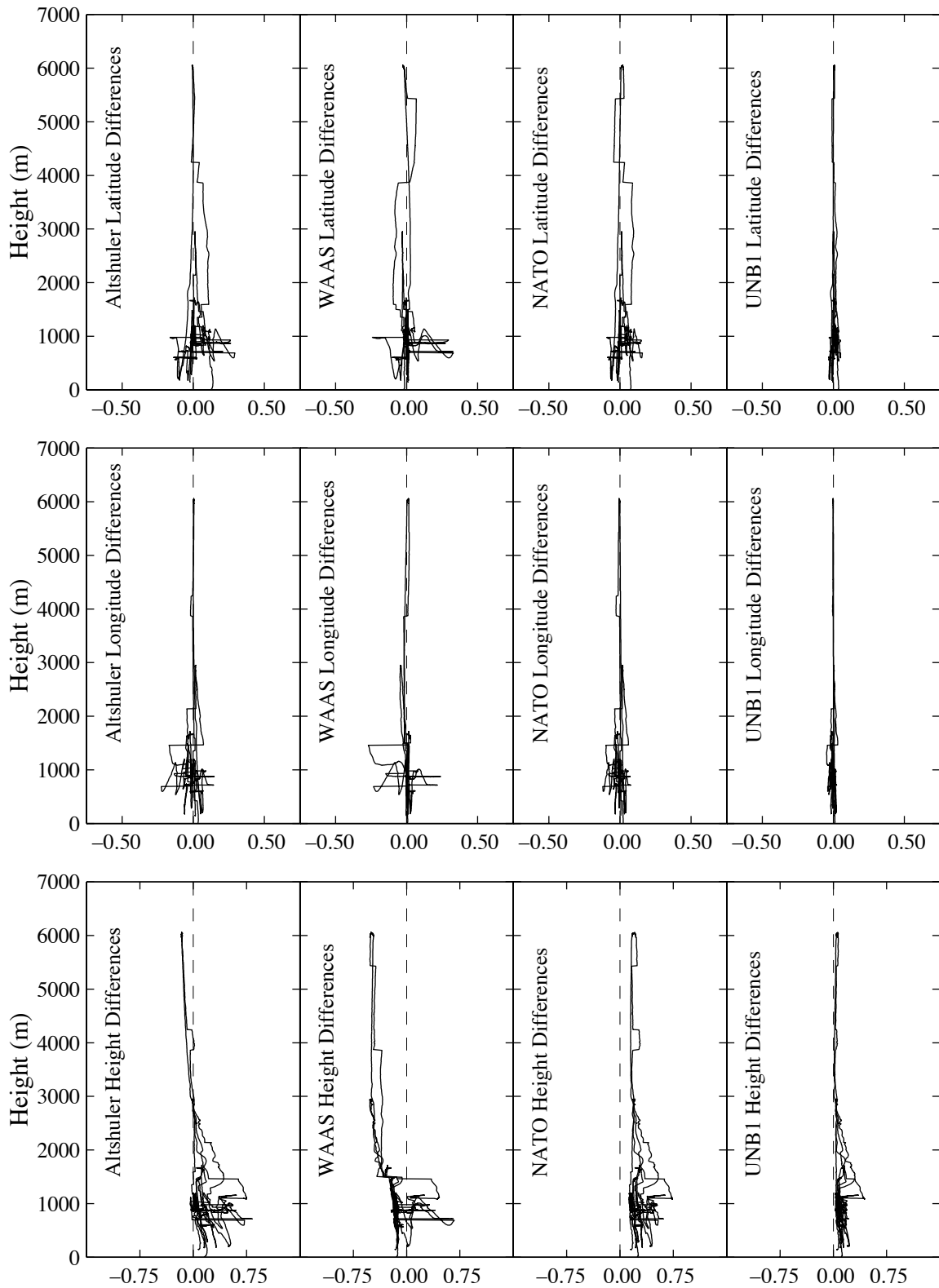
Figure B1.10. Solution Differences for Flight F512, March 17, 1995.
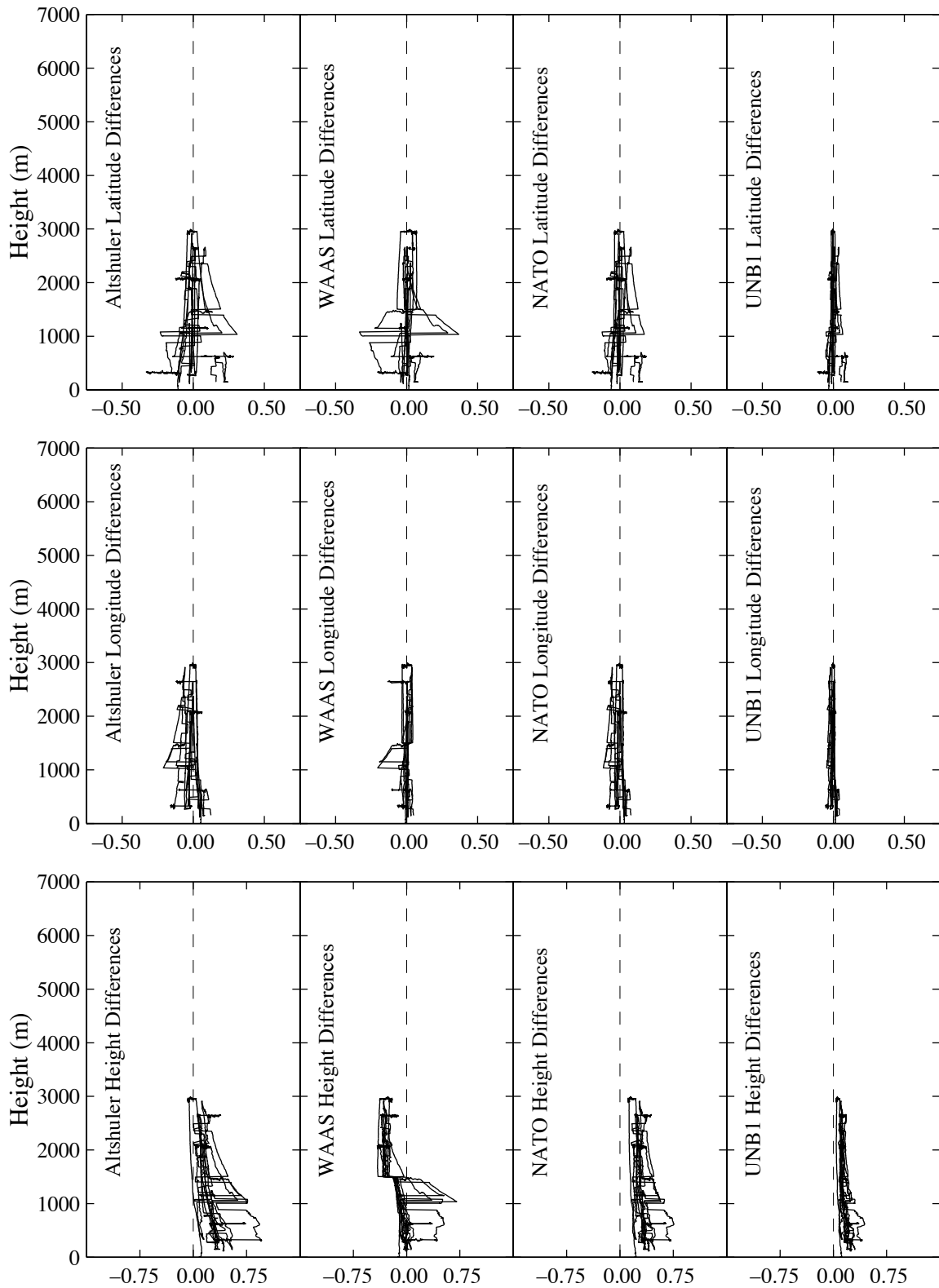
Figure B1.11. Solution Differences for Flight F513, March 18, 1995.
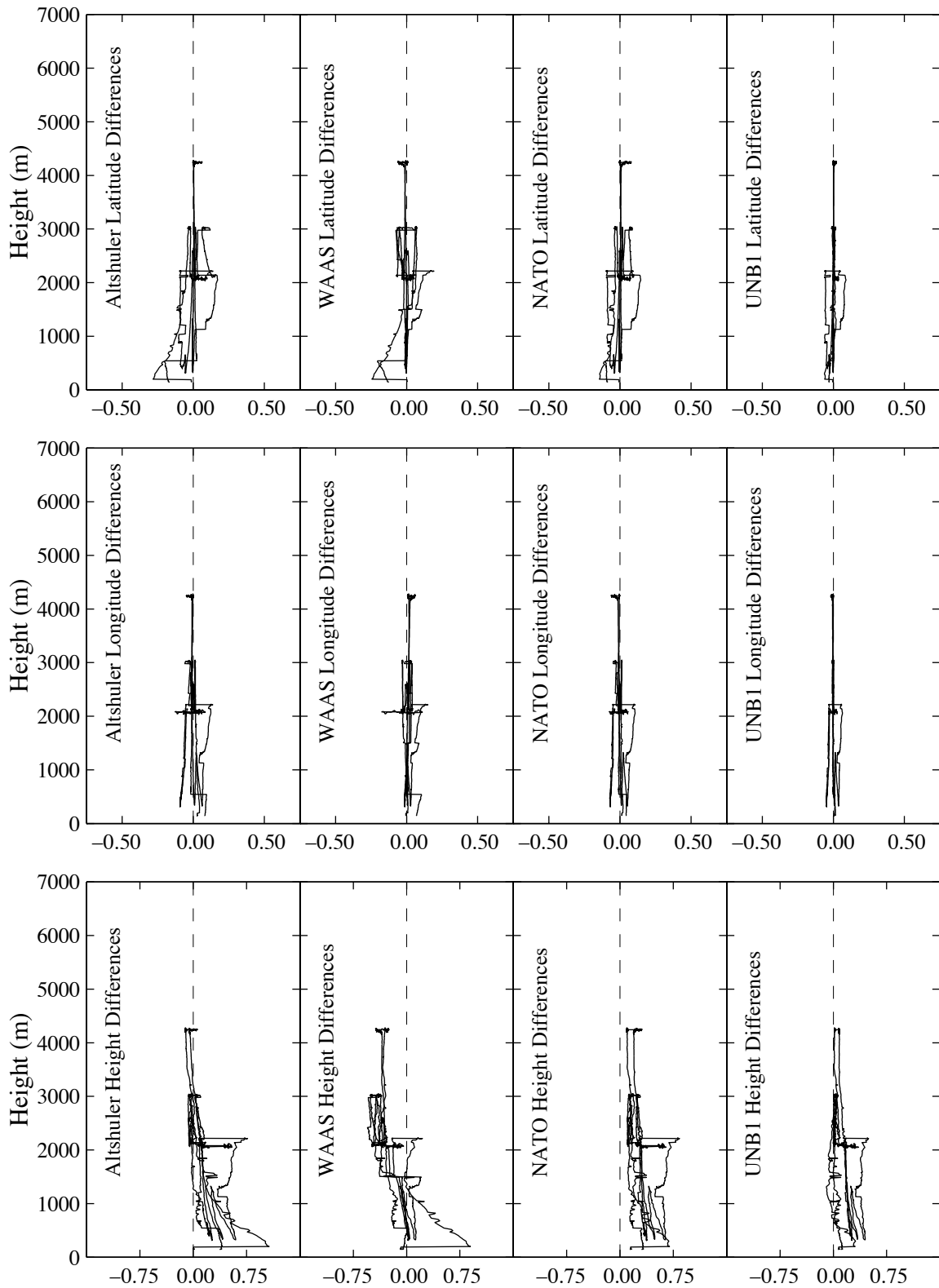
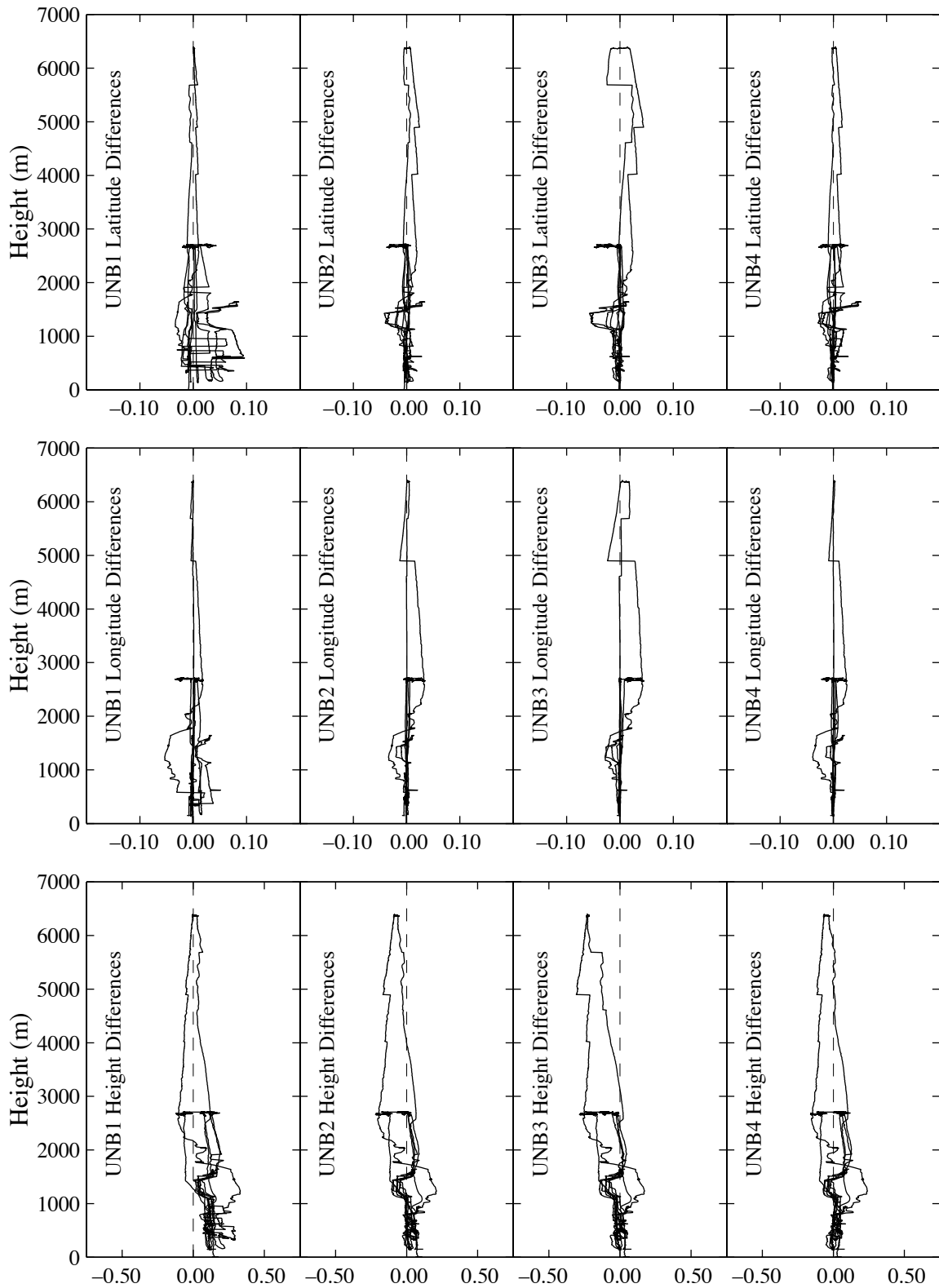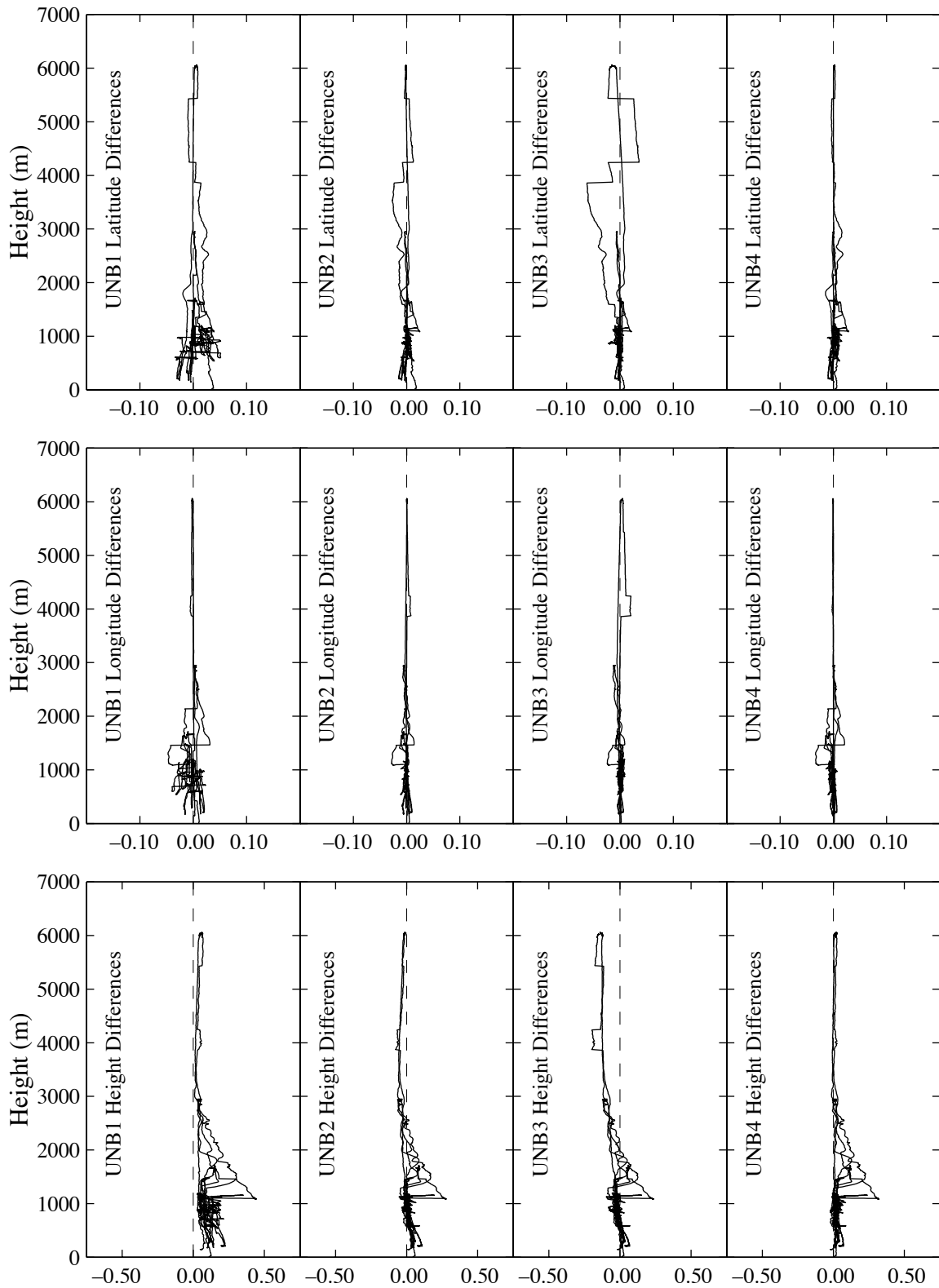**Figure B1.12. Solution Differences for Flight F516, March 22, 1995.**

APPENDIX B2 Navigation-Type Models:

Solution Position Differences With Respect To Time

The following plots present the same information as the previous section, that is the differences between the benchmark solutions and those calculated with the navigation-type tropospheric delay models. However the differences are now plotted against time. In addition, for the purposes of providing more information, each plot also shows the distance of the aircraft from the reference station, the relative Position Dilution of Precision (PDOP, as a function of the differential satellite geometry) and the height of the aircraft. (See Figure 3.3 for an example in the main part of the report.)
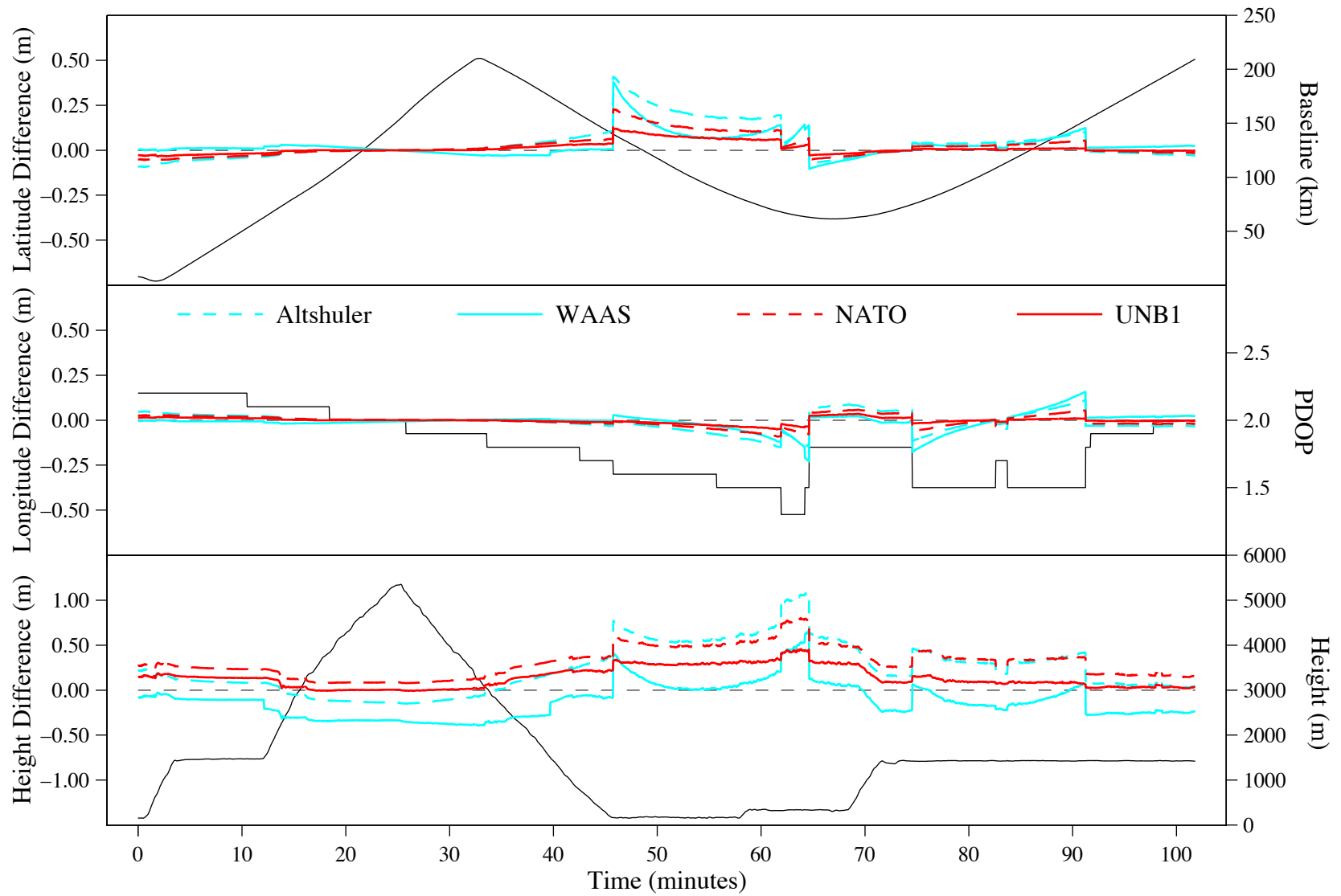
Figure B2.1. Solution Differences for Flight F503, March 03, 1995.
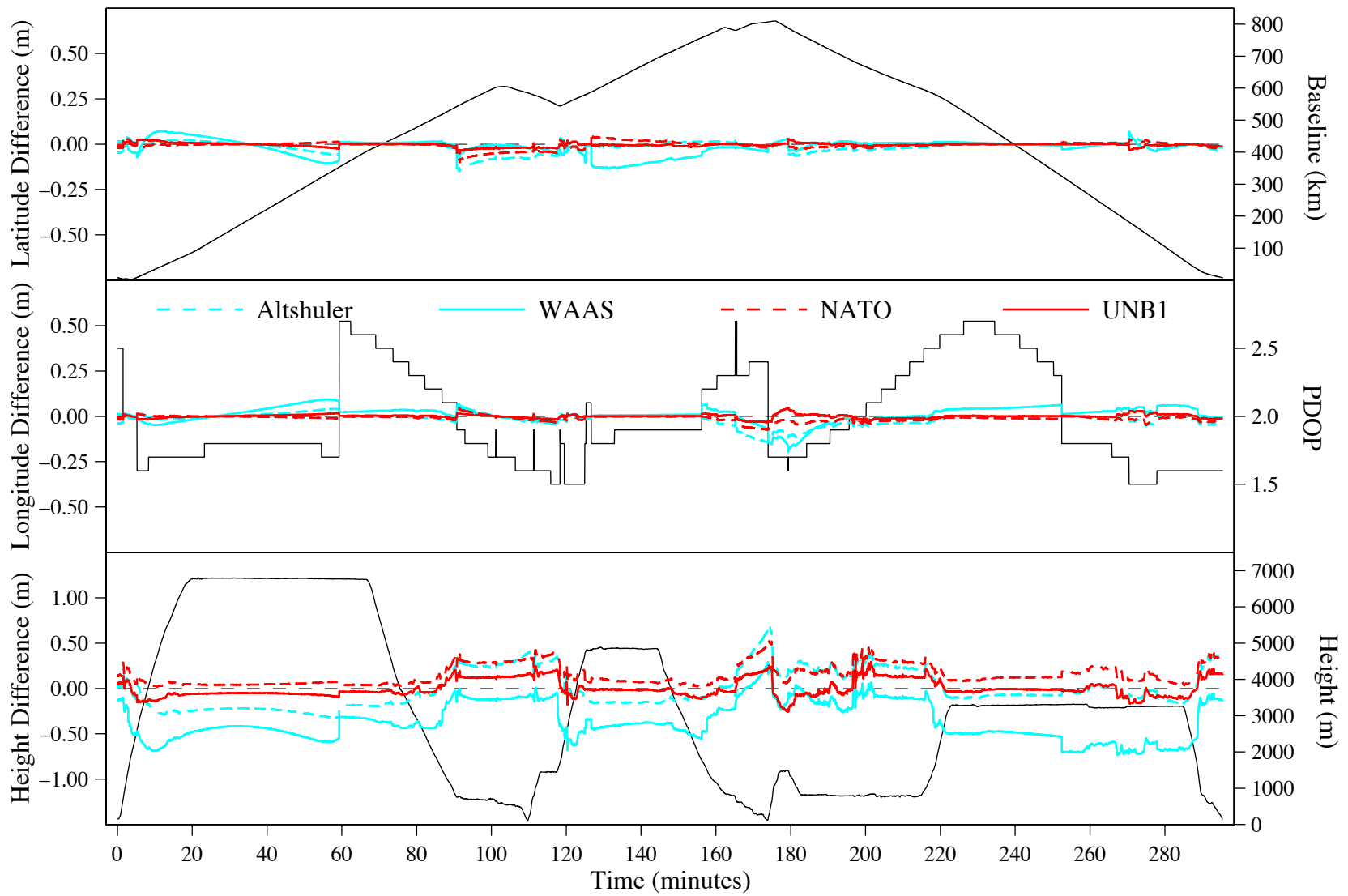
Figure B2.2. Solution Differences for Flight F504, March 06, 1995.

114
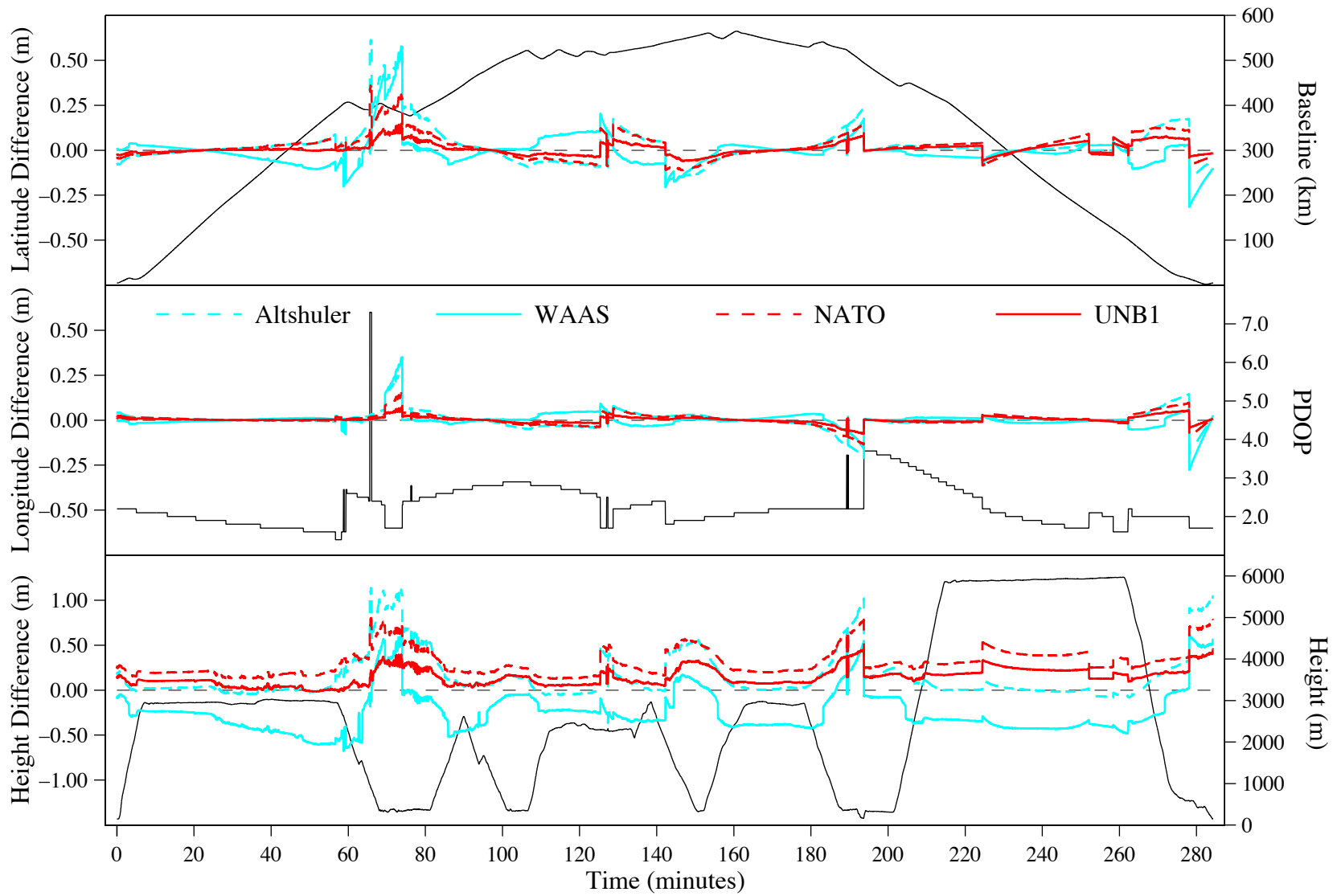
Figure B2.3. Solution Differences for Flight F505, March 07, 1995.
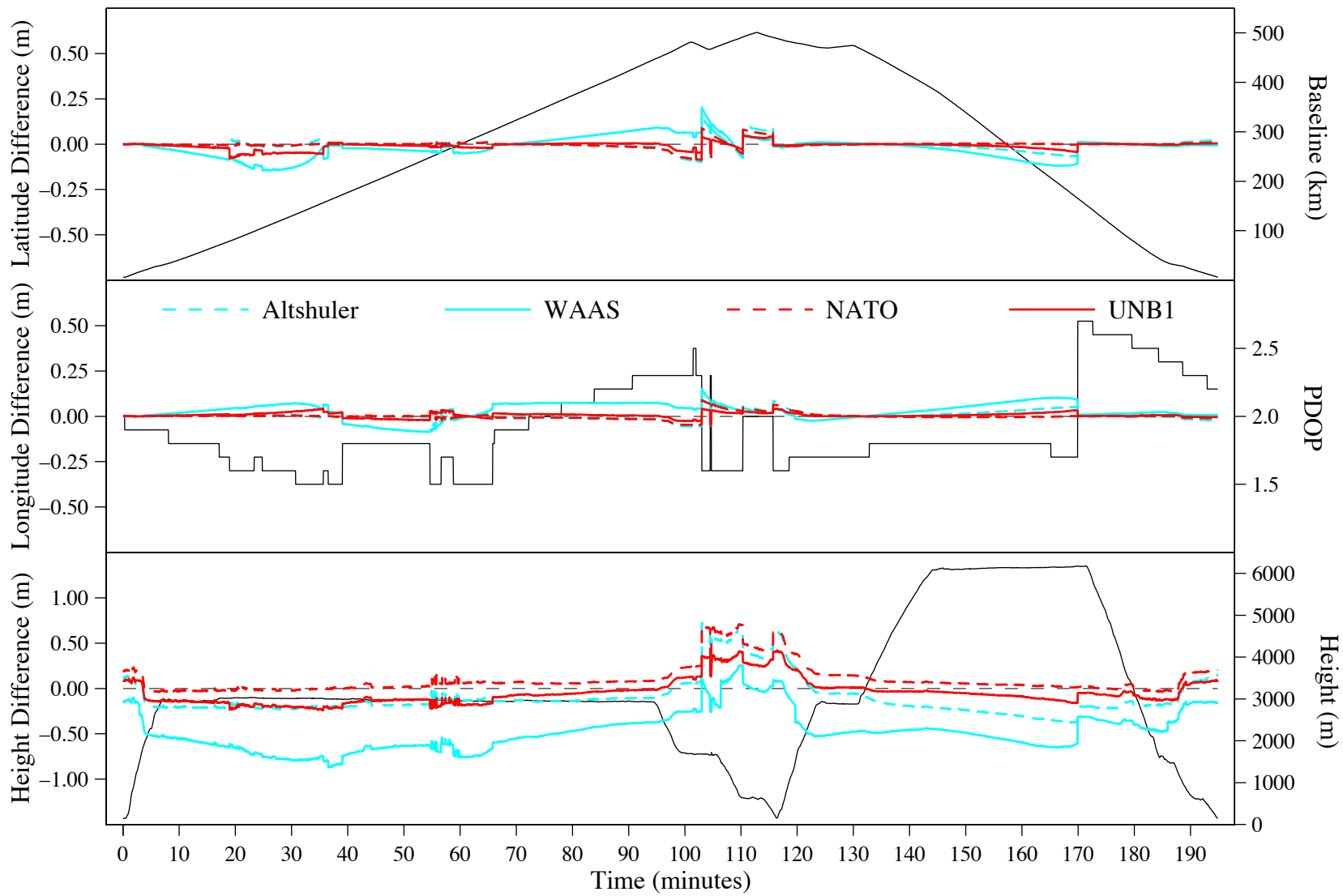
Figure B2.4. Solution Differences for Flight F506, March 08, 1995.
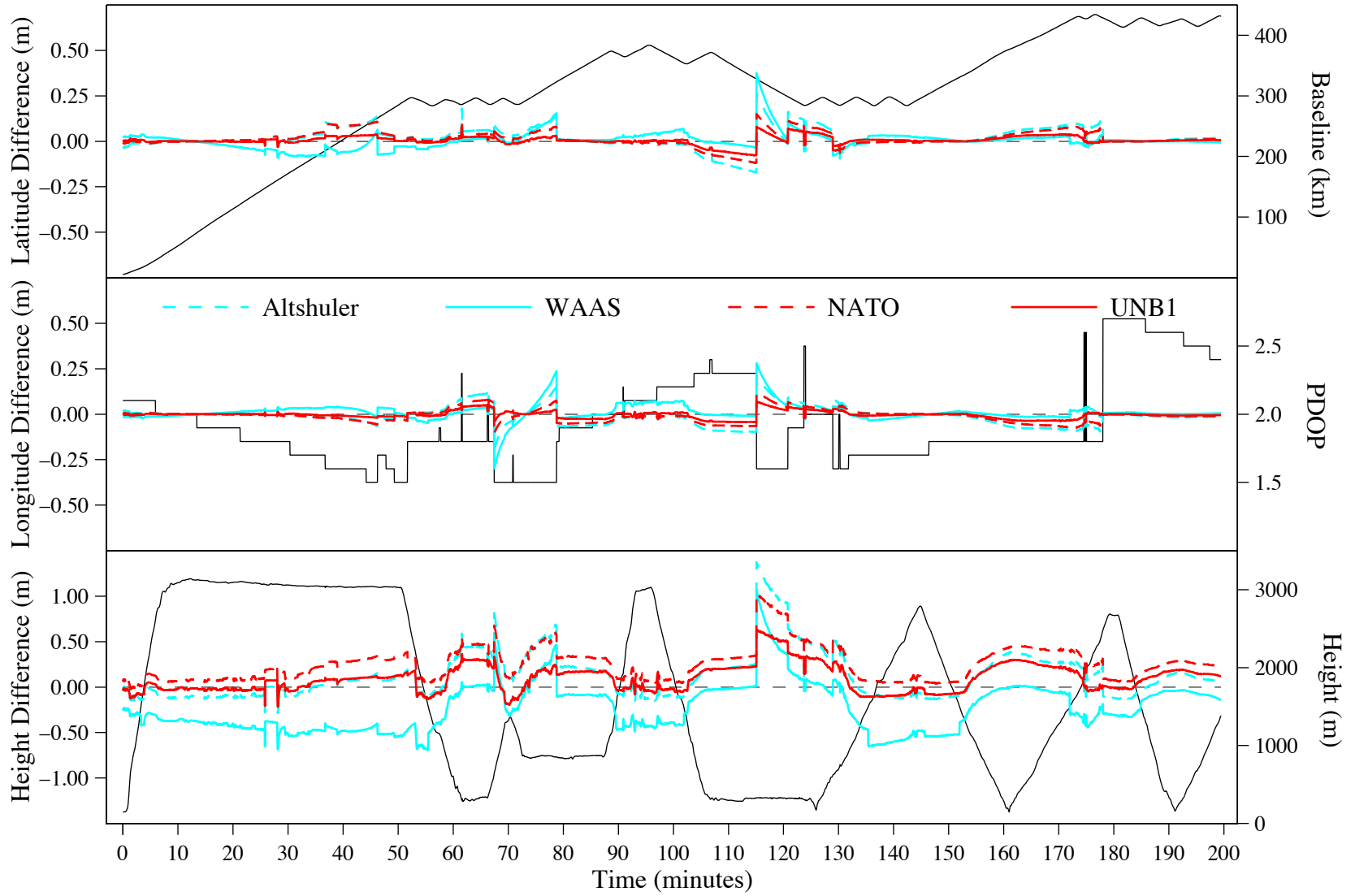
Figure B2.5. Solution Differences for Flight F507, March 09, 1995.
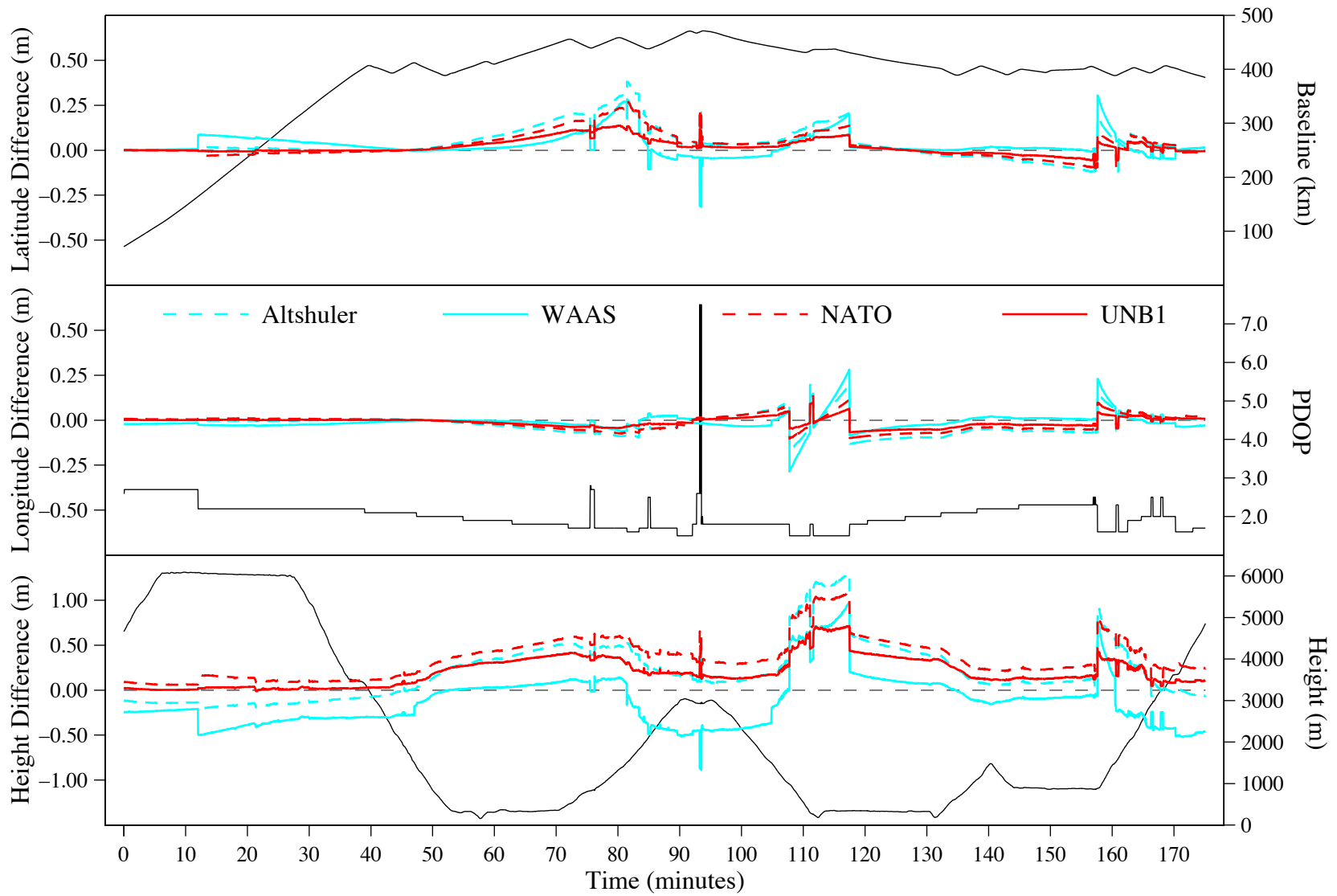
Figure B2.6. Solution Differences for Flight F508, March 10, 1995.
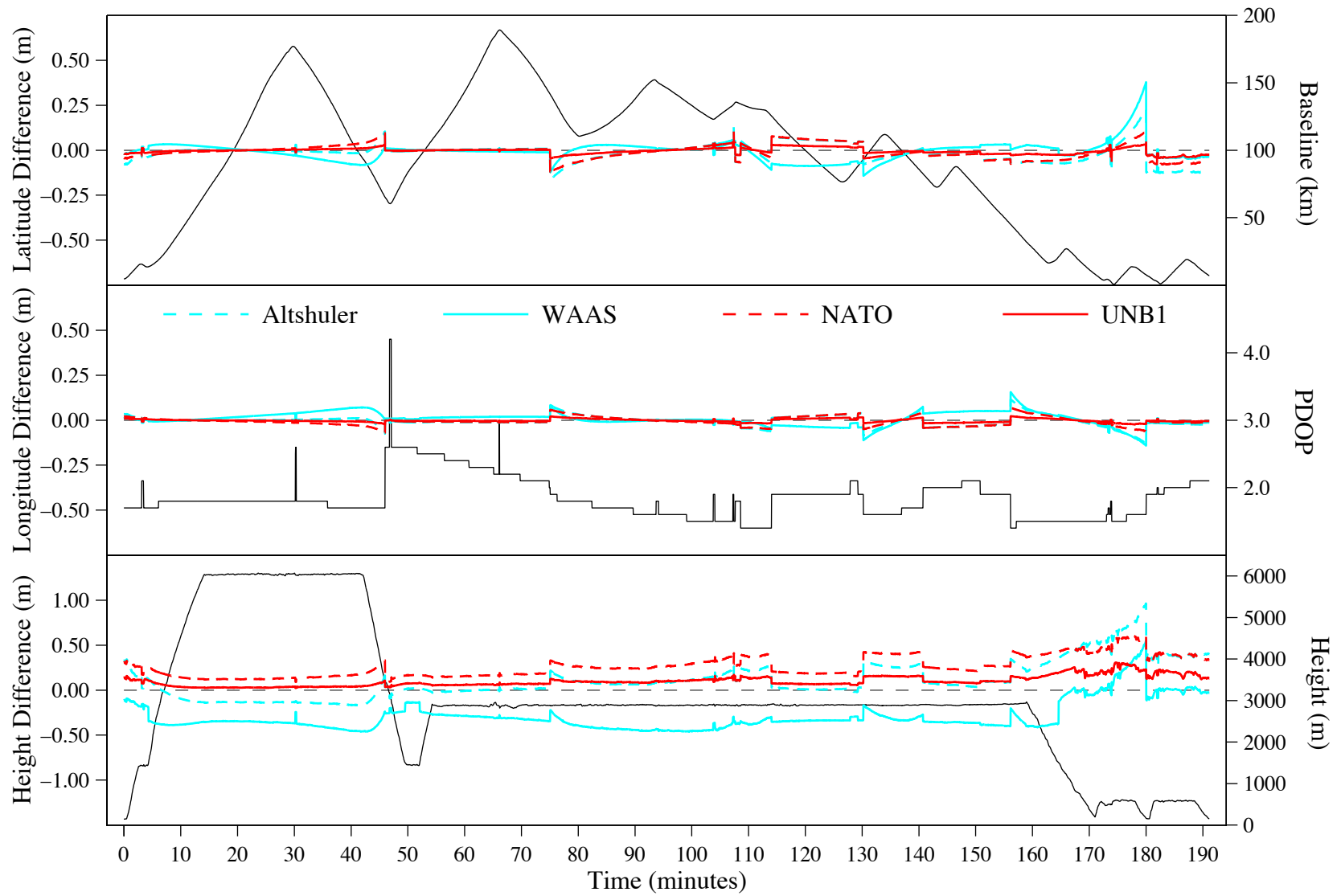
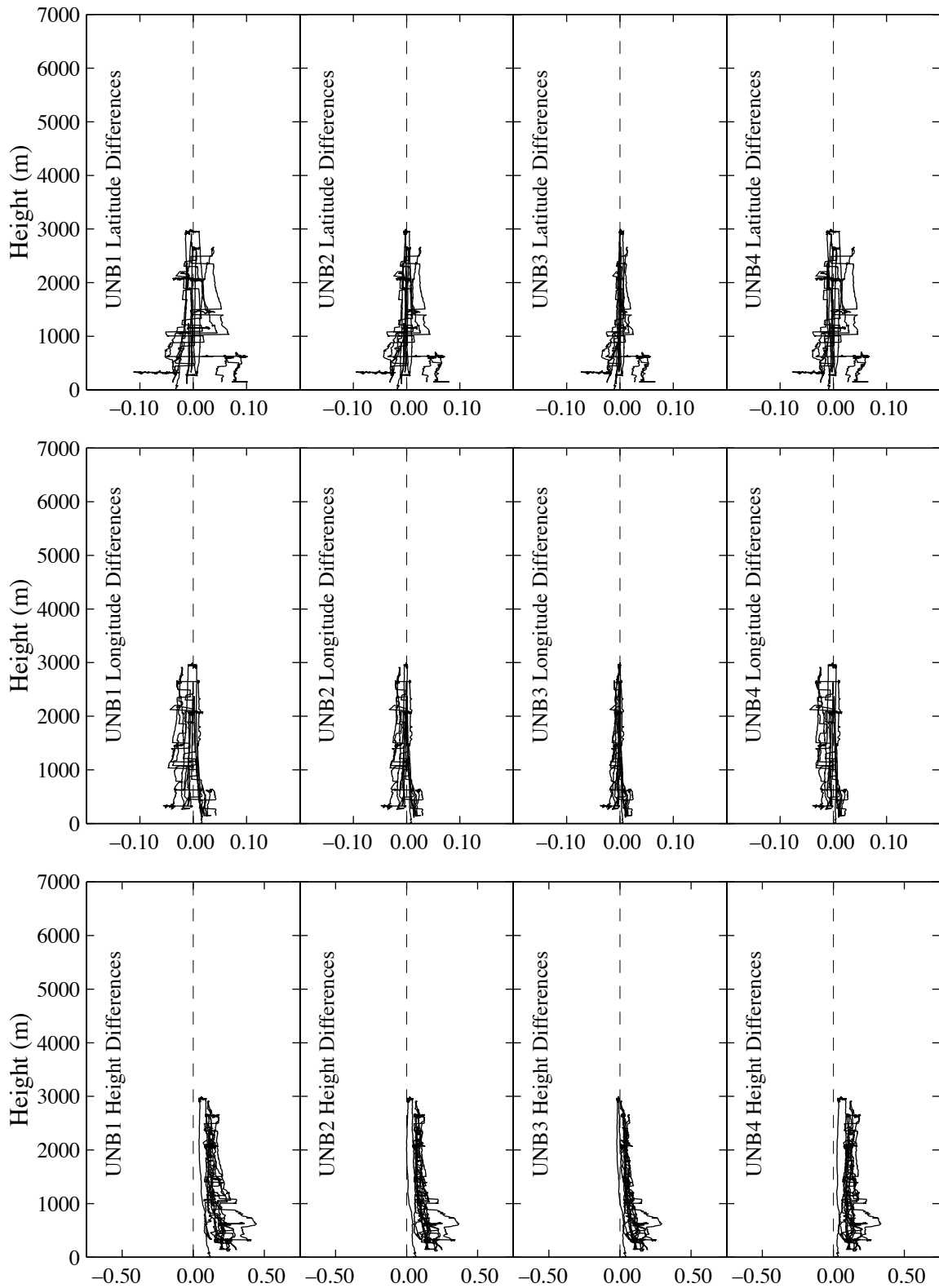**Figure B2.7. Solution Differences for Flight F509, March 13, 1995.**
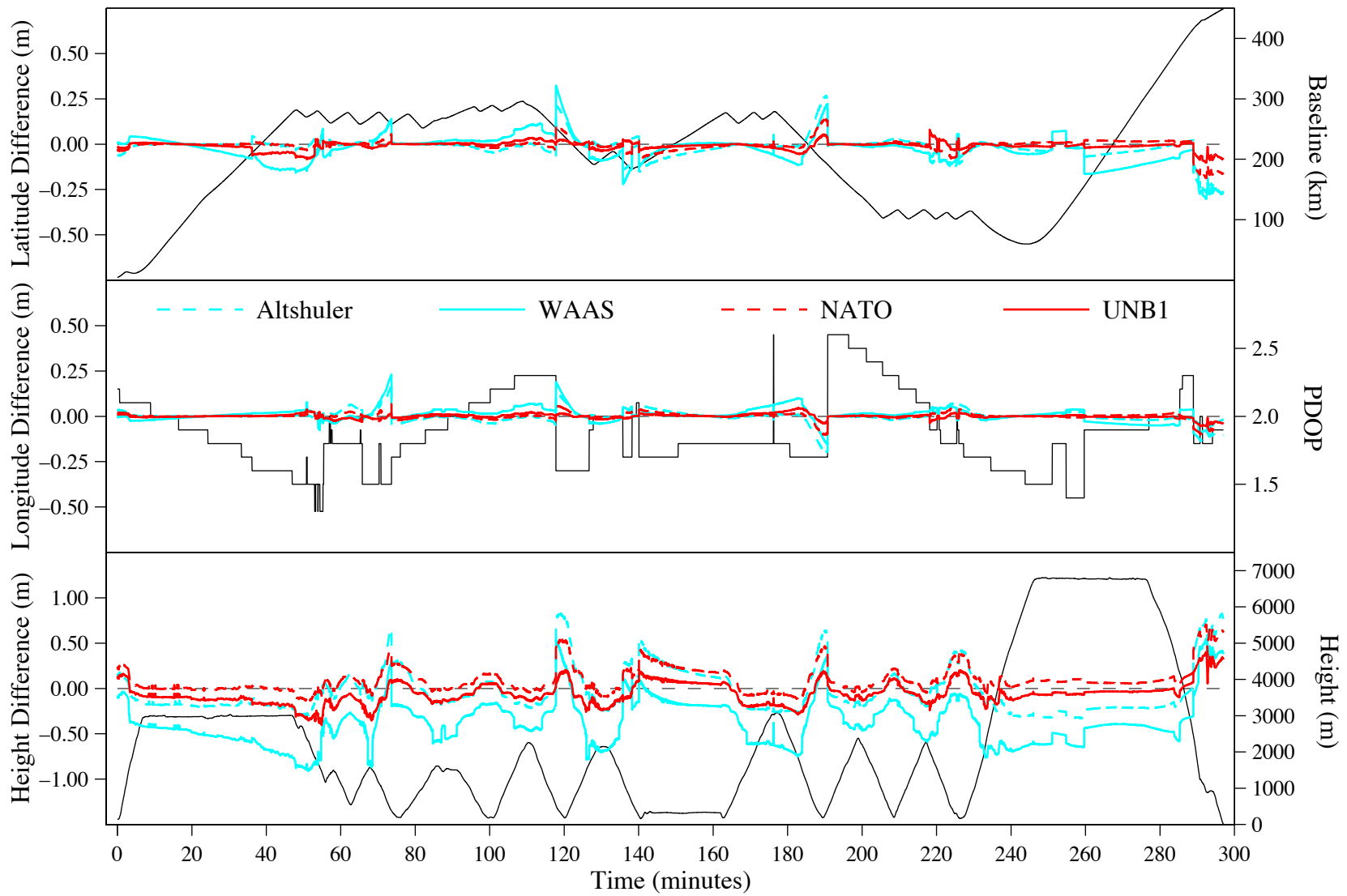
Figure B2.8. Solution Differences for Flight F510, March 14, 1995.
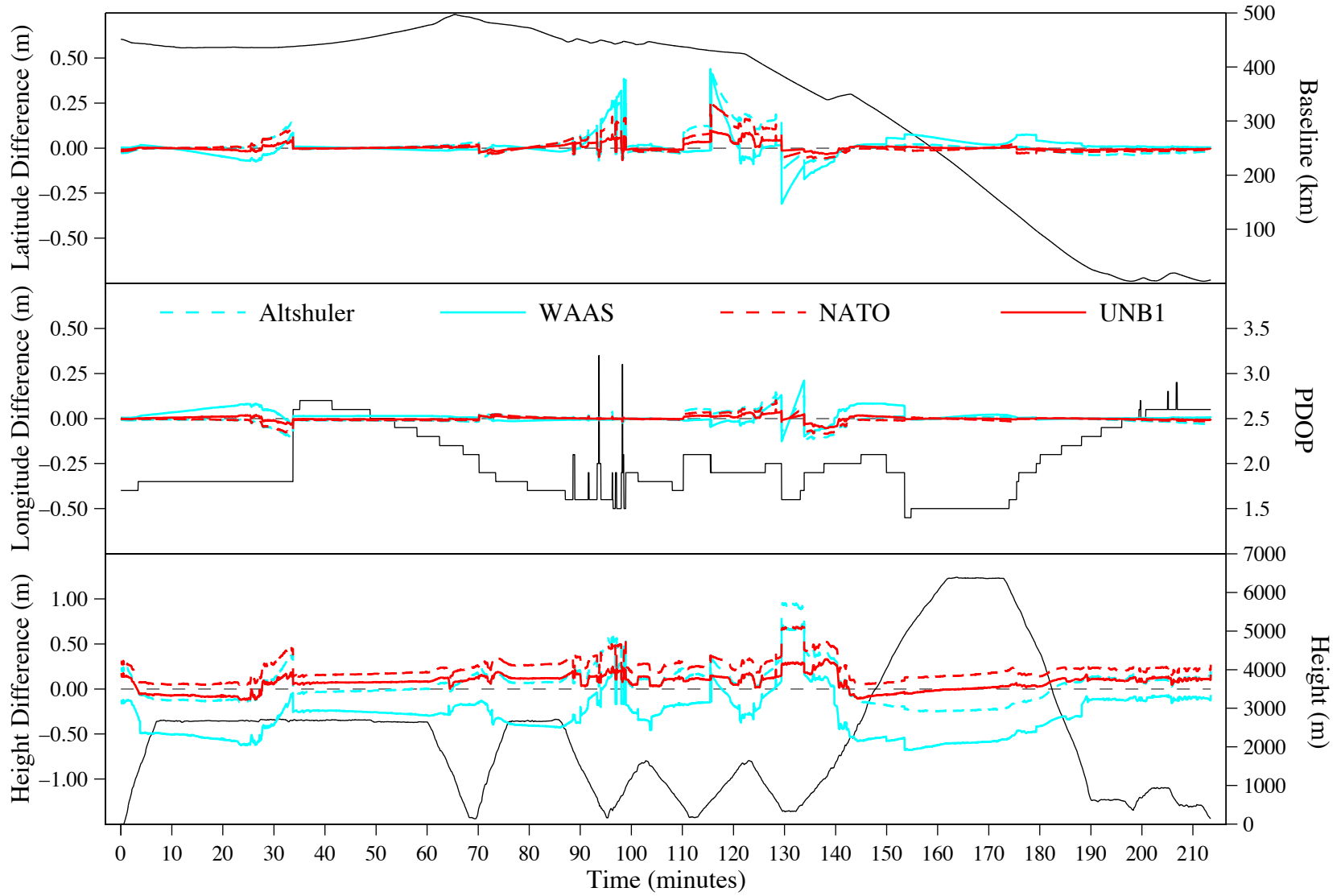
Figure B2.9. Solution Differences for Flight F511, March 15, 1995.
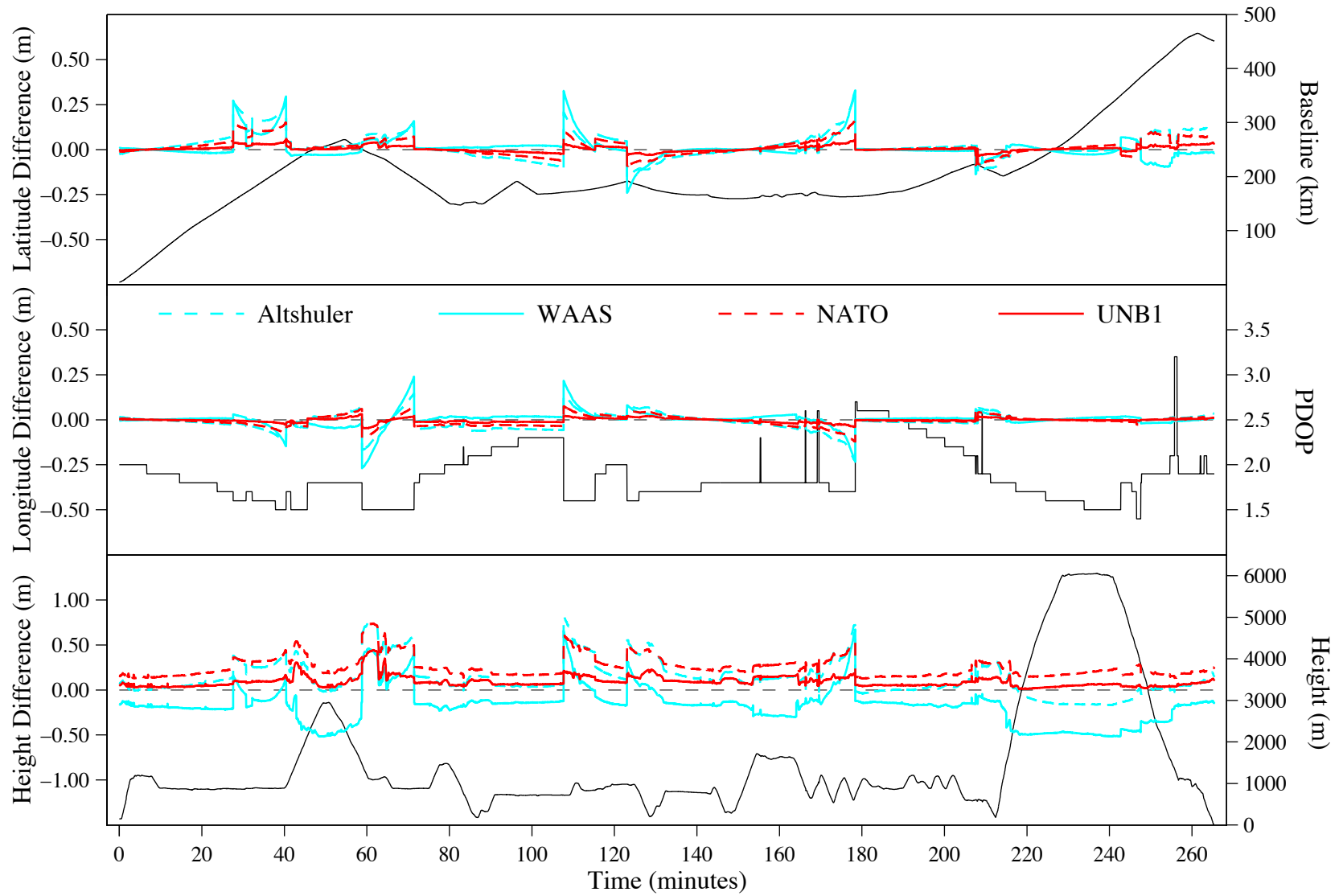
Figure B2.10. Solution Differences for Flight F512, March 17, 1995.
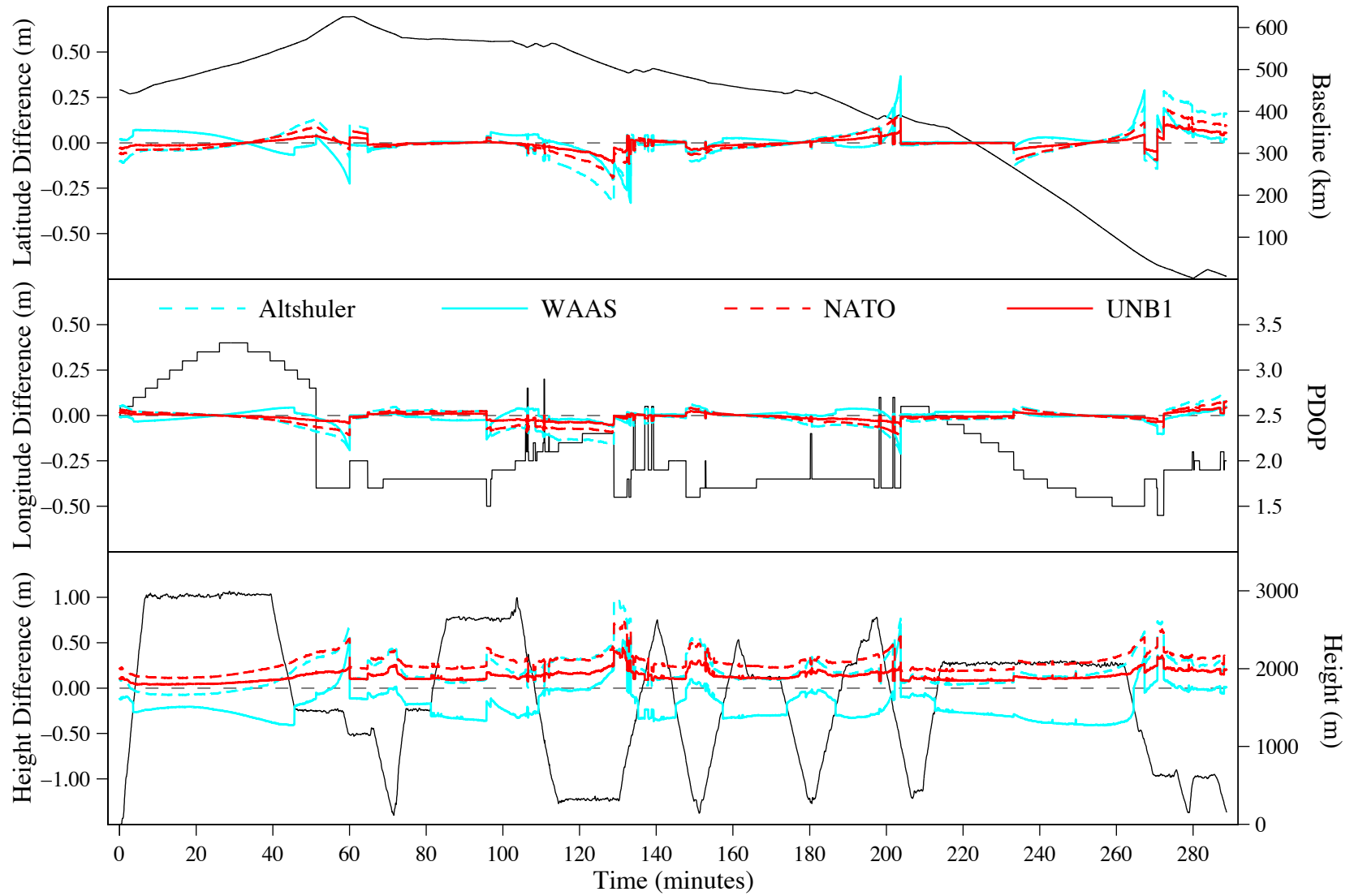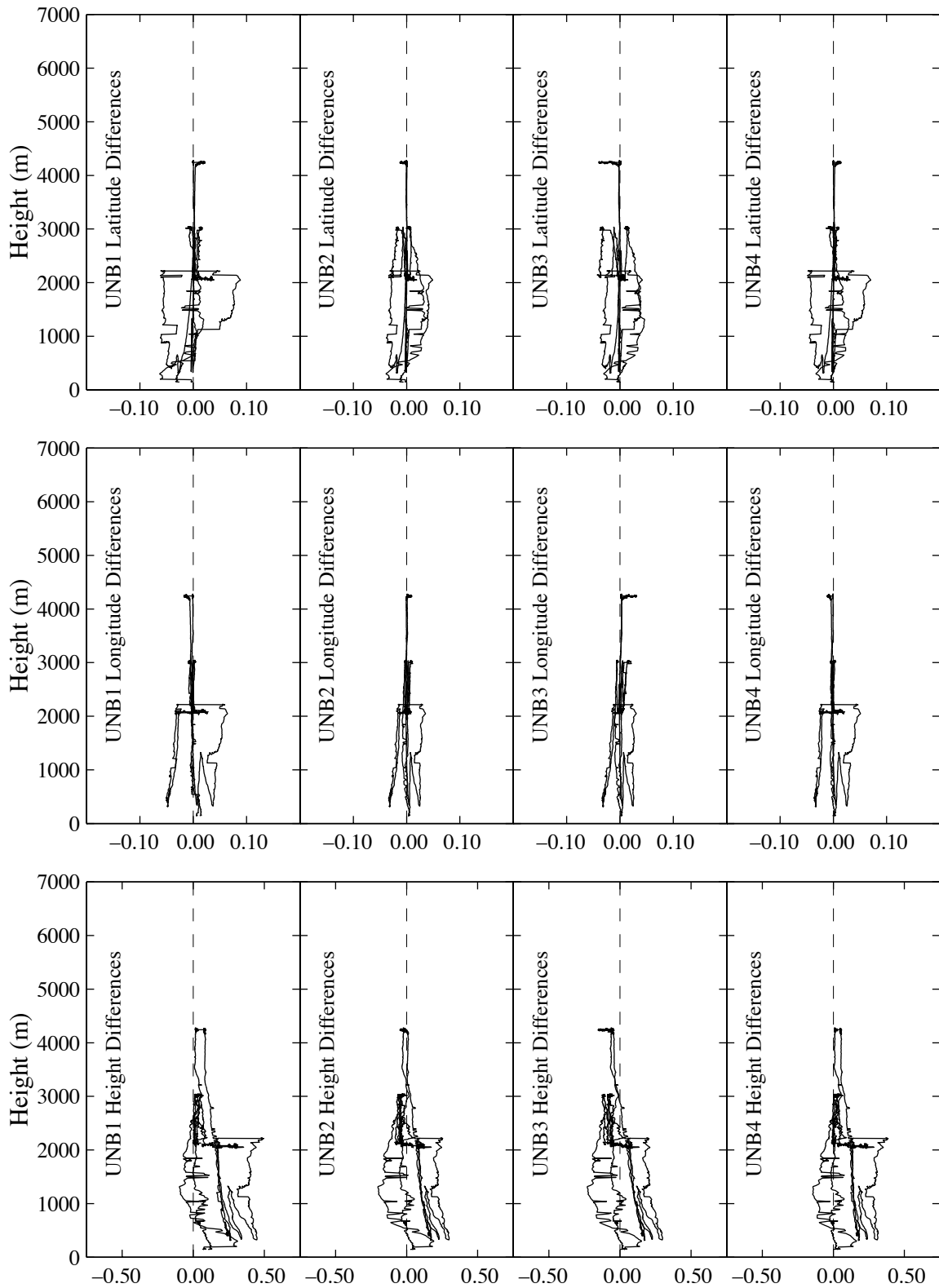
Figure B2.11. Solution Differences for Flight F513, March 18, 1995.
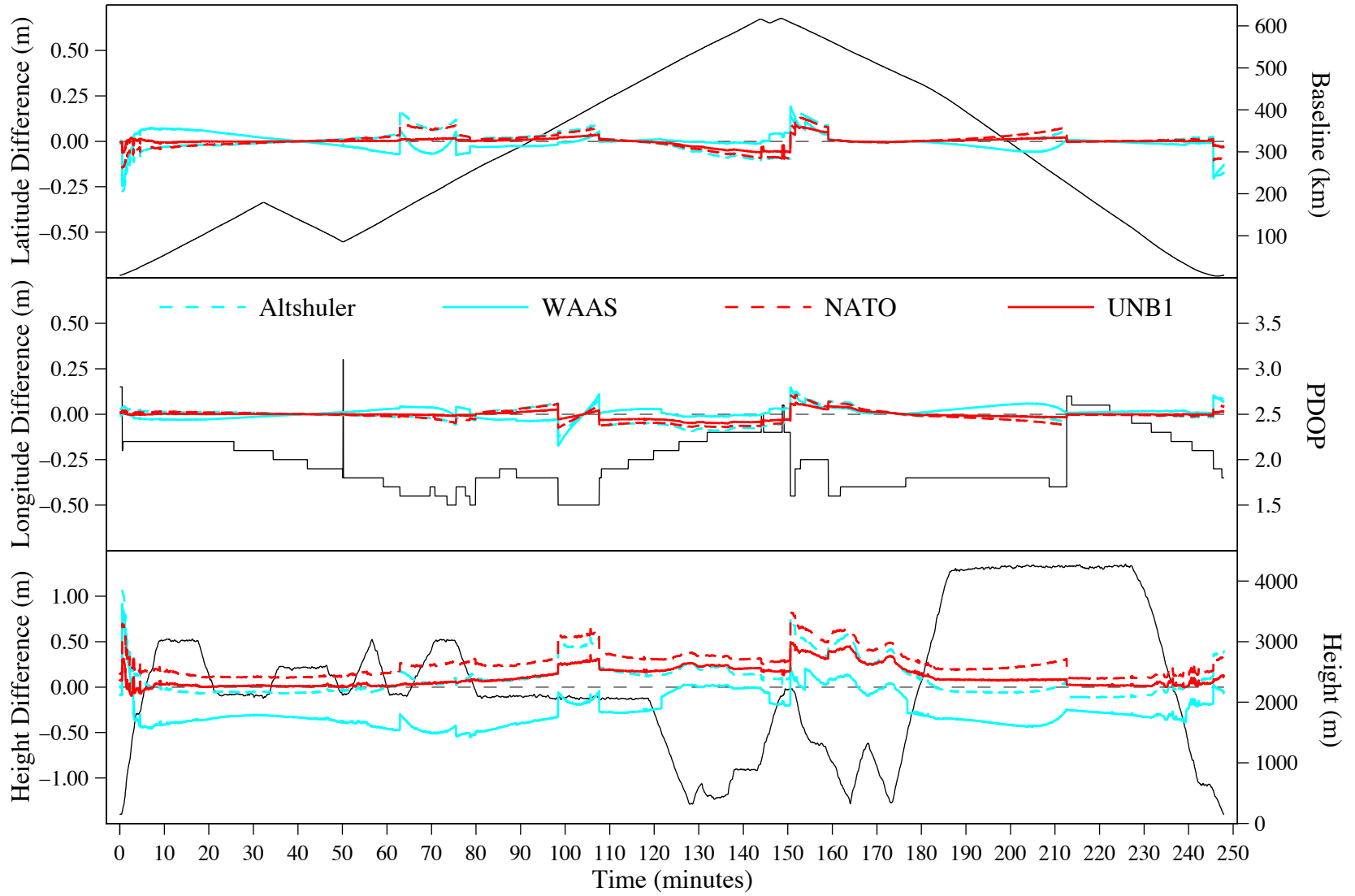
Figure B2.12. Solution Differences for Flight F516, March 22, 1995.

APPENDIX B3 UNB Models:

Solution Position Differences With Respect To Height

The following plots are of the same type as Figure 3.4 and Appendix B1, that is the position differences (in metres) between the UNB models solutions and the benchmark solutions. For the purposes of providing insight into the performance of the models, the differences are plotted against the aircraft height.

Figure B3.1. Solution Differences for Flight F503, March 03, 1995.

Figure B3.2. Solution Differences for Flight F504, March 06, 1995.

127

Figure B3.3. Solution Differences for Flight F505, March 07, 1995.

128

Figure B3.4. Solution Differences for Flight F506, March 08, 1995.

129

Figure B3.5. Solution Differences for Flight F507, March 09, 1995.

130

Figure B3.6. Solution Differences for Flight F508, March 10, 1995.

Figure B3.7. Solution Differences for Flight F509, March 13, 1995.

Figure B3.8. Solution Differences for Flight F510, March 14, 1995.

133

Figure B3.9. Solution Differences for Flight F511, March 15, 1995.

134

Figure B3.10. Solution Differences for Flight F512, March 17, 1995.

135

Figure B3.11. Solution Differences for Flight F513, March 18, 1995.

Figure B3.12. Solution Differences for Flight F516, March 22, 1995.

APPENDIX B4 Meteorological Data Recorded at the Aircraft

The following plots display the ambient meteorology of pressure, temperature and water vapour recorded at the aircraft. The first two parameters were recorded directly, the latter was derived from relative humidity measurements. For clarity they are plotted against aircraft height to give an indication of the vertical atmospheric profiles encountered during the flights. For further clarity, the pressure plot is split into two discontinuous parts. In this way the potential bias present at either the top and/or bottom of the profile is more clearly visible.

In addition, the values given by the UNB models calculated at the reference station location are plotted for comparison purposes. These will differ slightly from the model values computed at the aircraft, depending on the latitudinal separation from the reference station, but the general trends are easily seen with these plots.
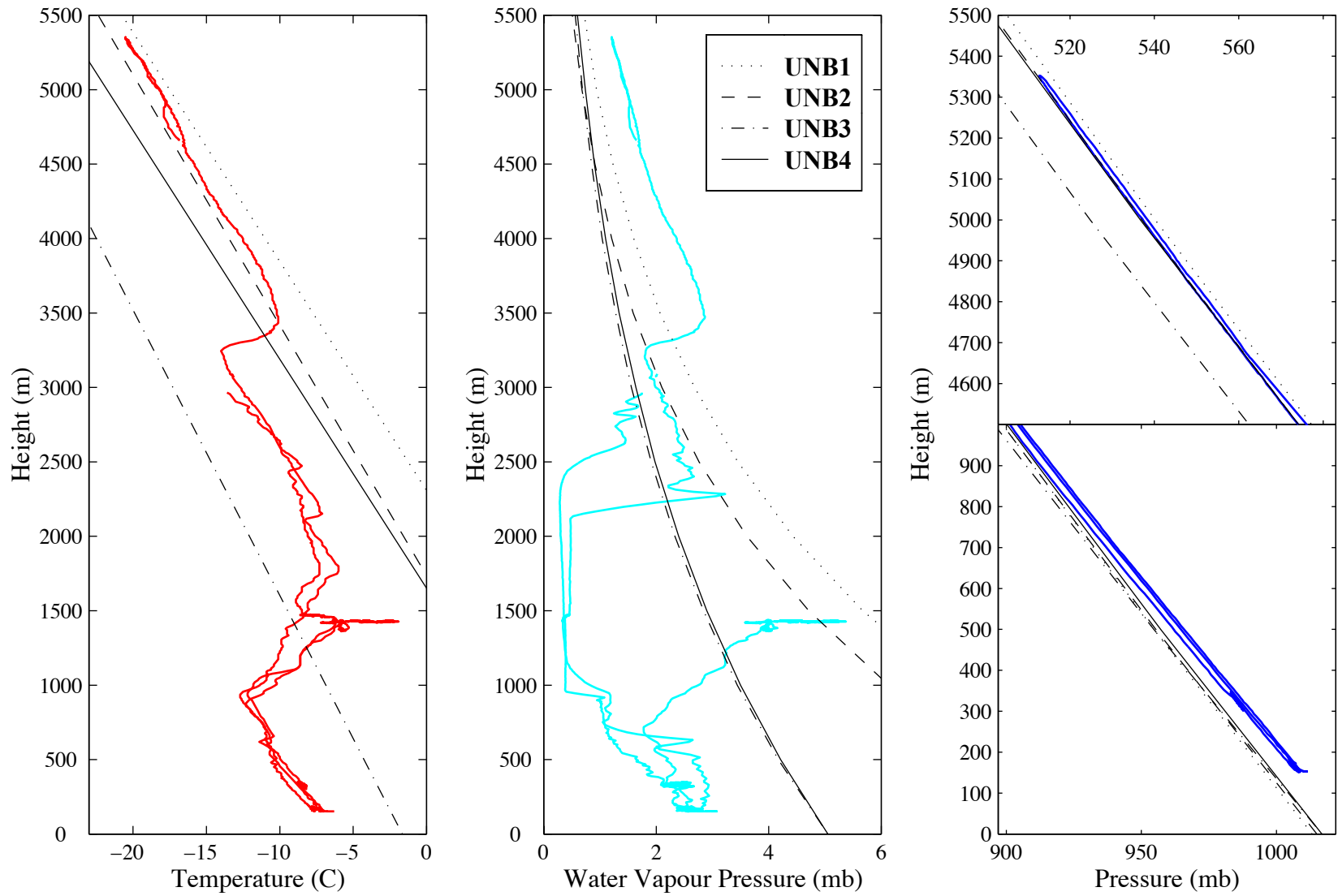
Figure B4.1. Meteorology recorded on Flight F503, March 03, 1995.
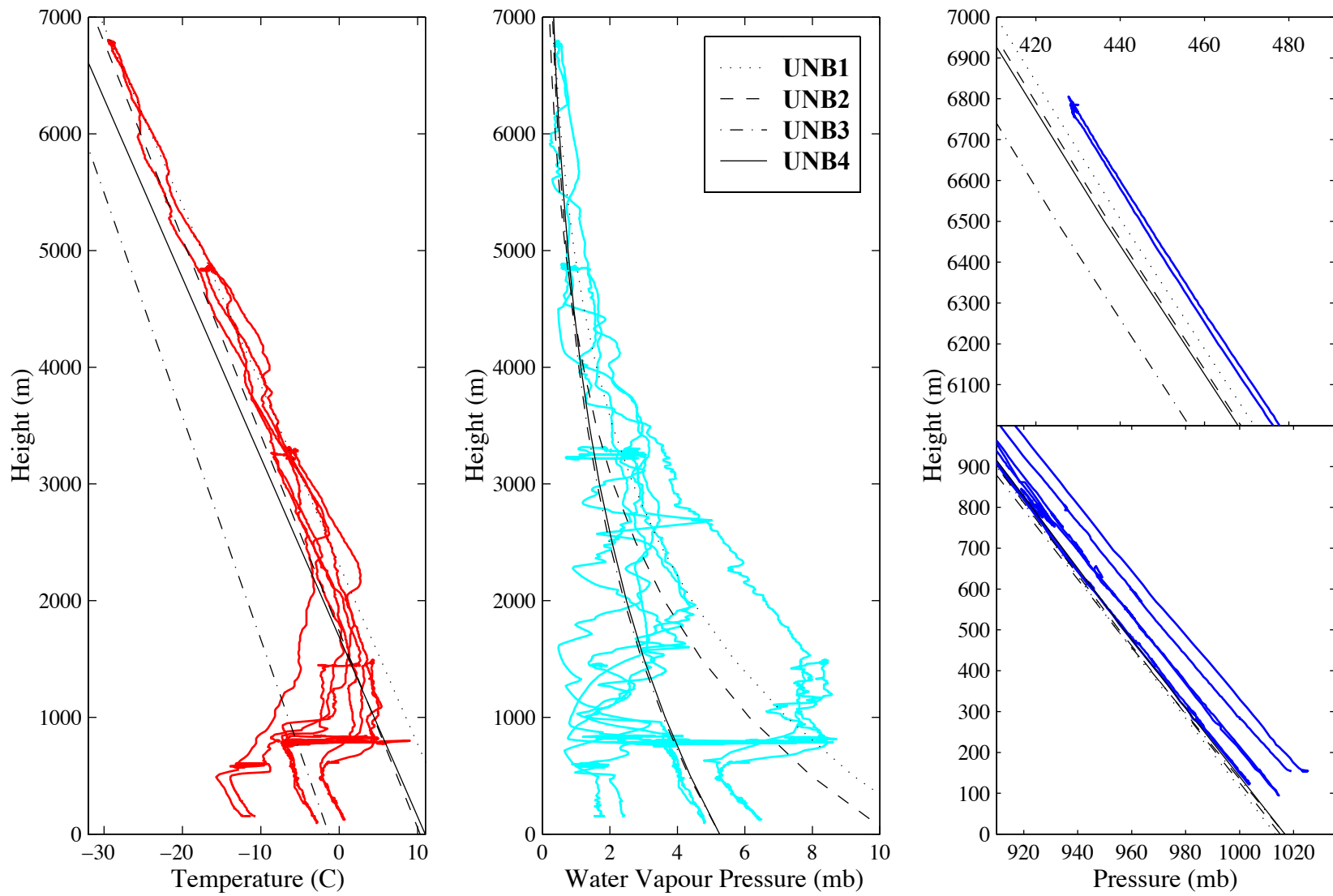
Figure B4.2. Meteorology recorded on Flight F504, March 06, 1995.
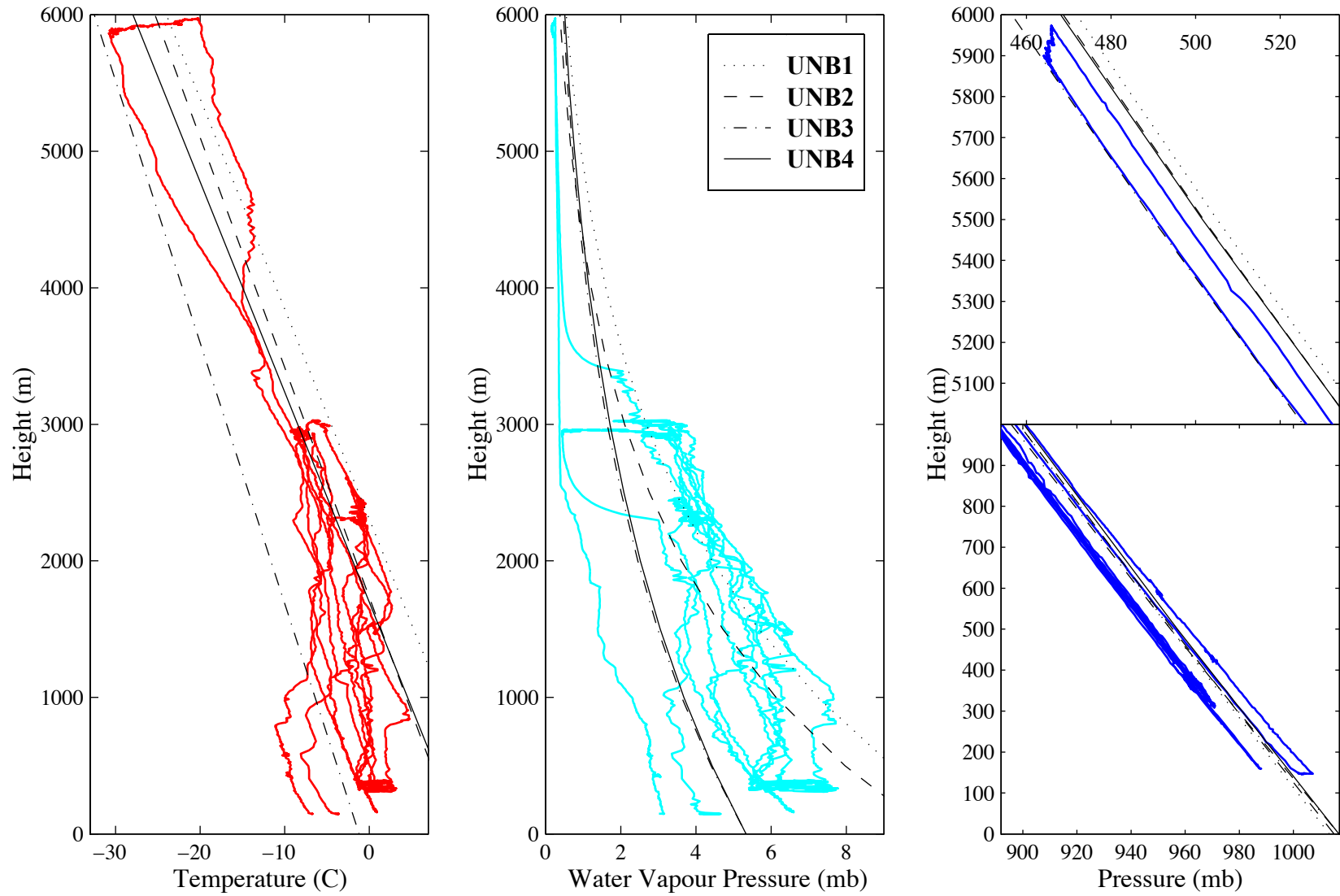
Figure B4.3. Meteorology recorded on Flight F505, March 07, 1995.
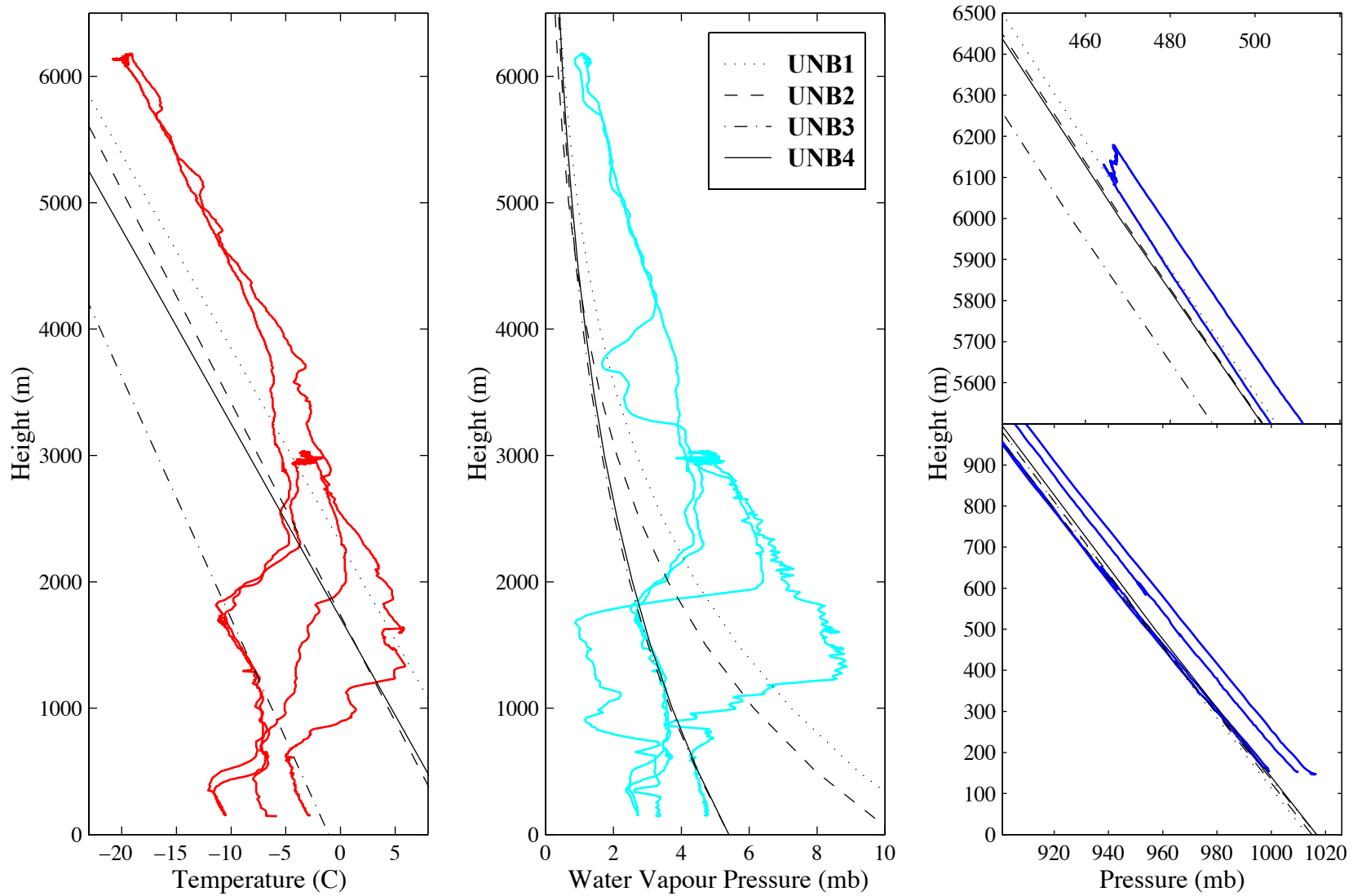
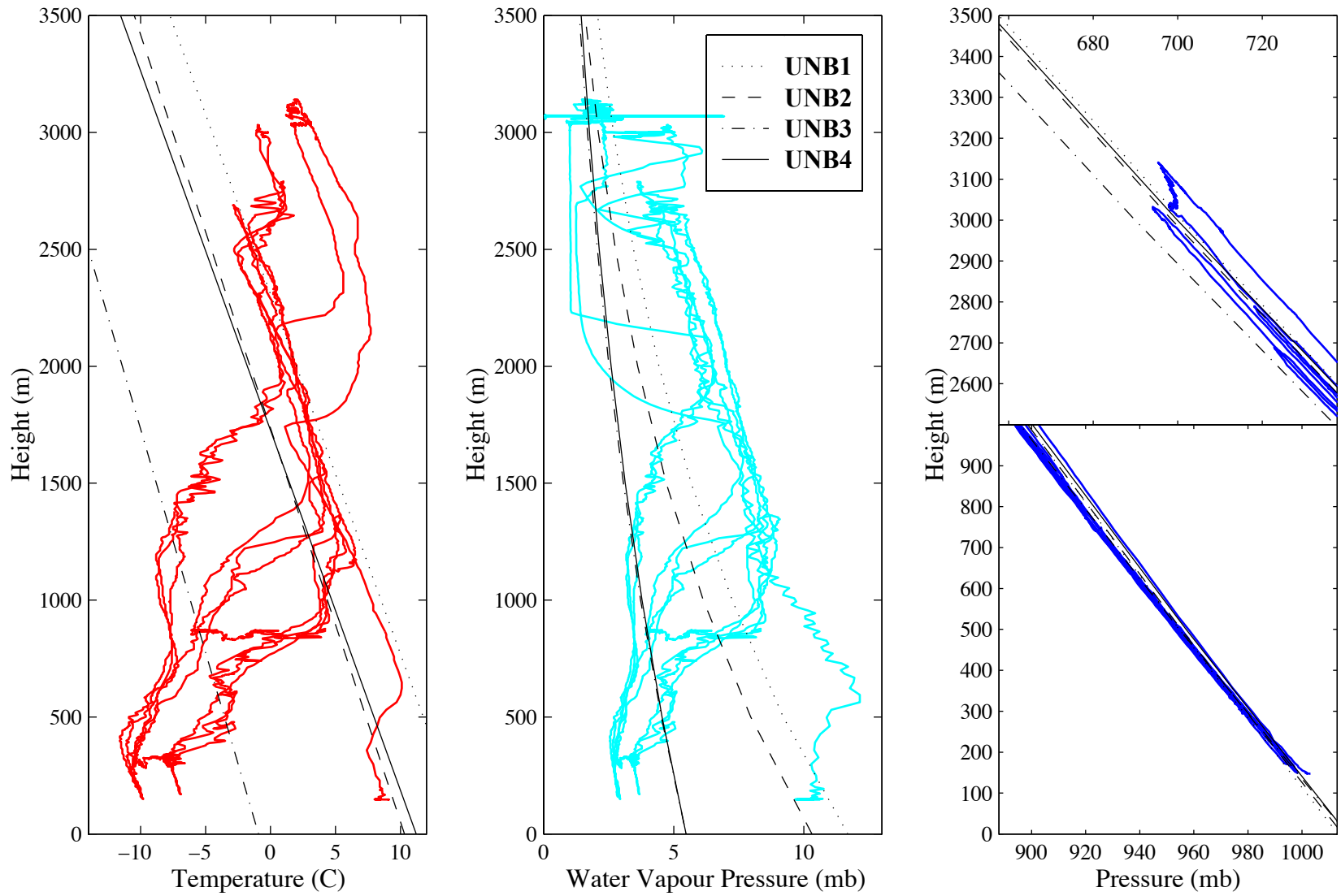**Figure B4.4. Meteorology recorded on Flight F506, March 08, 1995.**

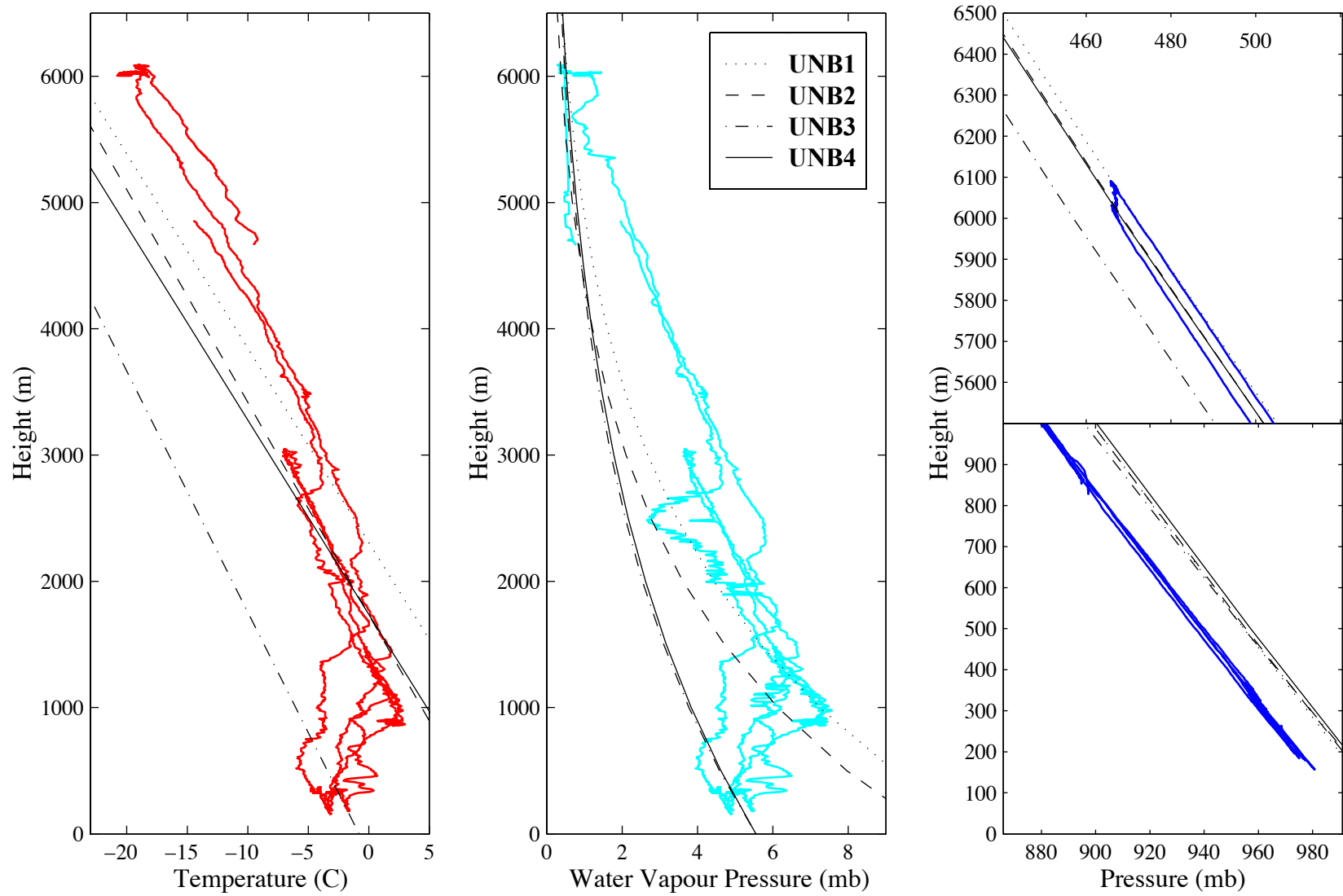**Figure B4.5. Meteorology recorded on Flight F507, March 09, 1995.**

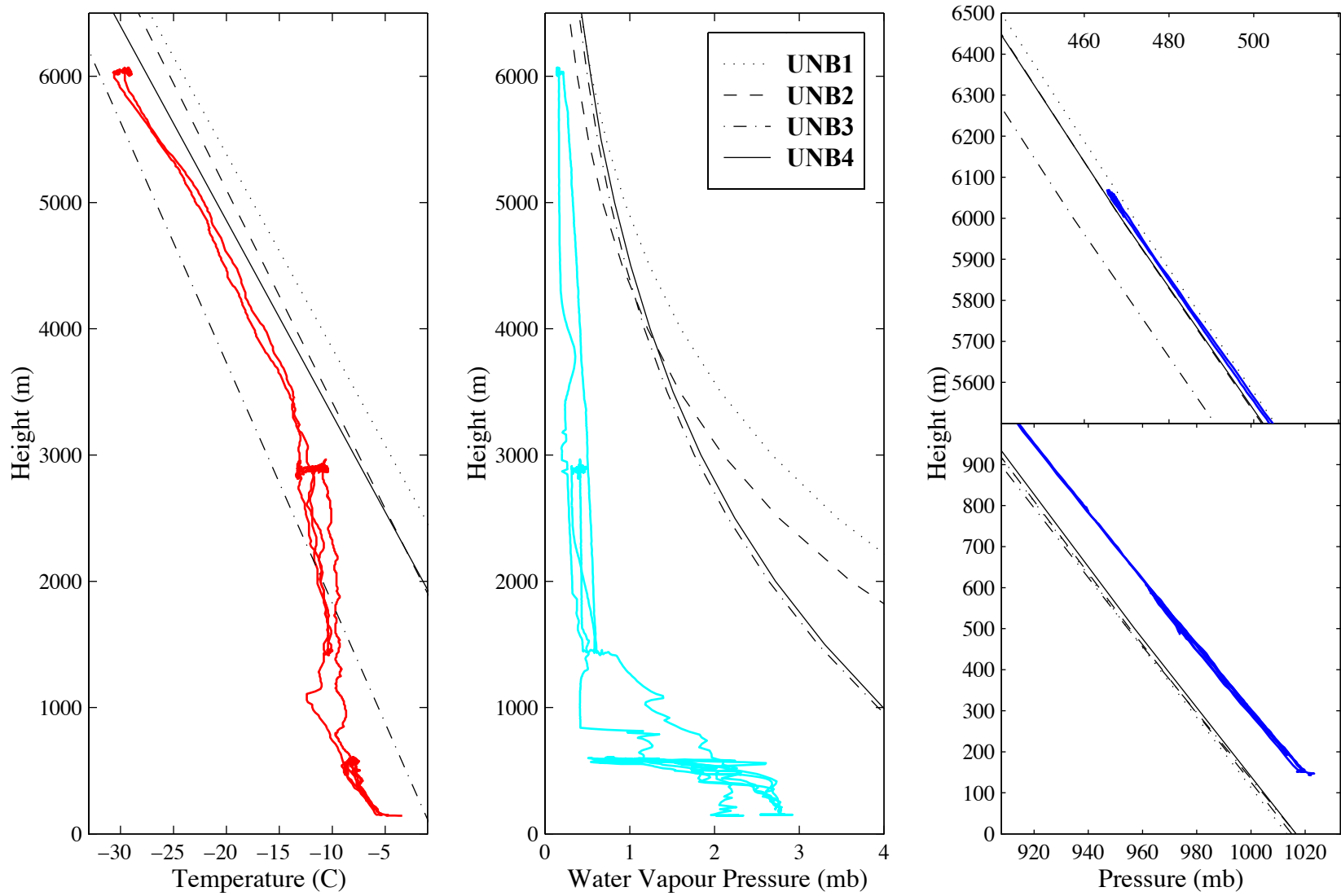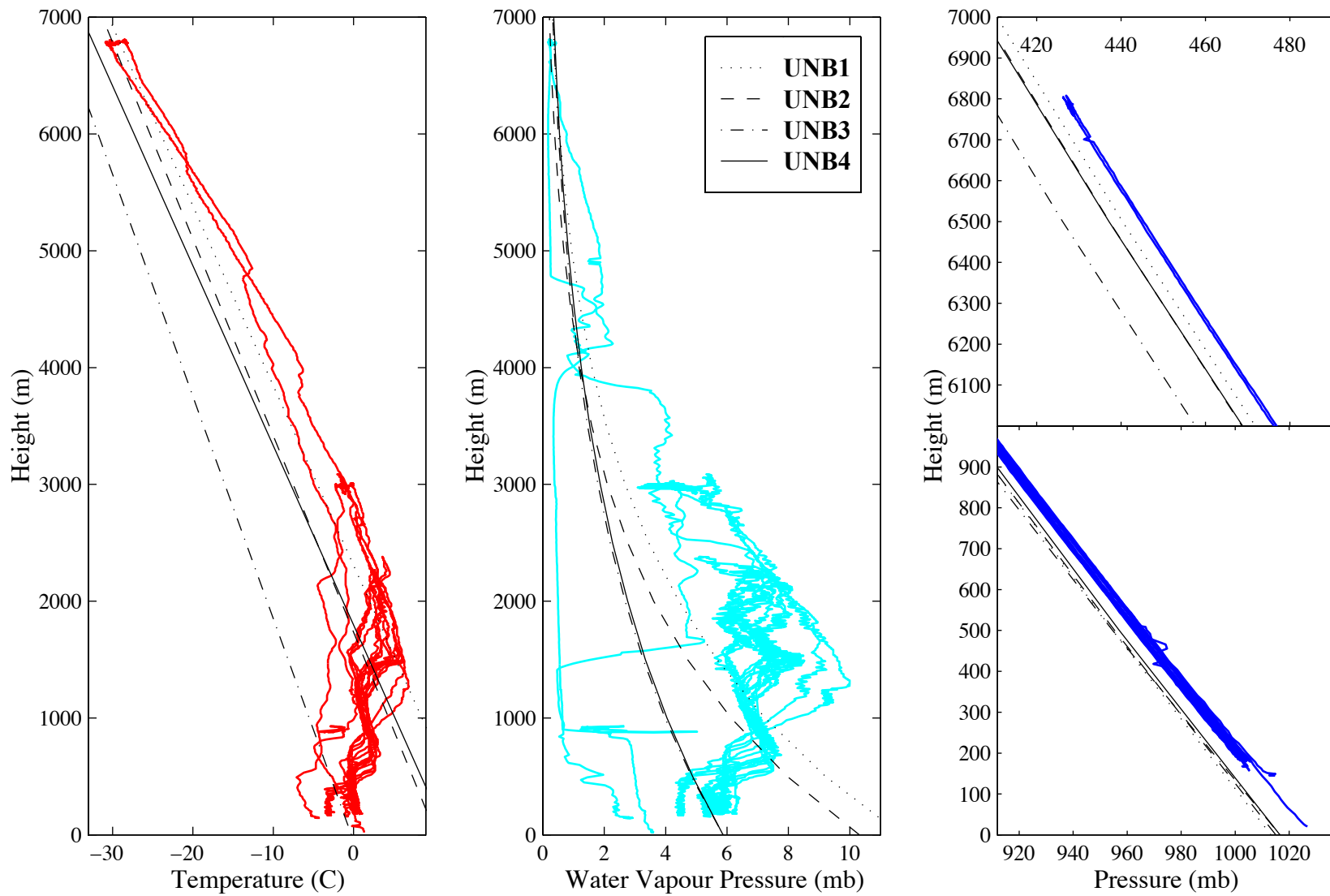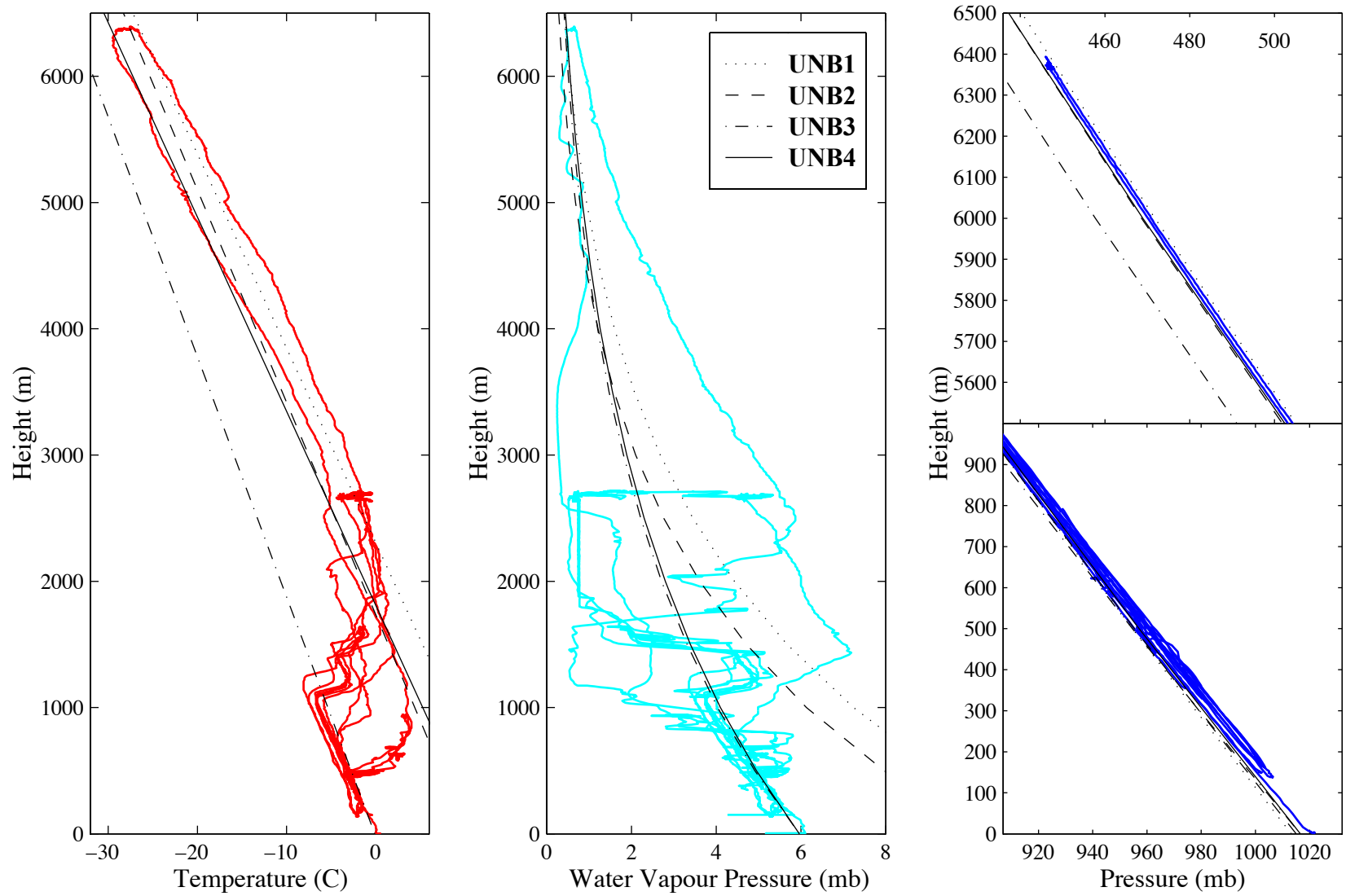**Figure B4.6. Meteorology recorded on Flight F508, March 10, 1995.**

Figure B4.7. Meteorology recorded on Flight F509, March 13, 1995.

Figure B4.8. Meteorology recorded on Flight F510, March 14, 1995.

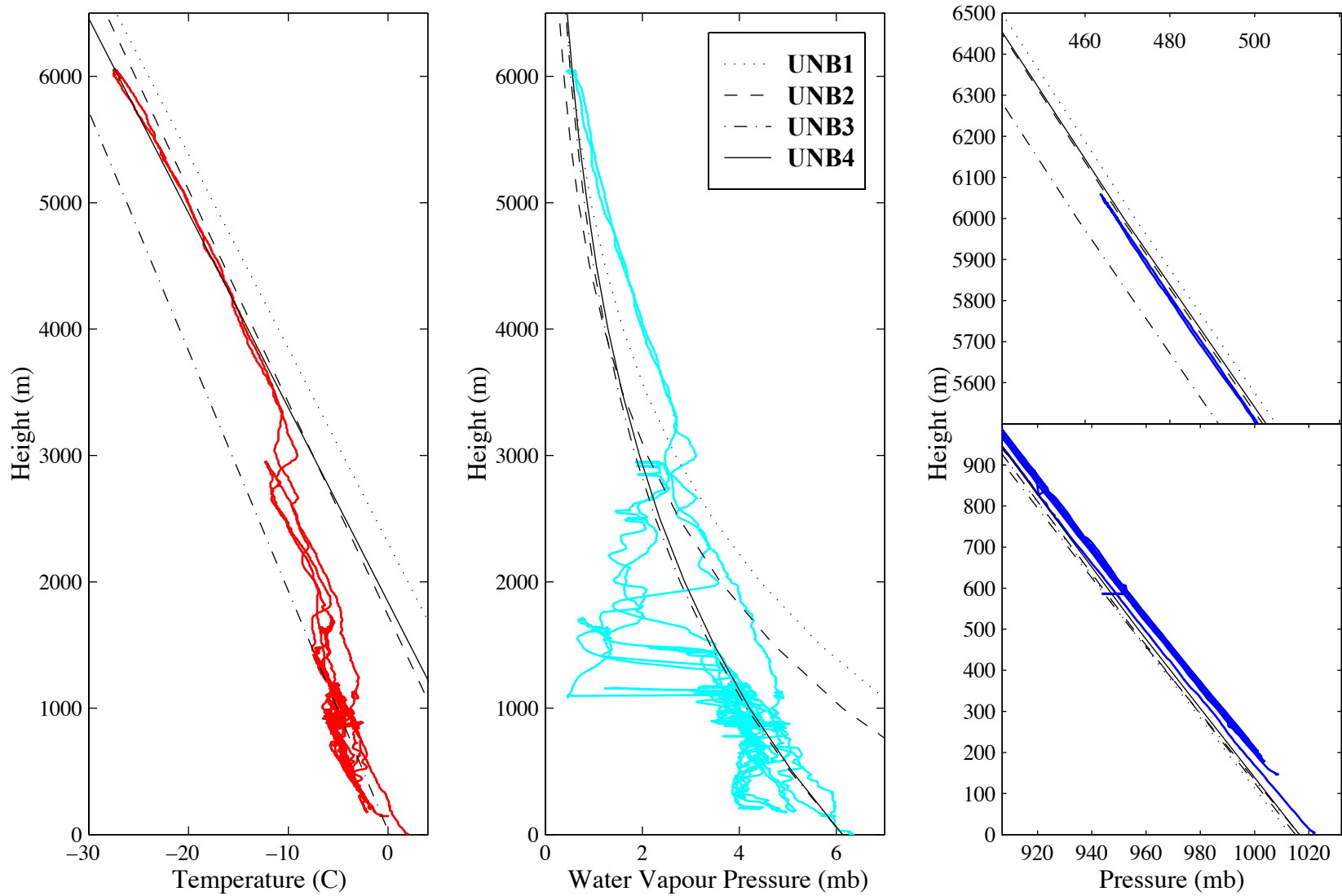**Figure B4.9. Meteorology recorded on Flight F511, March 15, 1995.**

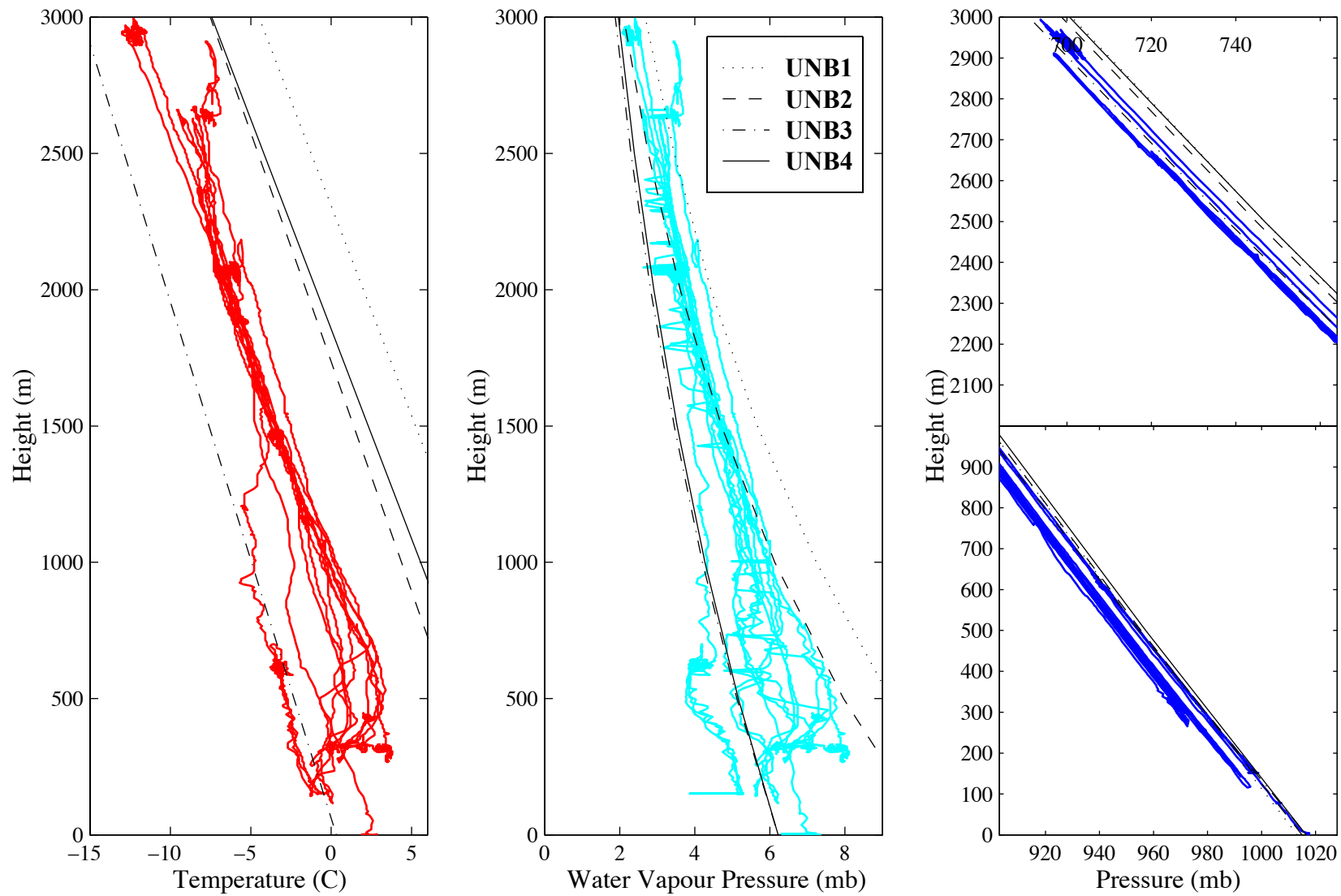**Figure B4.10. Meteorology recorded on Flight F512, March 17, 1995.**

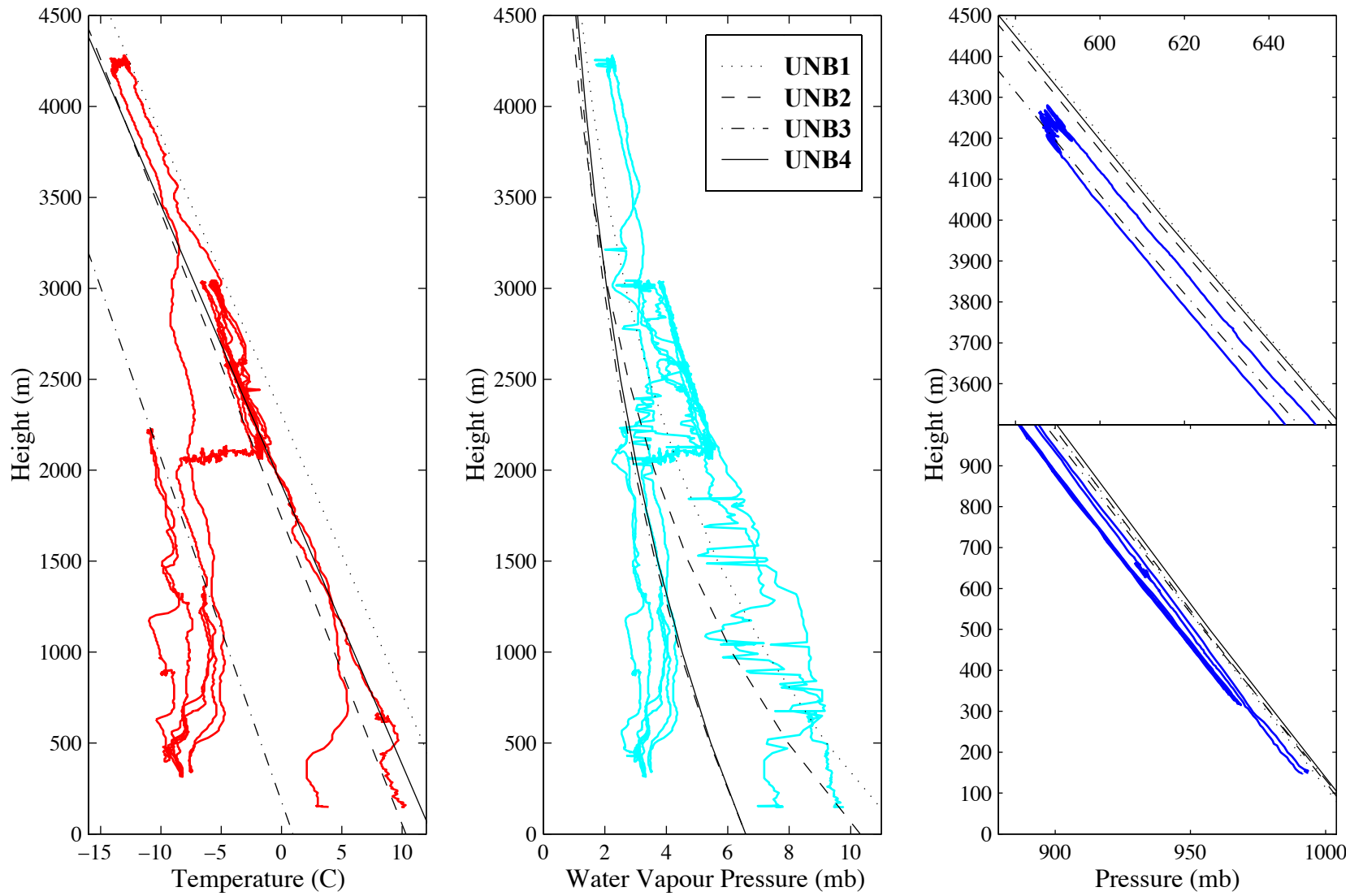**Figure B4.11. Meteorology recorded on Flight F513, March 18, 1995.**

Figure B4.12. Meteorology recorded on Flight F516, March 22, 1995.

APPENDIX B5 Frequency Polygon Plots of the Ray-Trace Residuals

These plots present, in a comprehensive form, the ray-trace residuals for the UNB and initially proposed WAAS models for each of the thirteen stations that provided radiosonde data. The residuals for each elevation angle at which the models were tested were grouped into 75 bins. The plots for the zenith, 30, 20, 15, 10 and 5 degree residuals are superimposed on the same axes, however the drastically different shapes allow easy identification. Each polygon for a given station has the same area (equal number of data points). The general trend of the frequency polygons is the same: the zenith residuals are the most leptokurtic (pointed) with the other elevation angles becoming progressively more platykurtic (flat) down to 5 degrees.

Because the emphasis of these plots is on the model performance at each station, the limits and scale of the x-axis are kept constant for each station. The stations are represented in order of decreasing latitudinal position.
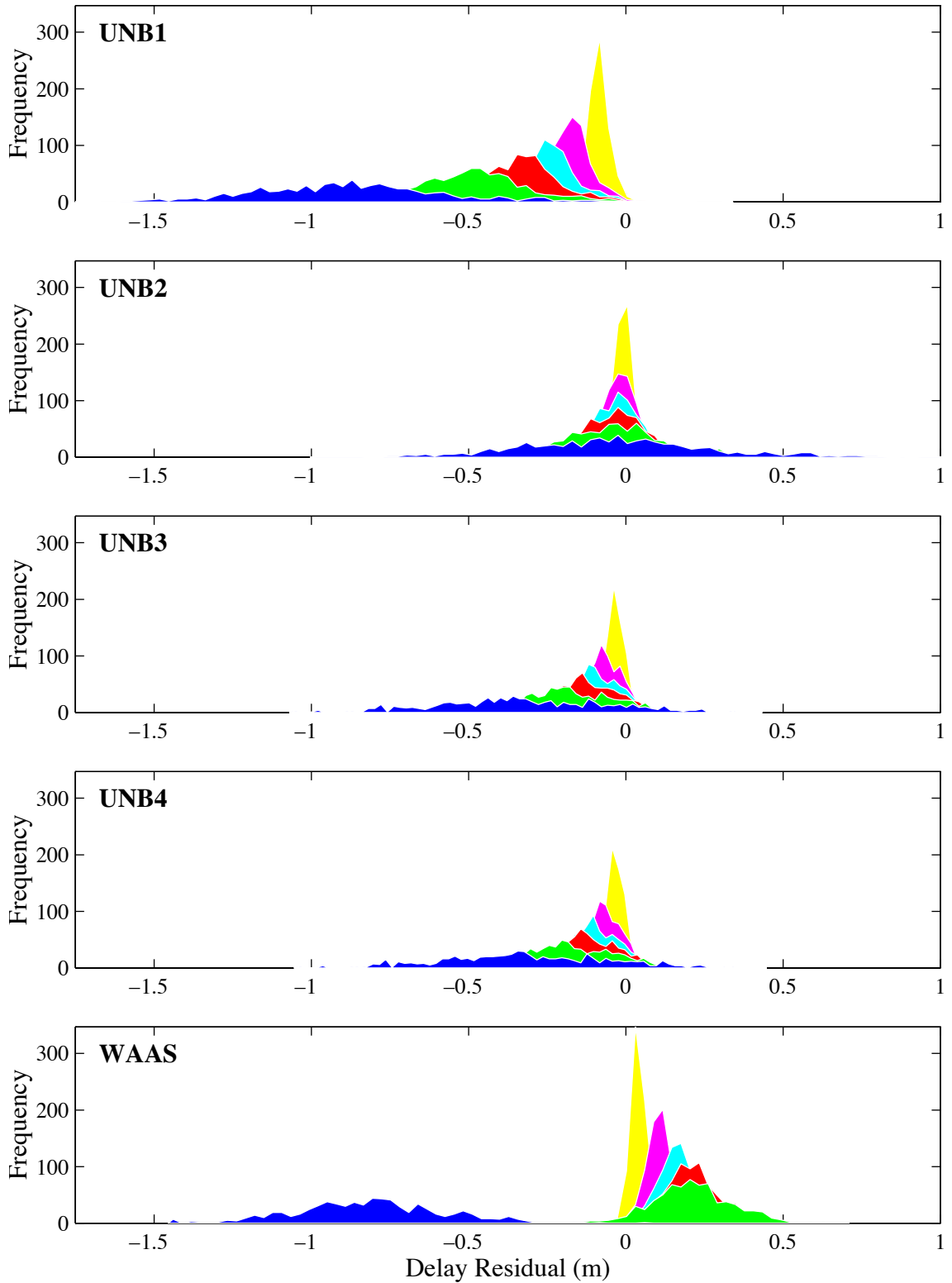
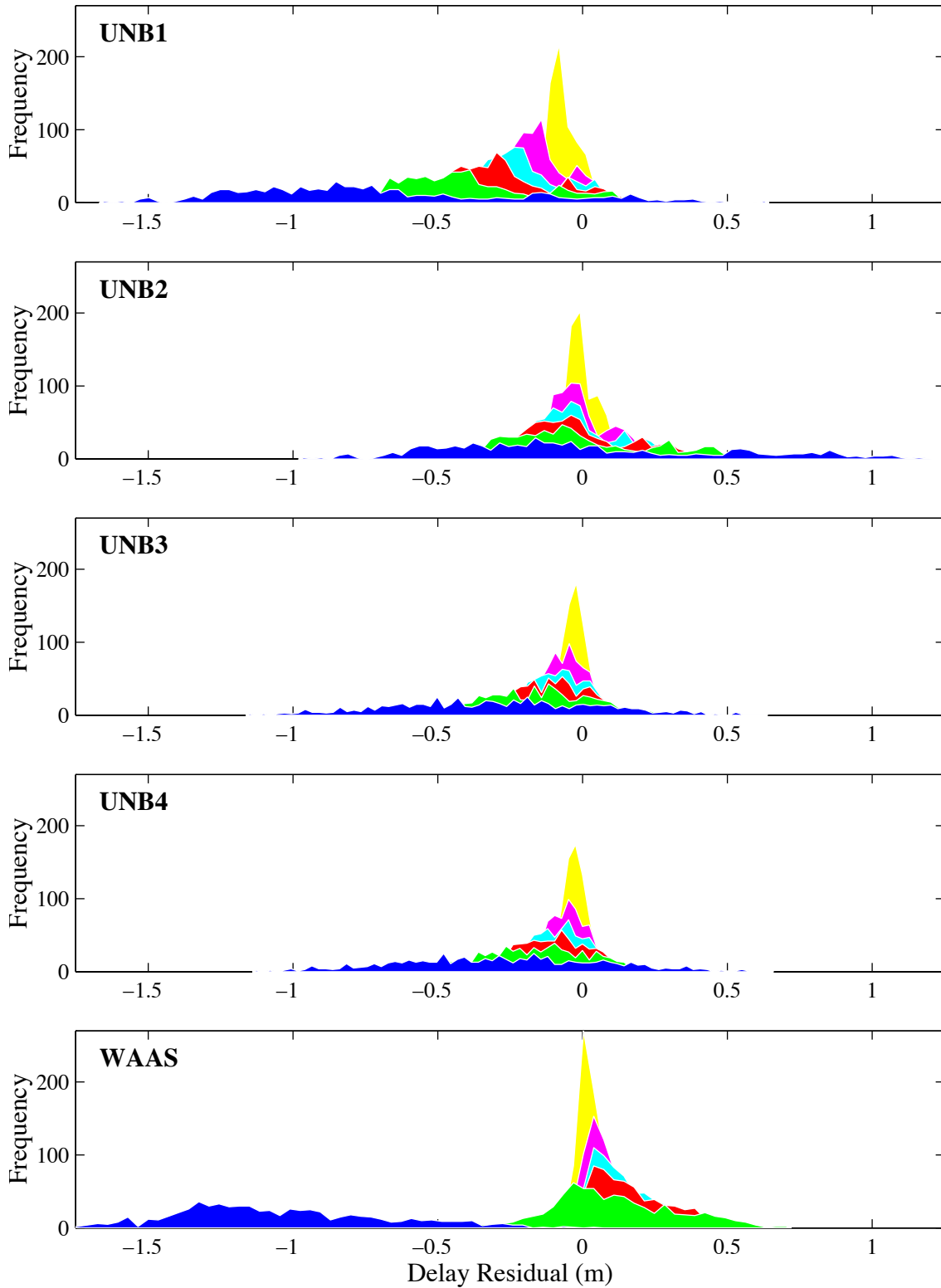**Figure B5.1. Frequency distributions of ray−trace residuals for Alert.**

Figure B5.2. Frequency distributions of ray−trace residuals for Kotzebue.
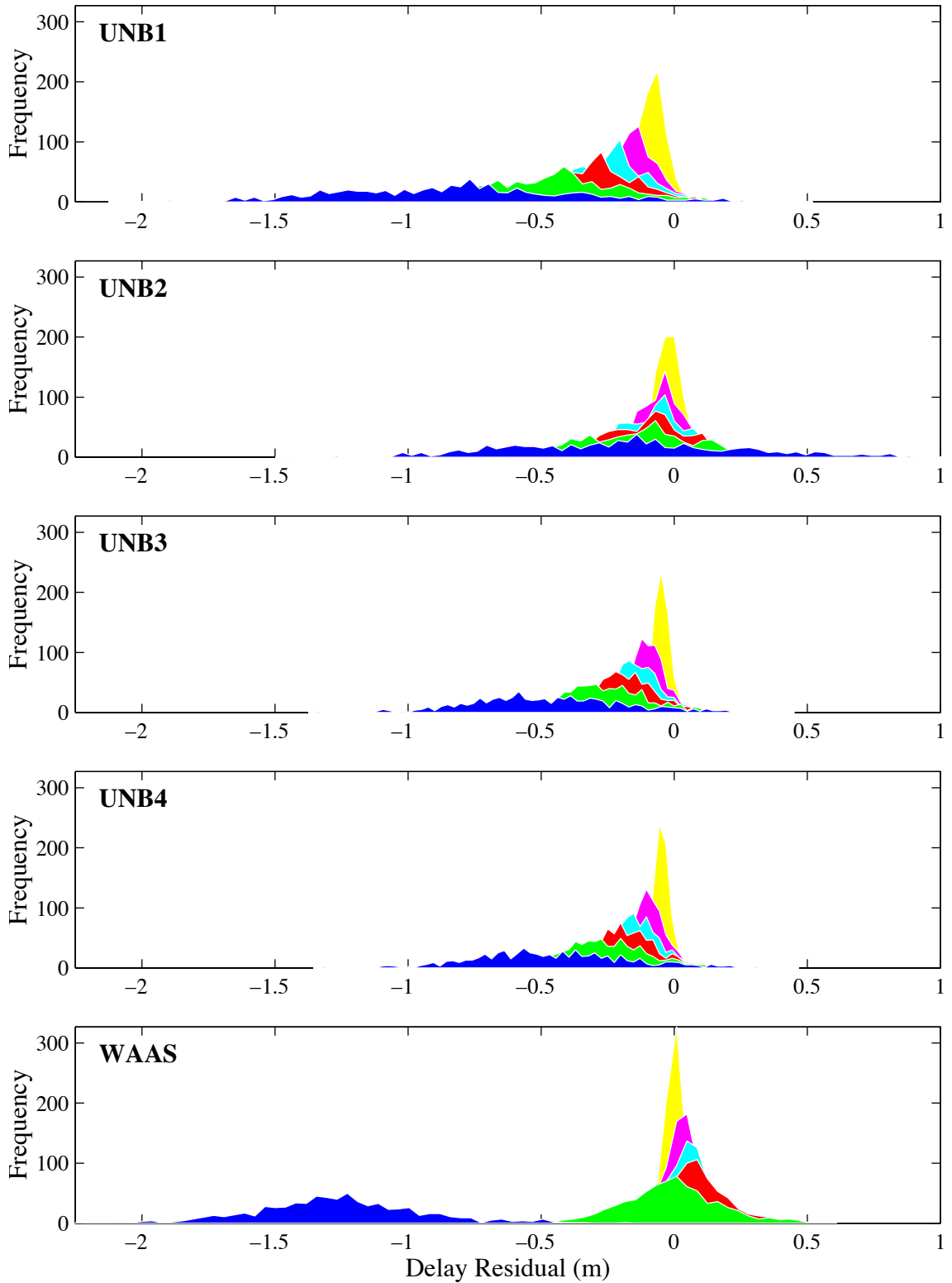
153

Figure B5.3. Frequency distributions of ray–trace residuals for Iqaluit.
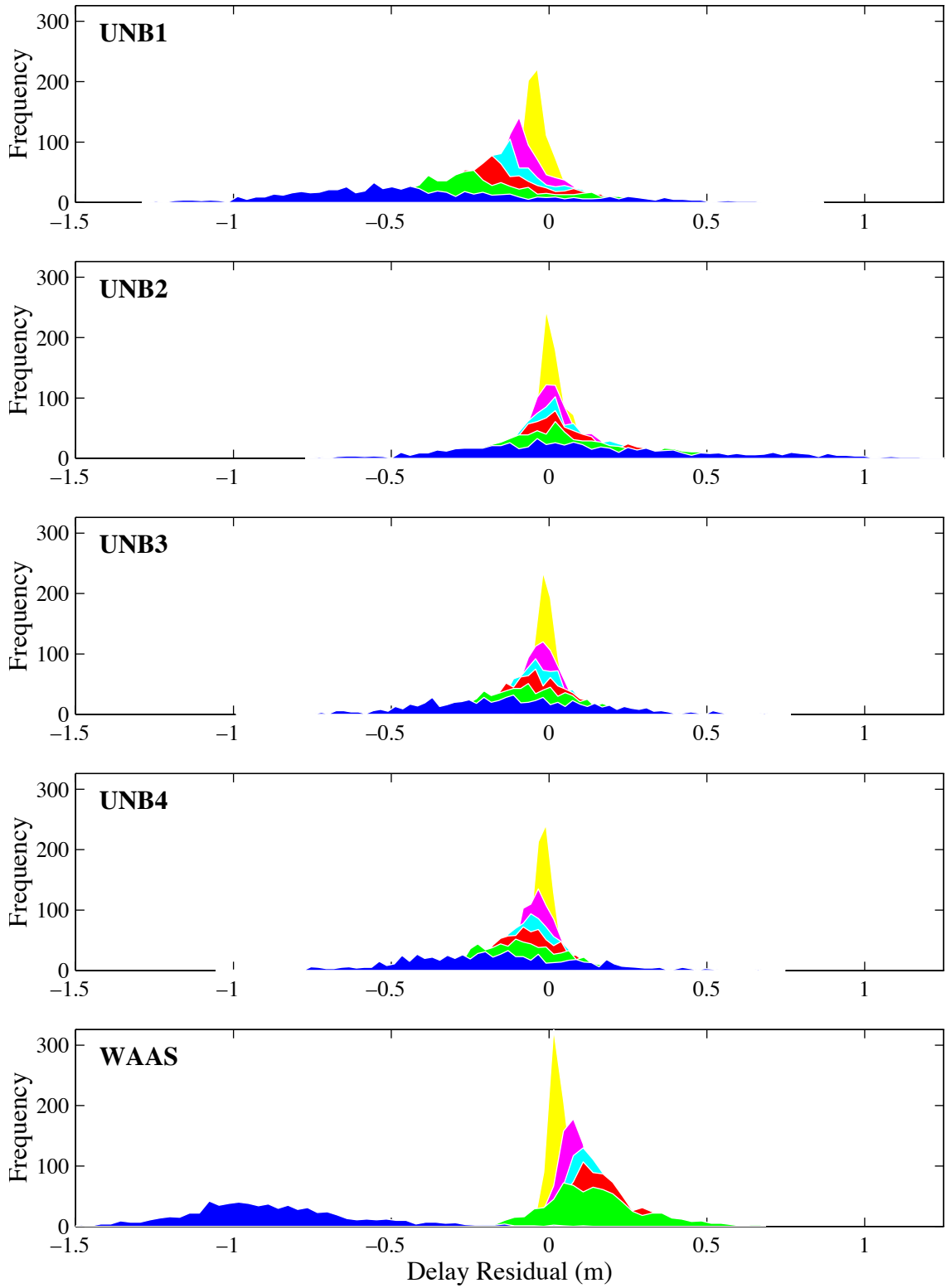
Figure B5.4. Frequency distributions of ray–trace residuals for Whitehorse.

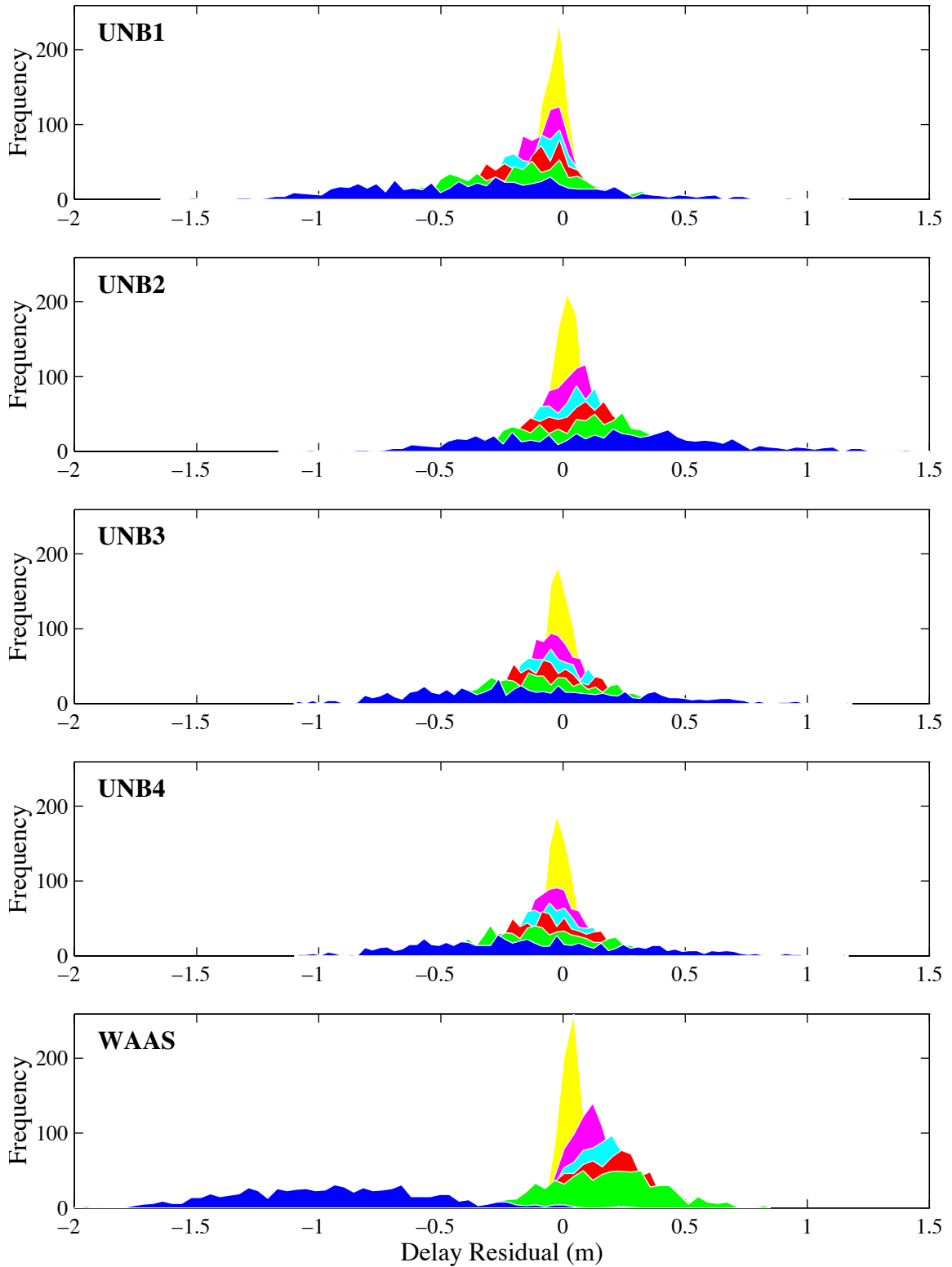**Figure B5.5. Frequency distributions of ray–trace residuals for Landvetter.**

Figure B5.6. Frequency distributions of ray−trace residuals for The Pas.

157

Figure B5.7. Frequency distributions of ray−trace residuals for St. John's.

Figure B5.8. Frequency distributions of ray−trace residuals for Denver.

159
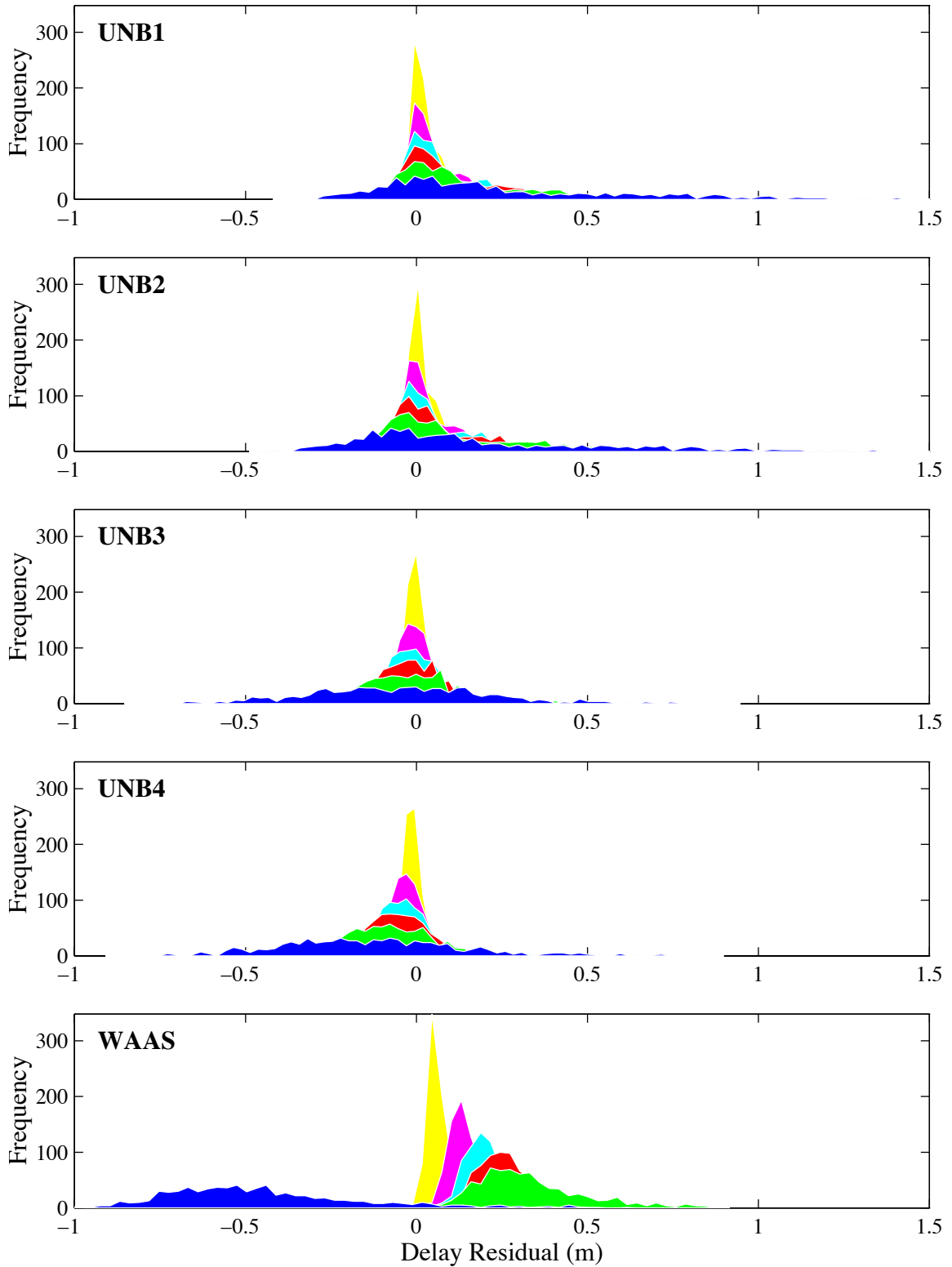
Figure B5.9. Frequency distributions of ray−trace residuals for Grand Jnc.

160
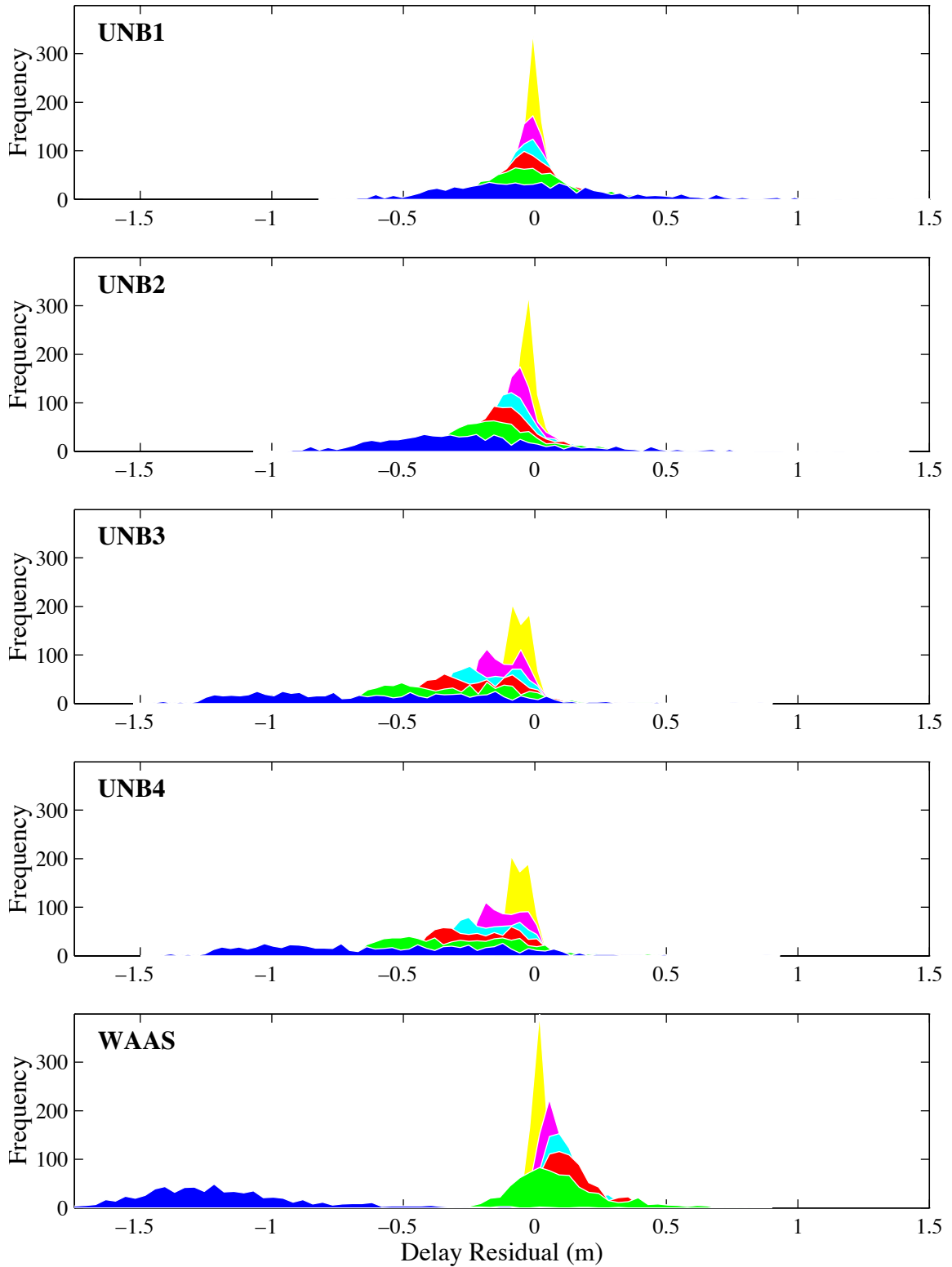
Figure B5.10. Frequency distributions of ray−trace residuals for Oakland.
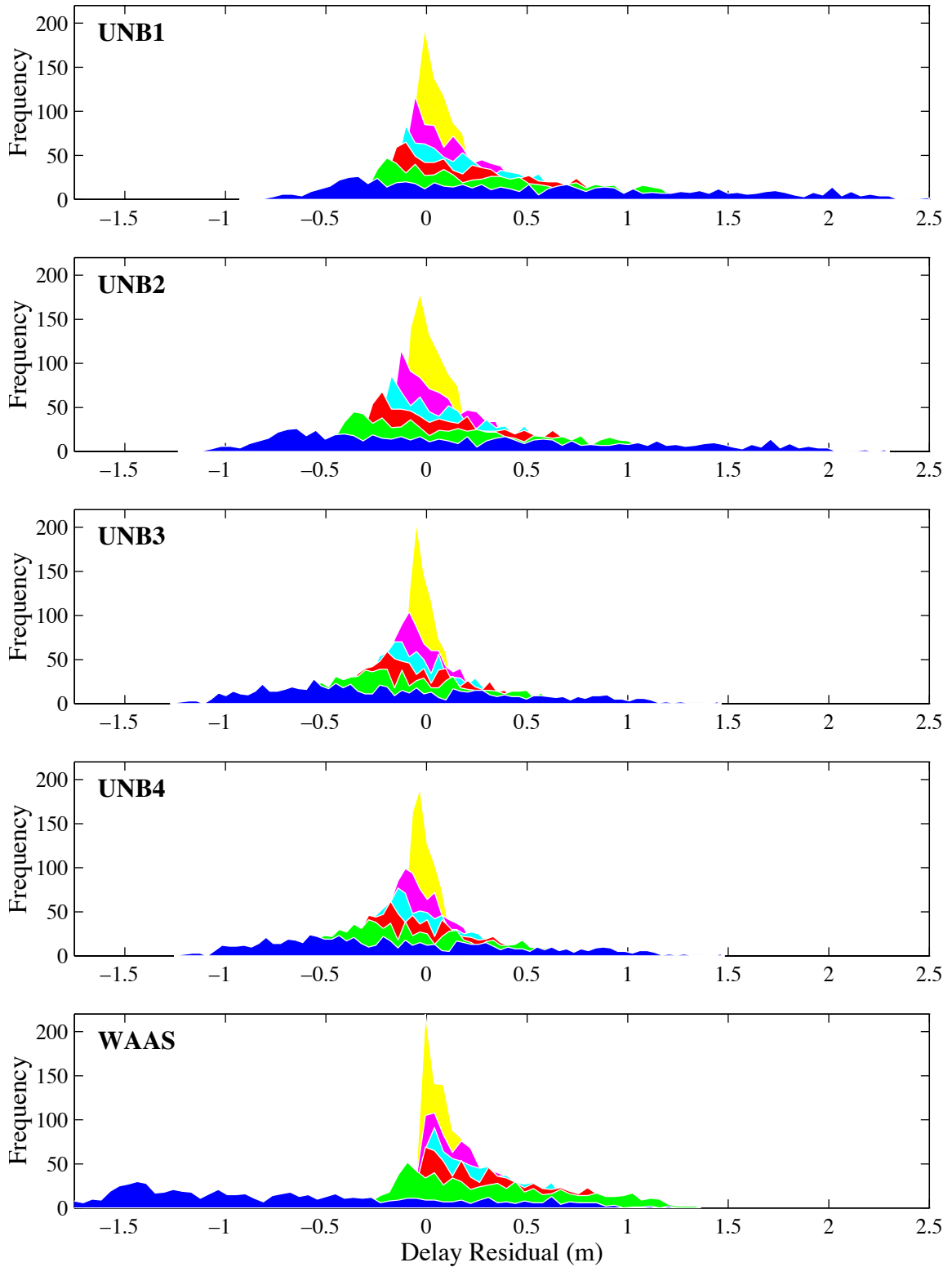
Figure B5.11. Frequency distributions of ray–trace residuals for Nashville.

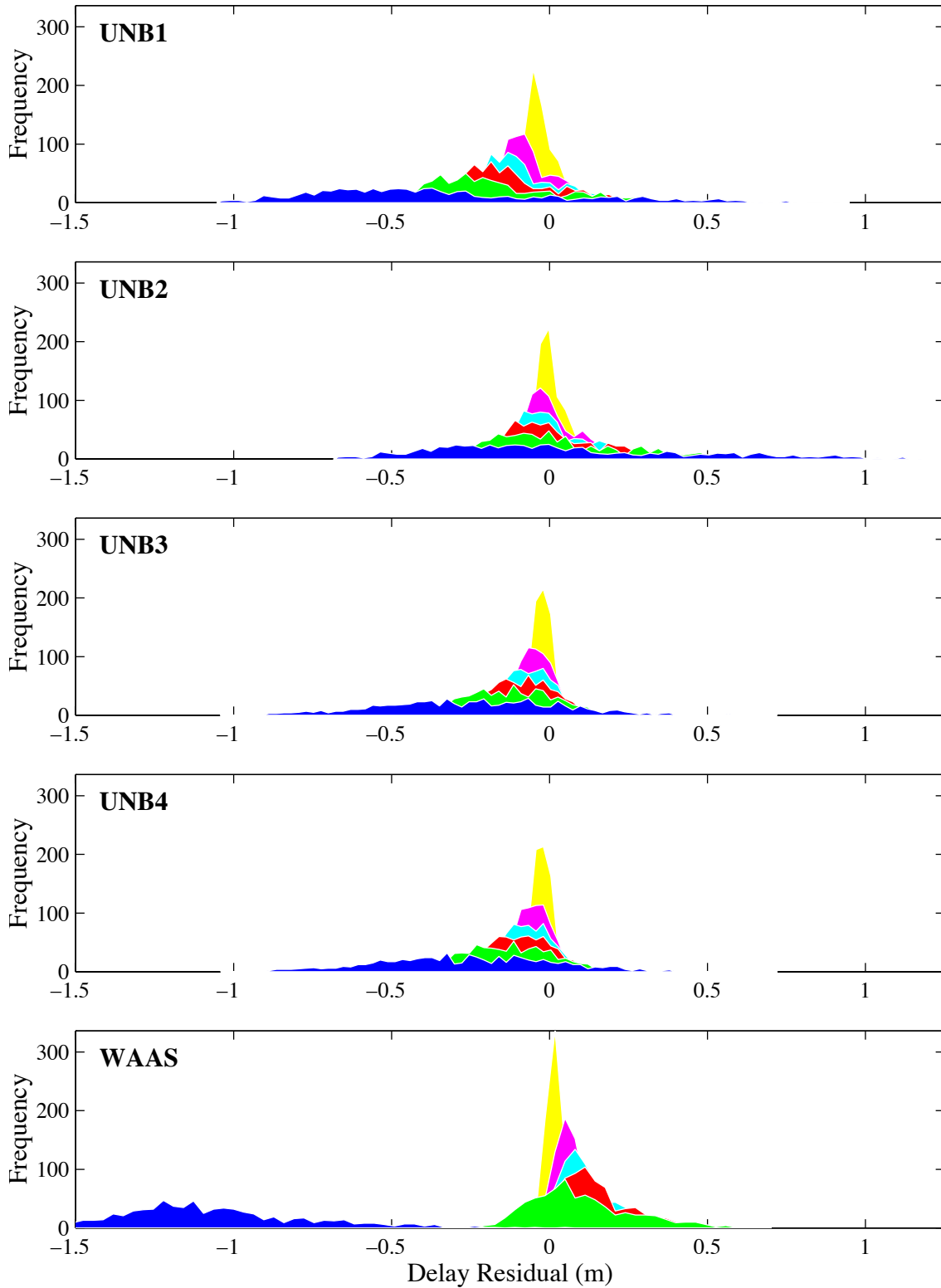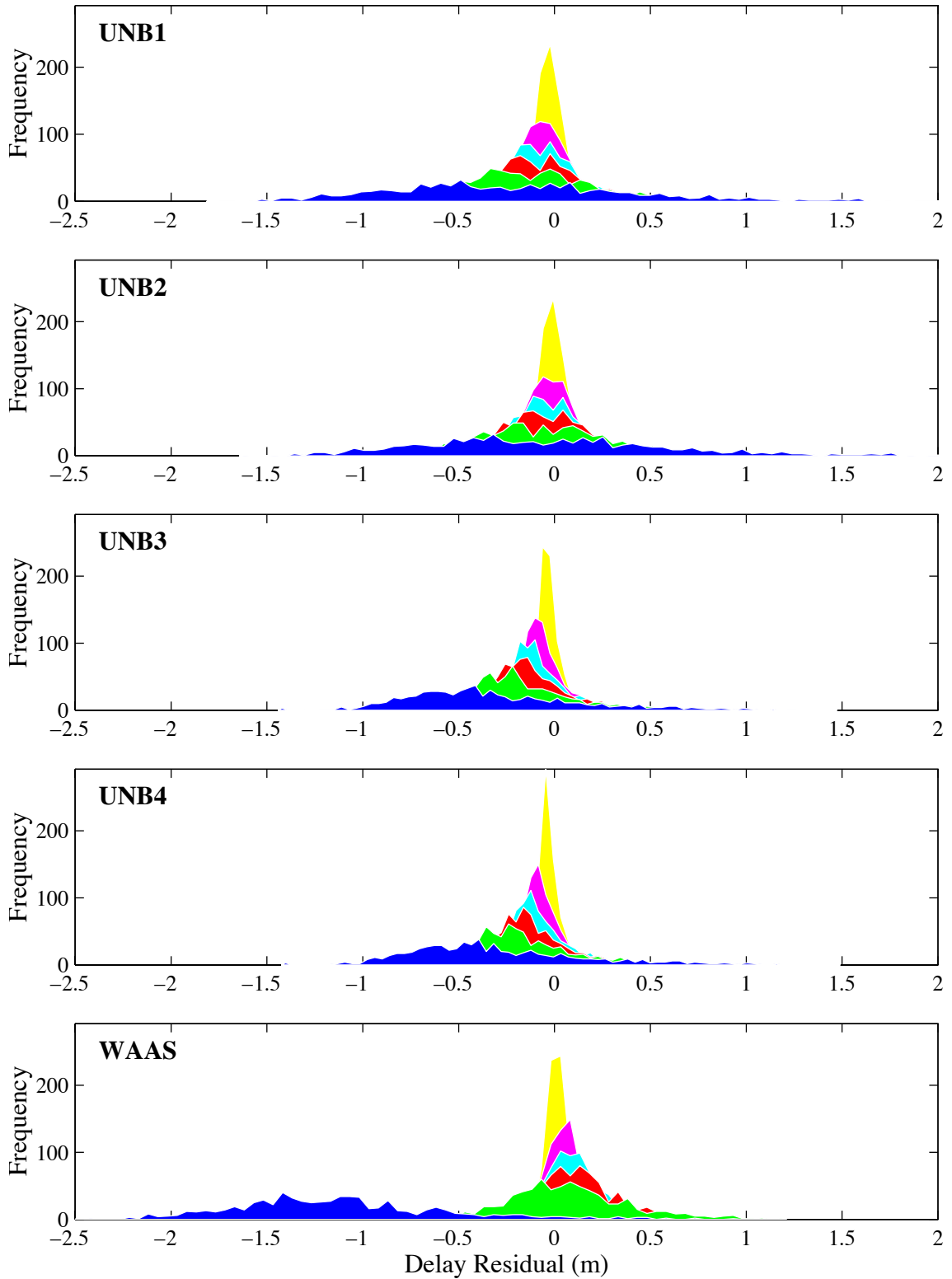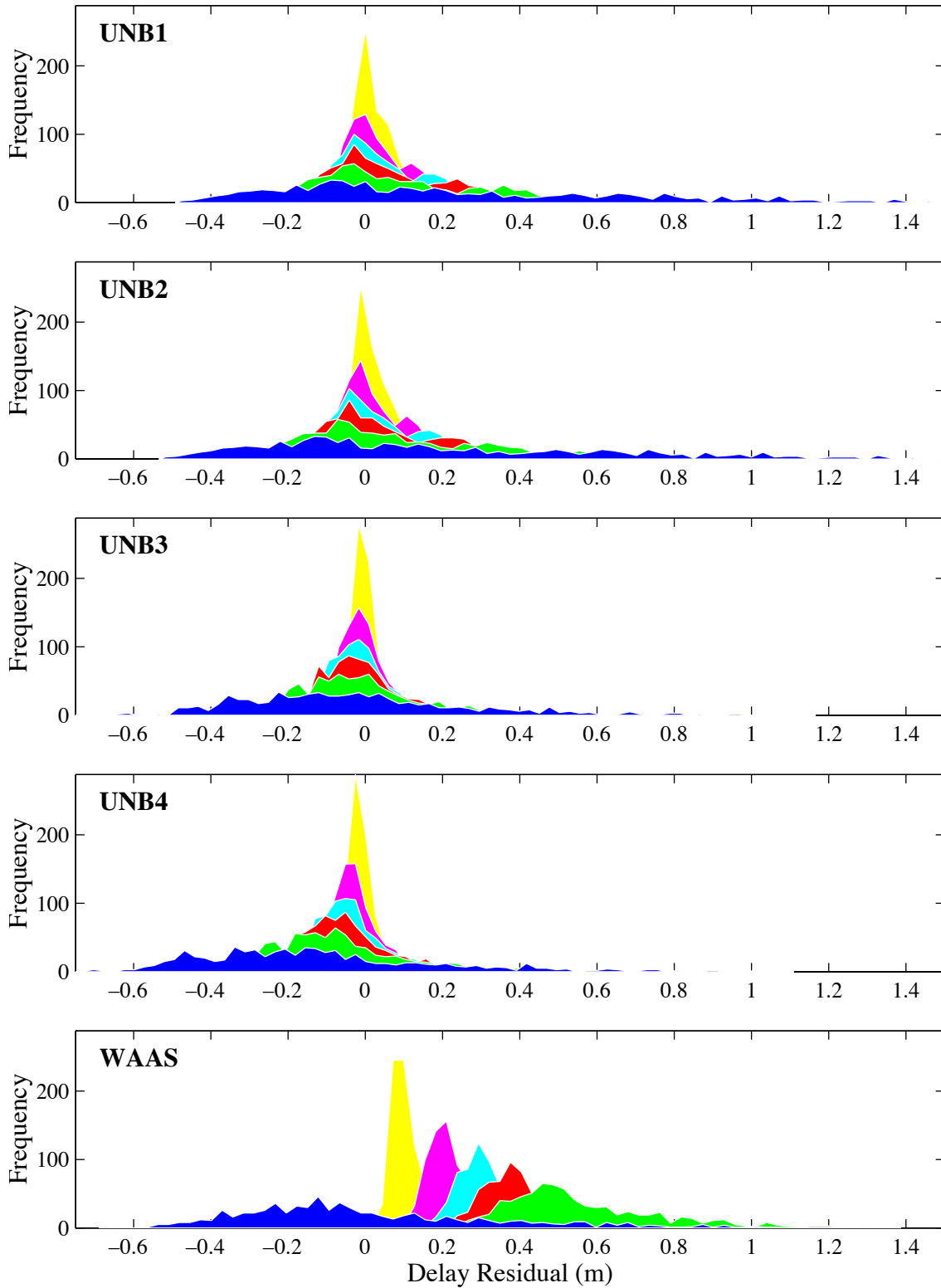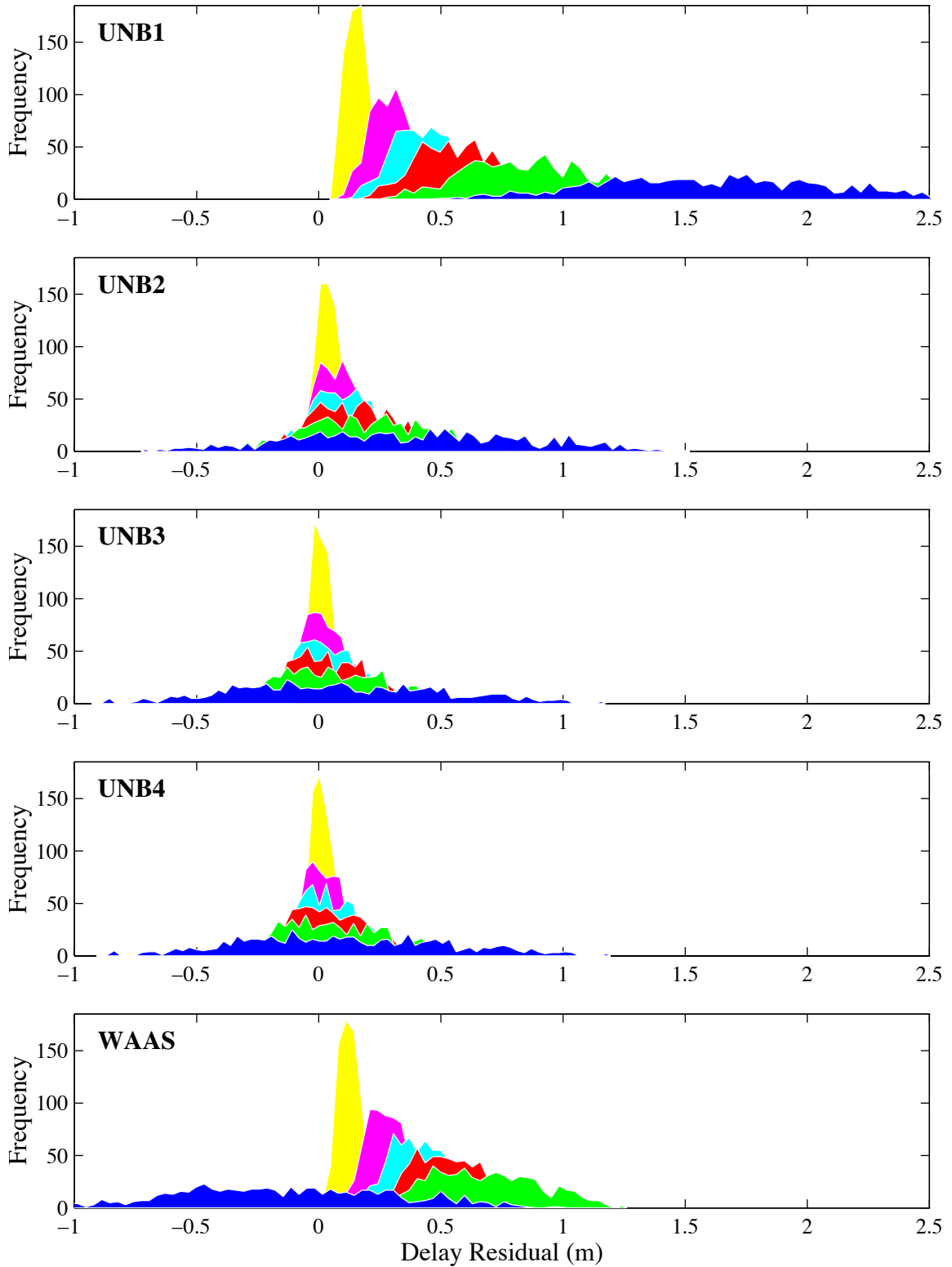**Figure B5.12. Frequency distributions of ray−trace residuals for San Juan.**
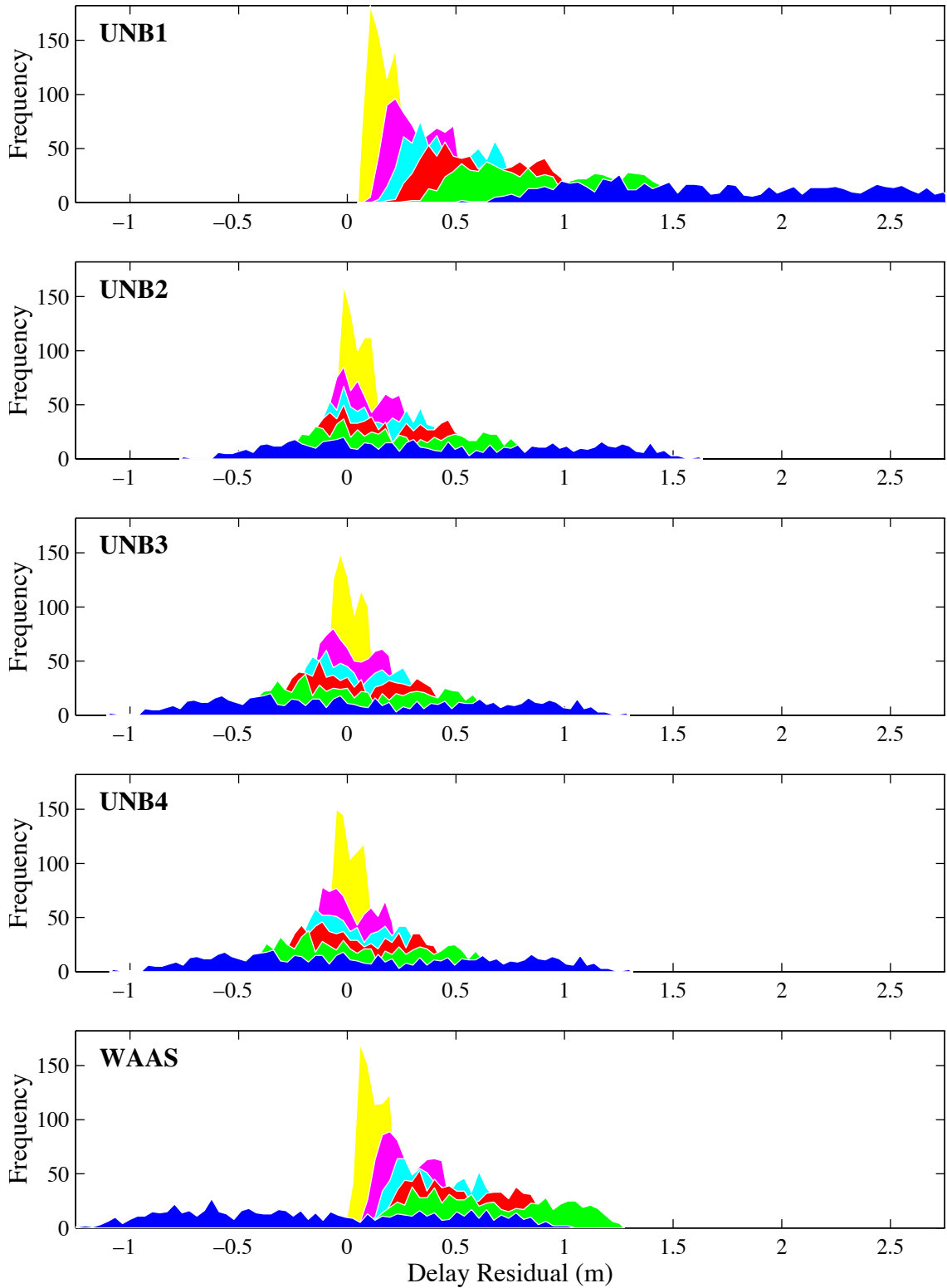
Figure B5.13. Frequency distributions of ray−trace residuals for Guam.

APPENDIX C
PRACTICAL IMPLEMENTATION

This appendix deals with various points about the practical implementation of the UNB3 tropospheric propagation delay model. Appendix C1 is a self-contained section summarising the model and describing all the necessary components of the algorithm. Section C2 details some considerations on the practical implementation of the software required to compute the delay. Section C3 outlines an equation to compute suitable *a priori* weights that might be required in a least-squares adjustment or Kalman filter.

APPENDIX C1 Tropospheric Delay Algorithm

The tropospheric delay model to be applied by the user shall take the form:

$$d_{trop} = d_{hyd}^z \cdot m_{hyd} + d_{wet}^z \cdot m_{wet}, \qquad\qquad (\text{C.1})$$

where the range delays caused by the atmospheric gases in hydrostatic equilibrium and water vapour are dealt with separately. For each component, the expected delay at the user's zenith is computed first (d_{hyd}^z and d_{wet}^z respectively) and then mapped to the satellite "line-of-sight" by the corresponding mapping function (m_{hyd} and m_{wet} respectively).

The algorithms used for the zenith delays and mapping functions are commonly used in space geodesy and are based on the work of *Saastamoinen* [1972] and *Niell* [1996] respectively. A look-up table of atmospheric parameters is used to drive the zenith delay algorithms. This was first described in Section 3.3.2 and is repeated here for convenience. This table is based on similar tables already provided for the mapping functions. They are the fundamental components of the model and have been derived from one source — the 1966 U.S. Standard Atmosphere Supplements [*Dubin et al.*, 1966]. A value for each parameter is computed from the tables based on the user's position (latitude and height) and time (day-of-year).

The zenith delay algorithms require mean-sea-level values of the following atmospheric parameters: pressure (P_0, mbar), temperature, (T_0, Kelvin), water vapour pressure (e_0, mbar), temperature lapse rate (β, Kelvin/metre) and water vapour "lapse

rate" (λ, dimensionless). These are extracted from Table C.1 and interpolated to the user's time and position with the equation:

$$\xi(\phi, t) = \xi_{avg}(\phi_i) + \left[\xi_{avg}(\phi_{i+1}) - \xi_{avg}(\phi_i)\right] \cdot m$$
$$- \left(\xi_{amp}(\phi_i) + \left[\xi_{amp}(\phi_{i+1}) - \xi_{amp}(\phi_i)\right] \cdot m\right)$$
$$\cdot \cos\left(\frac{2\pi(t - 28)}{365.25}\right)$$

(C.2a)

for the latitude range $15° < |\phi| < 75°$ and

$$\xi(\phi, t) = \xi_{avg}(\phi_i) - \xi_{amp}(\phi_i) \cdot \cos\left(\frac{2\pi(t - 28)}{365.25}\right)$$

(C.2b)

for latitudes $|\phi| \leq 15°$ and $|\phi| \geq 75°$. For the interpolation, $m = (\phi - \phi_i)/(\phi_{i+1} - \phi_i)$; ϕ is the absolute value of the user's latitude and the subscripts refer to the nearest tabular latitudes to the required one; t is the day-of-year; and ξ represents the required parameter. In the Southern Hemisphere the amplitude values should change sign and this can be achieved by adding 182.625 to the user's day of year.

The next step is to compute the factors to scale these values to the user's height:

$$\kappa_{hyd} = \left(1 - \frac{\beta H}{T_0}\right)^{\frac{g}{R_d \beta}},$$

(C.3)

$$\kappa_{wet} = \left(1 - \frac{\beta H}{T_0}\right)^{\frac{\lambda' g}{R_d \beta} - 1},$$

(C.4)

(where $\lambda' = \lambda + 1$, $g = 9.80665$ m/s^2, $R_d = 287.054$ J/kg/K and the user's height, H, is expressed in units of metres above mean-sea-level). It should be noted that these functions only precisely model physical conditions upto the altitude of the tropopause.

The relative model error will increase above that region, however the absolute delay continues to decrease exponentially and the functions remain approximately correct. Both functions remain numerically valid for heights upto and including $H = T_0/\beta$ where they become zero. The maximum height at latitude 15°N/S, for example, is ~47.6 km. At this altitude the magnitude of the total zenith delay is usually on the order of several millimetres only, and the correction could be ignored for most practical purposes.

**Table C.1. Meteorological parameter values for the
hydrostatic and wet zenith delays.**

Lat.	Average				
	P_0	T_0	e_0	β	λ
15	1013.25	299.65	26.31	$6.30 \cdot 10^{-3}$	2.77
30	1017.25	294.15	21.79	$6.05 \cdot 10^{-3}$	3.15
45	1015.75	283.15	11.66	$5.58 \cdot 10^{-3}$	2.57
60	1011.75	272.15	6.78	$5.39 \cdot 10^{-3}$	1.81
75	1013.00	263.65	4.11	$4.53 \cdot 10^{-3}$	1.55
Lat.	Amplitude				
	P_0	T_0	e_0	β	λ
15	0.00	0.00	0.00	$0.00 \cdot 10^{-3}$	0.00
30	-3.75	7.00	8.85	$0.25 \cdot 10^{-3}$	0.33
45	-2.25	11.00	7.24	$0.32 \cdot 10^{-3}$	0.46
60	-1.75	15.00	5.36	$0.81 \cdot 10^{-3}$	0.74
75	-0.50	14.50	3.39	$0.62 \cdot 10^{-3}$	0.30

The sensitivity functions to model the refraction effect are:

$$\tau_{hyd}^z = \frac{10^{-6} k_1 R_d}{g_m} \ , \tag{C.5}$$

$$\tau_{wet}^z = \frac{10^{-6} k_3' R_d}{g_m \lambda' - \beta R_d} \ , \tag{C.6}$$

(where k_1 = 77.604 K/mbar, k_3' = 382000 K^2/mbar, and g_m = 9.784(1–2.66·10^{-3}cos(2ϕ)–

2.8·10^{-7}H) m/s^2) and the zenith range delays (in metres) can be computed according to:

$$d_{hyd}^z = \tau_{hyd}^z \cdot \kappa_{hyd} \cdot P_0 \; , \tag{C.7}$$

$$d_{wet}^z = \tau_{wet}^z \cdot \kappa_{wet} \cdot \frac{e_0}{T_0} \; . \tag{C.8}$$

For the hydrostatic mapping function, equation (C.2) is used to compute values for a_{hyd}, b_{hyd}, and c_{hyd} from Table C.2. The mapping function value is given by:

$$m_{hyd} = \frac{1 + \dfrac{a_{hyd}}{1 + \dfrac{b_{hyd}}{1 + c_{hyd}}}}{\sin(E) + \dfrac{a_{hyd}}{\sin(E) + \dfrac{b_{hyd}}{\sin(E) + c_{hyd}}}} + \left(\frac{1}{\sin(E)} - \frac{1 + \dfrac{a_{hgt}}{1 + \dfrac{b_{hgt}}{1 + c_{hgt}}}}{\sin(E) + \dfrac{a_{hgt}}{\sin(E) + \dfrac{b_{hgt}}{\sin(E) + c_{hgt}}}} \right) \cdot \frac{H}{1000}$$

$$\tag{C.9}$$

where E is the satellite elevation angle, a_{hgt} = 2.53·10^{-5}, b_{hgt} = 5.49·10^{-3}, c_{hgt} = 1.14·10^{-3}.

For the wet delay mapping function, the parameter values from Table C.3 are interpolated using a simplified form of equation (C.2) because there is no annual variation:

$$\xi(\phi,t) = \xi_{avg}(\phi_i) + \left[\xi_{avg}(\phi_{i+1}) - \xi_{avg}(\phi_i) \right] \cdot m \tag{C.10a}$$

for the latitude range 15° < $|\phi|$ < 75° and

$$\xi(\phi,t) = \xi_{avg}(\phi_i) \tag{C.10b}$$

for latitudes $|\phi|$ ≤ 15° and $|\phi|$ ≥ 75°.

A simplified form of equation (C.9) provides the wet delay mapping function:

$$m_{wet} = \frac{1 + \dfrac{a_{wet}}{1 + \dfrac{b_{wet}}{1 + c_{wet}}}}{\sin(E) + \dfrac{a_{wet}}{\sin(E) + \dfrac{b_{wet}}{\sin(E) + c_{wet}}}}$$

(C.11)

Table C.2. Parameter values for the hydrostatic delay mapping function.

Lat.	Average		
	a_{hyd}	b_{hyd}	c_{hyd}
15	$1.2769934 \cdot 10^{-3}$	$2.9153695 \cdot 10^{-3}$	$62.610505 \cdot 10^{-3}$
30	$1.2683230 \cdot 10^{-3}$	$2.9152299 \cdot 10^{-3}$	$62.837393 \cdot 10^{-3}$
45	$1.2465397 \cdot 10^{-3}$	$2.9288445 \cdot 10^{-3}$	$63.721774 \cdot 10^{-3}$
60	$1.2196049 \cdot 10^{-3}$	$2.9022565 \cdot 10^{-3}$	$63.824265 \cdot 10^{-3}$
75	$1.2045996 \cdot 10^{-3}$	$2.9024912 \cdot 10^{-3}$	$64.258455 \cdot 10^{-3}$
Lat.	Amplitude		
	a_{hyd}	b_{hyd}	c_{hyd}
15	0.0	0.0	0.0
30	$1.2709626 \cdot 10^{-5}$	$2.1414979 \cdot 10^{-5}$	$9.0128400 \cdot 10^{-5}$
45	$2.6523662 \cdot 10^{-5}$	$3.0160779 \cdot 10^{-5}$	$4.3497037 \cdot 10^{-5}$
60	$3.4000452 \cdot 10^{-5}$	$7.2562722 \cdot 10^{-5}$	$84.795348 \cdot 10^{-5}$
75	$4.1202191 \cdot 10^{-5}$	$11.723375 \cdot 10^{-5}$	$170.37206 \cdot 10^{-5}$

Table C.3. Parameter values for the wet delay mapping function.

Lat.	Average		
	a_{wet}	b_{wet}	c_{wet}
15	$5.8021897 \cdot 10^{-4}$	$1.4275268 \cdot 10^{-3}$	$4.3472961 \cdot 10^{-2}$
30	$5.6794847 \cdot 10^{-4}$	$1.5138625 \cdot 10^{-3}$	$4.6729510 \cdot 10^{-2}$
45	$5.8118019 \cdot 10^{-4}$	$1.4572752 \cdot 10^{-3}$	$4.3908931 \cdot 10^{-2}$
60	$5.9727542 \cdot 10^{-4}$	$1.5007428 \cdot 10^{-3}$	$4.4626982 \cdot 10^{-2}$
75	$6.1641693 \cdot 10^{-4}$	$1.7599082 \cdot 10^{-3}$	$5.4736038 \cdot 10^{-2}$

APPENDIX C2 General Considerations

Table C.4 indicates some example execution times for calculating the tropospheric delay using the existing and new models. The computations were done on a Sun Microsystems 85 MHz MicroSPARC II. As can be seen, UNB4 takes approximately 6 times longer to return the delay than the Altshuler model or the initially proposed WAAS model. Apart from the fact that the UNB model's code is not optimised for speed, there are several other factors that can be considered to improve execution time. While it is important that a new delay determination be made at every epoch (see Section 2.2.3), the coefficients of the model change slowly with time and horizontal position. Hence, the meteorological parameters and the mapping function coefficients can be sampled less often.

Table C.4. Execution times for tropospheric delay models.

Delay Model	Time (sec) per 1,000,000 evaluations
Altshuler	10
WAAS	10
NATO	8
UNB1	53
UNB2	58
UNB3	60
UNB4	55
$NMF_h{}^{\dagger}$	19
$NMF_w{}^{\dagger}$	12

†Hydrostatic and wet mapping functions respectively for UNB1/2/3/4.

It is recommended that the look-up tables that represent the meteorological parameters and the mapping function coefficients be implemented as variable size arrays with the latitude values explicitly specified. In this way, not only can updated parameter

values be provided at a future date, but more values representing greater spatial coverage could be implemented. For example, it would probably be wise to explicitly specify the Southern Hemisphere parameter values for UNB3, in case "true" (as opposed to Northern Hemisphere) values are made available at a later date.

Because of the added complexity of the UNB3 algorithm over the other navigation-type models, it may appear attractive to compute a sample of discrete zenith delay values across the range of time and space represented by the model, and then derive a simpler algorithm, such as a polynomial, to approximate these values. It is strongly recommended that this **not** be done. This was, in effect, what happened with the Altshuler model and subsequently again with the initially proposed WAAS model. The "better" performance of the NATO model over these two models is due in part because it returns to the source of the models (CRPL Reference Atmosphere-1958) and presents it in its most basic form. In the same way, the generality of the UNB models lends them a great flexibility, not only in their application, but also in their implementation (vis-à-vis updating or expanding the parameter values).

APPENDIX C3 Model Weights

Applying the error propagation law to equation (C.1), and assuming no correlation between terms, provides:

$$\sigma^2_{d_{trop}} = \left(d^z_{hyd}\right)^2 \cdot \sigma^2_{m_{hyd}} + \left(m_{hyd}\right)^2 \cdot \sigma^2_{d^z_{hyd}} + \left(d^z_{wet}\right)^2 \cdot \sigma^2_{m_{wet}} + \left(m_{wet}\right)^2 \cdot \sigma^2_{d^z_{wet}} \quad .(\text{ C.12 })$$

We can evaluate this equation under standard atmospheric conditions (d^z_{hyd} = 2.30 m, d^z_{wet} = 0.12 m), at five degrees elevation angle ($\overline{m_{hyd}}$ = 10.1441, $\overline{m_{wet}}$ = 10.7467), with zenith delay errors for UNB3 from our data ($\sigma_{d^z_{hyd}}$ = 0.019 m, $\sigma_{d^z_{wet}}$ = 0.042 m), and five degree mapping function errors specified by *Niell* [1996] ($\sigma_{m_{hyd}}$ = 0.0038, $\sigma_{m_{wet}}$ = 0.0247) from a larger, independent set of radiosonde data, to arrive at:

$$\begin{aligned}\sigma^2_{d_{trop}} &= (0.008740)^2 + (0.192738)^2 + (0.002964)^2 + (0.451361)^2 \\ \therefore \quad \sigma_{d_{trop}} &\approx 0.49 \ m\end{aligned} \quad , \quad (\text{ C.13 })$$

which compares well with the value for UNB3 in Table 4.7 ($\approx$0.45 m).   From the individual components of equation (C.13), we can see that the errors in the Niell mapping functions contribute only a small amount to the total delay error and hence the primary error contribution is the error in the zenith delay determination.   Therefore, for practical purposes we are justified in writing:

$$\sigma^2_{d_{trop}} = \left(m_{hyd}\right)^2 \cdot \sigma^2_{d^z_{hyd}} + \left(m_{wet}\right)^2 \cdot \sigma^2_{d^z_{wet}} , \quad (\text{ C.14 })$$

as the equation which will provide the necessary *a priori* weights for the tropospheric delay at any elevation angle in a least-squares adjustment or Kalman filter.

<center>**VITA**</center>

Candidate's Full Name: John Paul Collins

Place and Date Of Birth: Newcastle-under-Lyme, Staffordshire, England
November 25, 1970

Permanent Address: 45 East Bank Ride
Forsbrook, Stoke-on-Trent
Staffordshire, ST11 9DS
England, U.K.

Universities Attended: University of East London
Longbridge Road, Dagenham
Essex, RM8 2AS
England, U.K.
1990-1993
B.Sc. (Hons.) Surveying and Mapping Sciences

University of New Brunswick
Department of Geodesy and Geomatics Engineering
Fredericton, N.B.
Canada, E3B 5A3
1994-1999

Publications and Conference Proceedings:

Mendes, V.B., J.P. Collins and R.B. Langley (1995). "The effect of tropospheric propagation delay errors in airborne GPS precise positioning." *Proceedings of ION GPS-95*, The 8th International Technical Meeting of the Satellite Division of The Institute of Navigation, Palm Springs, Calif., September 12-15, pp. 1681-1689.

Collins, J.P. and R.B. Langley (1996). "Mitigating tropospheric propagation delay errors in precise airborne GPS navigation." *Proceedings of PLANS '96*, IEEE Position, Location and Navigation Symposium, Atlanta, Ga., April 22-26, pp. 582-589.

Collins, J.P., R.B. Langley, and J. LaMance (1996). "Limiting factors in tropospheric propagation delay error modelling for GPS airborne navigation." *Proceedings of The 52nd Annual Meeting*, Institute of Navigation, Cambridge, Mass., June 19-21, pp. 519-528.

Collins, J.P. and R.B. Langley (1997). "Estimating the residual tropospheric delay for airborne differential GPS positioning." *Proceedings of ION GPS-97*, The 10th International Technical Meeting of the Satellite Division of The Institute of Navigation, Kansas City, Mo., September 16-19, pp. 1197-1206.

Collins, J.P. and R.B. Langley (1998). (Invited) "Estimating the residual tropospheric delay for airborne differential GPS positioning (a summary)." *Advances in Positioning and Reference Frames*, Ed. F.K. Brunner. International Association of Geodesy Symposia No. 118, Rio de Janeiro, Brazil, September 3-9, 1997. Springer-Verlag, New York, pp. 331-336.

Collins, J.P. and R.B. Langley (1998). "The residual tropospheric propagation delay: How bad can it get?" *Proceedings of ION GPS-98*, The 11th International Technical Meeting of the Satellite Division of The Institute of Navigation, Nashville, Tenn., September 15-18, pp. 729-738.

Collins, J.P. and R.B. Langley (1999). "Tropospheric Delay: Prediction for the WAAS user." *GPS World*, Vol. 10, No. 7, pp. 52-58.